Archives of Computational Methods in Engineering - **Preprint**

Challenges, tools and applications of tracking algorithms in the numerical modelling of cracks in concrete and masonry structures

Savvas Saloustros · Miguel Cervera · Luca Pelà

This is a pre-print of an article published in *Archives of Computational Methods in Engineering*. The final authenticated version is available online at: https://doi.org/10.1007/s11831-018-9274-3

Abstract The importance of crack propagation in the structural behaviour of concrete and masonry structures has led to the development of a wide range of finite element methods for crack simulation. A common standpoint in many of them is the use of tracking algorithms, which identify and designate the location of cracks within the analysed structure. In this way, the crack modelling techniques, smeared or discrete, are applied only to a restricted part of the discretized domain.

This paper presents a review of finite element approaches to cracking focusing on the development and use of tracking algorithms. These are presented in four categories according to the information necessary for the definition and storage of the crack-path. In addition to that, the most utilised criteria for the selection of the crack propagation direction are summarized.

The various algorithmic issues involved in the development of a tracking algorithm are discussed through the presentation of a local tracking algorithm based on the smeared crack approach. Challenges such as the modelling of arbitrary and multiple cracks propagating towards more than one direction, as well as multi-directional and intersecting cracking, are detailed. The presented numerical model is applied to the analysis of small- and large-scale masonry and concrete structures under monotonic and cyclic loading.

Keywords Computational failure mechanics · Strain localization · Tracking algorithms · Quasi-brittle materials · Monotonic and cyclic loading

Savvas Saloustros · Miguel Cervera · Luca Pelà

Department of Civil and Environmental Engineering
Universitat Politècnica de Catalunya, UPC-BarcelonaTech
Campus Nord UPC, Jordi Girona 1-3, 08034 Barcelona, Spain.

CIMNE - Centre Internacional de Mètodes Numèrics a l'Enginyeria
Campus Nord UPC, Gran Capità, S/N, 08034 Barcelona, Spain.

E-mail: savvas.saloustros@upc.edu
E-mail: miguel.cervera@upc.edu
E-mail: luca.pela@upc.edu

1 Introduction

Strain localization refers to the development of narrow bands within a loaded structure where material degradation and deformation concentrates, while the areas outside these bands tend to unload elastically. In structures made of quasi-brittle materials, the evolution of these strain localization bands, called hereafter *cracks*, can have a detrimental effect on the global structural behaviour. Especially when reinforcement is lacking, as in the case of unreinforced masonry structures, the development of the collapse mechanism depends on the relative location and propagation of dominant cracks within the structure.

Due to the high importance of cracking phenomena in the structural capacity and response, the engineering community has shown an earnest interest during the last century in their understanding and realistic prediction, to such an extent that two new engineering fields have emerged: Fracture Mechanics and Computational Failure Mechanics. In the first the mathematical and physical bases associated with the initiation and propagation of cracking are set, while in the latter these

principles are applied and further developed within a numerical framework.

This paper focuses on the advances in the computational modelling of cracking during the last decades and in particular on the use of tracking algorithms in strain localization analysis. These numerical procedures are used to define the zones within the structure where cracking is expected to occur. In this way, the numerical approach used for the simulation of cracking is only applied to these designated zones rather than in the whole structure.

The paper is structured in the following way. The next section presents a brief historical overview of finite element approaches used for the simulation of cracking. Section 3 focuses on the development and use of tracking algorithms, the encountered challenges and the various solutions proposed in the literature. Then, the rest of the paper discusses the algorithmic issues and the application of tracking algorithms through the presentation of a local tracking technique developed by the authors for the analysis of both concrete and masonry structures. Section 4 outlines the simulation of monotonic loading cases, and two applications are presented in Section 5. The modelling of cyclic loading is addressed in Section 6 and Section 7 includes a relative case-study. Section 8 presents a large-scale application of the local tracking algorithm to an existing unreinforced masonry structure. The paper closes with the conclusions and some considerations for future research.

2 Finite element approaches to cracking

2.1 Classical crack representations

The advance of digital computers and the development of the Finite Element Method (FEM) between the 1950s and 1960s offered to engineers a powerful tool for applying and testing the fracture mechanics theories developed in the first half of the 20th century (for a historical synopsis see Felippa [1]). Since then, a plethora of numerical methods have been developed focusing on the simulation of propagating cracks in solids. This section presents an outline of the most used of these methods adopting a categorization on the basis of the crack representation at discrete level into: the *Discrete or Discontinuous Crack Approach* and the *Smeared or Continuous Crack Approach*.

In the Discrete Crack Approach (DCA), a crack is simulated as an actual displacement discontinuity (called hereafter a *strong discontinuity*) within a single element or along the boundary of adjacent elements (see Fig. 1a). Upon crack initiation, the displacement field across a crack presents a *discrete* jump w and the associated, fictitious, strain field becomes unbounded, shown in Fig. 1c. This is achieved through the proper enrichment of the displacement field with discontinuous functions. Alternatively, in the Smeared Crack Approach (SCA), cracks are represented in a continuous setting, and their effect (in the displacement and strains) is *smeared* over a certain region of the discretized domain, called the localization-band, with width h including one or more elements, as illustrated in Fig. 1b. The first case, shown in Fig. 1d, corresponds to the *local* smeared crack approach, in which the displacement jump presents two weak discontinuities between the element within the localization-band and the adjacent ones, while the associated strains show a definite jump. The second case, shown in Fig. 1e, refers to the *regularised* smeared crack approach, where the use of more elements for representing the effect of the crack results in a smoother variation of the displacement and strain fields over the selected localization band h. A discrete crack is interpreted as the limit case of a smeared one having a localization-band with vanishing width, and conversely, a smeared crack is the regularization of a discrete crack over a certain width h.

Despite their substantial differences, discrete and smeared crack approaches define the relationship between stress and deformation embarking from the same starting point; the *cohesive-zone model*. The cohesive-zone model, introduced by Barenblatt [2] for brittle fracture and Dugdale [3] for ductile one, defines the relationship between traction forces and displacements at the surface of the crack. In 1976, Hillerborg et al. [4] adopted the cohesive-zone concept in their *fictitious crack model* for representing discontinuous cracking in quasi-brittle materials with the finite element method. In this fictitious crack model, the loss of cohesion in the forming crack was directly related to the experimentally measured fracture energy of the material. The same concept was formulated later in 1983 in the context of the smeared crack approach by Bažant and Oh [5]. Today, the bibliography riddles with constitutive models based on these predecessors, which have been developed within the framework of plasticity (e.g. [6, 7, 8, 9]), damage (e.g. [10, 11, 12, 13, 14]), a combination of plasticity and damage (e.g. [15, 16, 17, 18, 19]) and smeared cracking (e.g. [20, 21]).

2.2 The problem of directional mesh-bias dependency

Discrete and smeared crack approaches have seen many variations since their first applications during the 1960s, the former by Ngo and Skordelis [22] and Nilson [23] and the latter by Rashid [24]. The main motivation behind these developments has been the wide range of

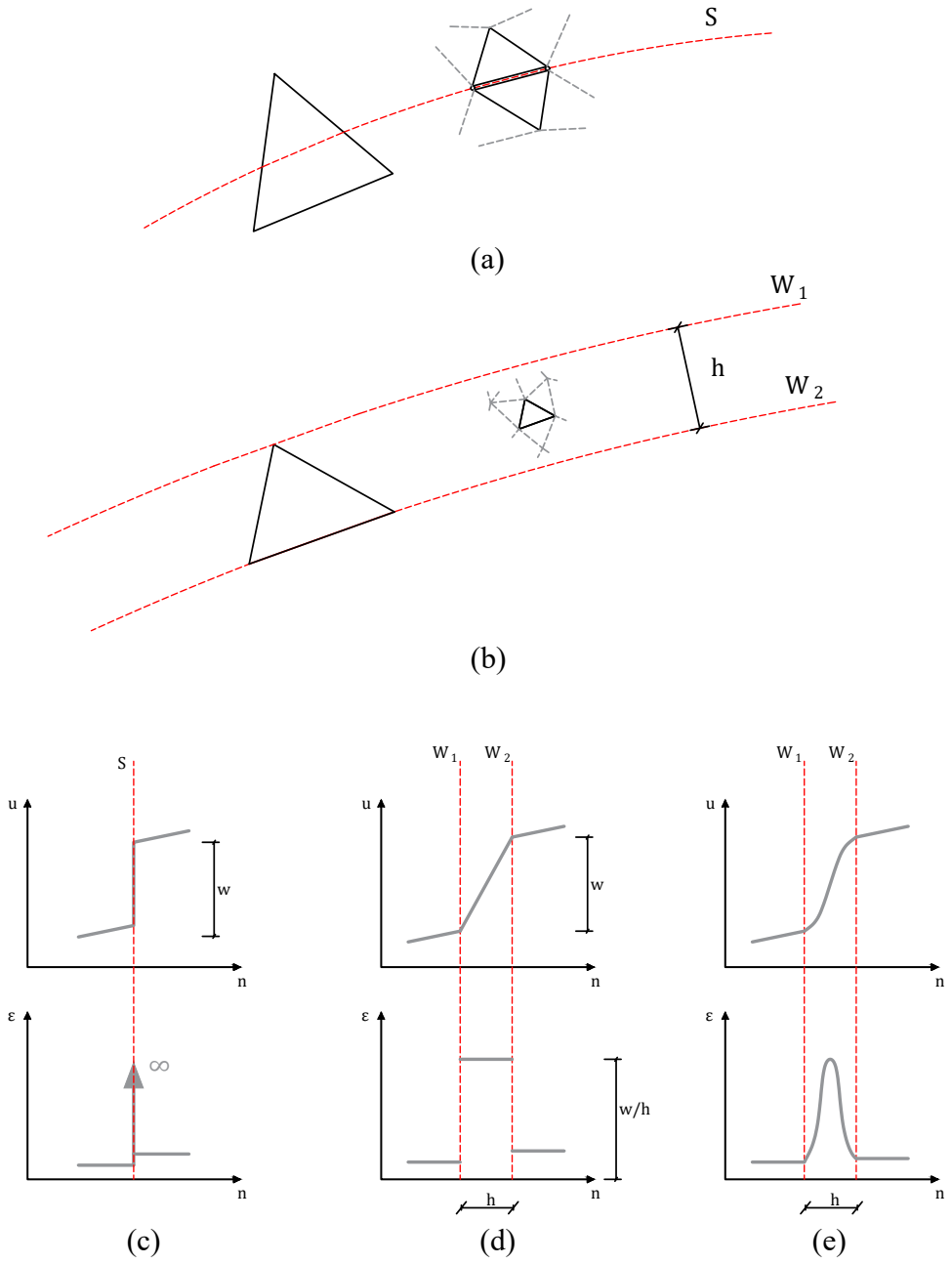

Fig. 1. (a) Discrete crack approach: the crack (shown with the red dashed curve S) is simulated either in the interior or across the boundaries of the finite elements. (b) Smeared crack approach: the effect of the crack is simulated within a zone of width h (bounded by the red dashed curves W_1, W_2) including one or more finite elements. Displacements and strains within the localization band of a (c) discrete crack approach, (d) local smeared crack approach and (e) regularised smeared crack approach.

engineering applications concerned with fracture simulation, varying from large-scale structures with arbitrary and multiple cracking to small-scale ones with few dominating cracks. The first cases need numerical tools that offer a balance between computational efficiency and correct crack localization. In the latter cases, the increasing importance of the accurate crack representation necessitates the elaboration of numerical approaches that can capture rigorously the crack propagation and the associated opening/closing kinematics.

Another equally important driving force for the development of various numerical methods has been the

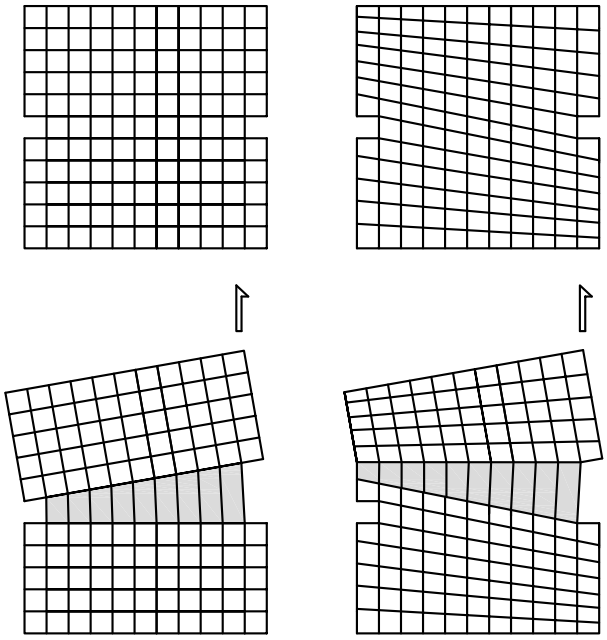

Fig. 2. Illustration of directional mesh-bias dependency in a mode I crack opening. Top: two meshes with different orientation of the finite elements' sides. Bottom: deformation and strain localization band (in grey) induced by a traction force applied at the top right end. The dependency of the localization band to the structure of the mesh is known as directional mesh-bias dependency.

unexpected numerical difficulties encountered in the simulation of cracks. Probably, the most significant of them is the observation that in a finite element analysis cracks have the tendency to propagate following the orientation of the finite elements' sides (see Fig. 2). This phenomenon became known as *directional mesh-bias dependency/sensitivity* and its underlying causes have been historically a matter of controversy. In particular, the origin of this pathology has been sought in the three ingredients of a computational failure model: (i) the underlying continuum theory, (ii) the constitutive model setting the linear and non-linear response of the material, and (iii) the spatial discretization procedure turning the continuum problem into a discrete one.

Early interpretations of the problem considered directional mesh-bias dependency as the result of mathematical features associated with the continuum model (e.g. [25, 26, 27]). Strain softening involves negative slope on the local stress-strain (or traction-displacement) relationship, usually represented by the use of a negative material tangent modulus. Due to the latter, the incremental equations of the Boundary Value Problem (BVP) lose ellipticity in quasi-static problems or hyperbolicity in dynamic ones. The alteration of the elliptic/hyperbolic character of the BVP results in the loss of uniqueness of the solution. As we will present later, efforts to recover the well-posedness of the BVP have been possible through modifications on the continuum or the constitutive model.

Along a different line, mesh-bias dependency has been considered to be the consequence of the approximation error involved in the discrete representation of the continuum differential equations [29, 30, 31]. The finite element method aims to approximate the solution of a continuum problem through its discretization into finite parts, i.e. the finite elements. The discretization procedure induces approximation errors in the pre- and post-peak range of the localization process. In the linear range, the discretization error originates from the differentiation process for obtaining the strains (and the stresses) from the known displacements. In the post-peak range, the discretization error is induced by the limited capacity of standard finite elements to reproduce separation modes in an adequate manner [32, 33]. Evidently, efforts to overcome these problems have pointed to the enhancement of the finite element method accuracy in the pre- and post-localization regiments.

Finally, a third apprehension of the problem considers the constitutive model as the possible flaw to the mesh-bias dependency of the numerical solution [34]. In this sense, the mesh-bias independency of the numerical solution can be alleviated through the proper definition of the constitutive model and the failure condition.

In the following we present an overview, without claiming completeness, of discrete and smeared crack approaches aiming to the mesh independent simulation of cracking within the context of the Finite Element Method (FEM). Other methodologies outside the FEM field, such as meshfree approaches, boundary element methods or discrete element methods will not be covered here. For a general review the reader is also referred to Rabczuk et al. [35].

2.3 Discrete crack approaches

The Discrete Crack Approach (DCA) represents closely the condition induced by an open crack, provoking displacement discontinuities within the fractured solid. The concept is based on the long tradition of Fracture Mechanics that, naturally, have defined the criteria for crack initiation and propagation in discrete crack approaches.

The DCA was preferred in the first endeavours for crack simulation with the finite element method [22, 36]. In these applications, cracks were modelled by

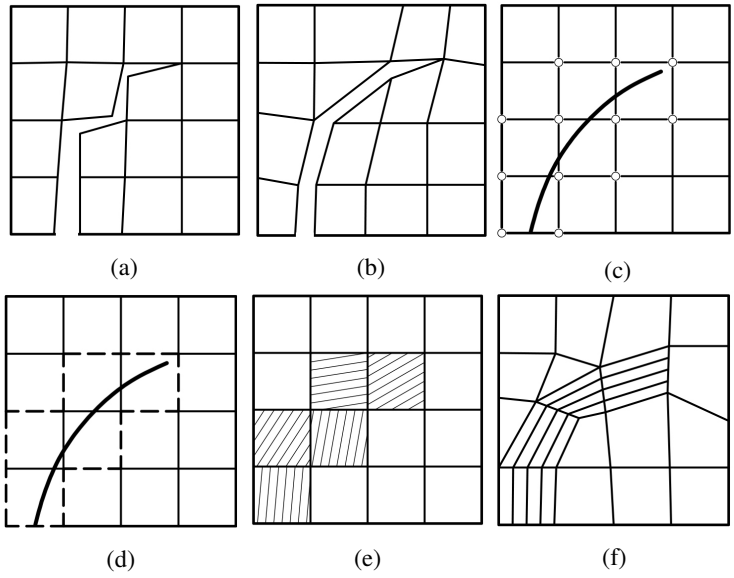

Fig. 3. Discrete (DCA) and Smeared (SCA) crack approaches for the representation of a curved crack. (a) DCA: Inter-element crack approaches with nodal separation or introduction of cohesive interface elements at the sides of the finite elements, (b) DCA: Remeshing, (c) DCA: Nodal enrichment in partition of unity methods, (d) DCA-SCA: elements with embedded discontinuities. (e) SCA: local weak discontinuities, (f) Remeshing and local SCA. (Image adapted from Cervera and Chiumenti [28]).

means of separating elements, upon satisfying a failure condition. The crack geometry was represented by the element edges and an additional set of nodes was introduced so that the interpolation across the element edges could be discontinuous. A subsequent alternative was the use of discrete interface elements along the crack boundaries [37, 4]. These strategies became known as *inter-element crack approaches* or *discrete-interface approaches*.

Inter-element crack approaches have an obvious limitation; cracks can develop only across the element boundaries and therefore the crack geometry depends on the mesh topology (Fig. 3a). To overcome this problem, two solutions have been proposed. The first one is to use a mesh with predefined element orientations aligned with crack-paths that are a priori known, estimated (through preliminary analyses) [38, 39, 40] (Fig. 4) or coincide with weak zones of the simulated material, as the mortar-unit interface in masonry structures [41, 42, 43, 44, 45, 46] (Fig. 5). The second choice is the use of a crack propagation criterion and the continuous adaptation of the mesh topology, so that the crack direction coincides with the finite elements' sides (Fig. 3b). The crack could be then simulated either by introducing a discrete interface or an additional set of nodes [47, 48, 49, 50, 51, 52, 53] (see Fig. 6). These approaches are based on graphic-aided design algorithms and became known as *remeshing techniques*. Remeshing

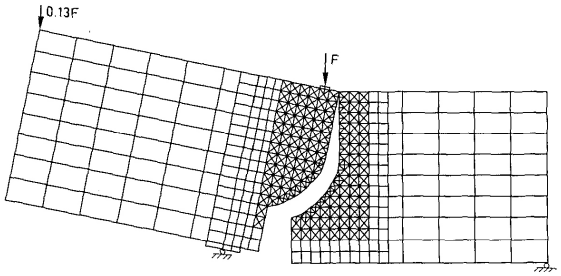

Fig. 4. Simulation of crack propagation in a four-point shear test on a single-edge notched concrete beam, with predefined crack-path using discrete interfaces in Rots [38].

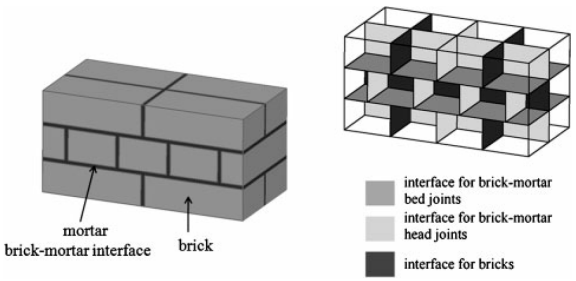

Fig. 5. Modelling of masonry with discrete interfaces in Macorini and Izzuddin [45].

is still an important part of several strain localization techniques (e.g. [54, 55, 56]).

The increased computational cost due to the addition of nodes and the increase of the bandwidth of the

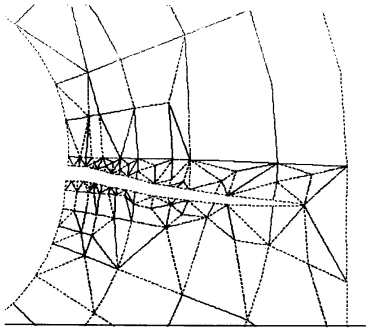

Fig. 6. Remeshing in the simulation of a propagating crack within a lug in Saouma and Zatz [47].

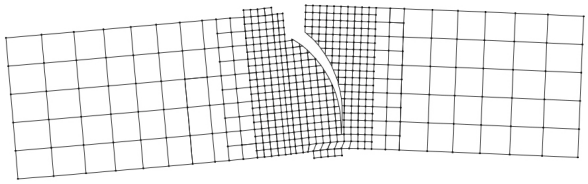

Fig. 7. Simulation of crack propagation in a four-point shear test on a single-edge notched concrete beam with the Discrete Strong Discontinuity Approach in Dias-da-Costa et al. [67].

stiffness matrix, as well as the intrinsic errors due to the projections of the variable fields from the old to the new mesh, make remeshing methods cumbersome for the simulation of evolving cracks. The answer to this was to simulate the effect of a crack within an element so that remeshing and nodal addition are not necessary. This concept led to the development of the *Embedded Finite Element Method (E-FEM)* in which crack discontinuities are embedded within a finite element. An early effort towards this direction can be traced in the work of Johnson and Scott [57]. Some years later, Dvorkin et al. [58] set the basis for the introduction of a strong discontinuity within a finite element. The approach raised much interest in the following years and different versions of elements with embedded strong discontinuities were developed (e.g. [59, 60, 61, 62, 63, 64, 65, 66]) (Fig. 3d). The *Discrete Strong Discontinuity Approach* is based on the same concepts of E-FEM but, as implied by its name, represents the cracks as actual discontinuities by introducing global nodes in the elements crossed by the crack-path [67] (Fig. 7). Early reviews of the different variations of embedded strong discontinuity methods are given by Jirásek [68] and Oliver et al. [69].

In the end of the 20th century, Belytschko and Black [70] and Möes et al. [71] proposed the *eXtended Finite Element Method (X-FEM)* as an alternative to the existing approaches for crack simulation. In X-FEM, the displacement discontinuities are captured through the

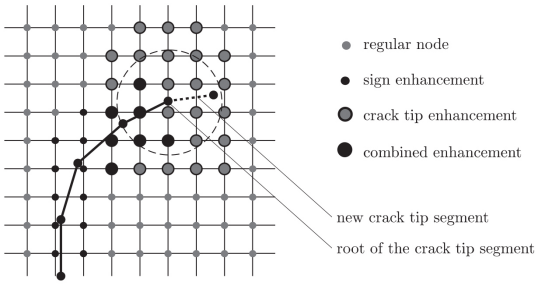

Fig. 8. Nodal enrichment of elements crossed by a crack and surrounding the crack-tip in the eXtended Finite Element Method (X-FEM). (Image from Dumstorff and Meschke [90]).

kinematic enrichment of the nodes at elements crossed by a crack, based on the partition of unity concept [72, 73] (Fig. 3c). Additional enrichments are applied to the nodes surrounding the crack-tip within a certain area (see Fig. 8), which are used for the computation of the near-tip stress intensity factors and, thus, of the stress field. The method became very popular, since it avoids the use of remeshing algorithms, and saw many variations in the following years such as the *Hansbo method* (or *Phantom node method*) [74, 75, 76] and the *Generalised Finite Element Method* [77, 78, 79, 80, 81]. Reviews of the different versions of the X-FEM can be found in [82, 83, 84, 85, 86], while comparisons between E-FEM and X-FEM in [87, 88, 89].

A common characteristic for many of the aforementioned strong discontinuity approaches is the use of devices that define the crack propagation direction and ensure crack-path continuity, the so-called *tracking algorithms*. Through them, the potential location of the crack, and thus the elements or nodes that require the kinematic enrichment can be identified. It should be noted here that the use of tracking algorithms is, in principle, not essential in E-FEM [65, 91, 92]. However, potential misalignment of the embedded discontinuities across neighbouring elements provokes spurious stress locking [93] and mesh-dependent results [94, 95]. For this reason, tracking algorithms are commonly adopted by E-FEM approaches.

To overcome the necessity of crack-path continuity through tracking algorithms, Remmers et al. [96, 97] developed the *cohesive segments method*. Here, the crack is represented in a piecewise linear way, as shown in Fig. 9, with a collection of overlapping cohesive segments that extend through three consecutive finite elements. Displacement discontinuities are captured exploiting the partition of unity method by nodal enrichment and their magnitude is governed by cohesive relationships. The *cracking node method* by Song and Belytschko [98] is a similar approach in which crack seg-

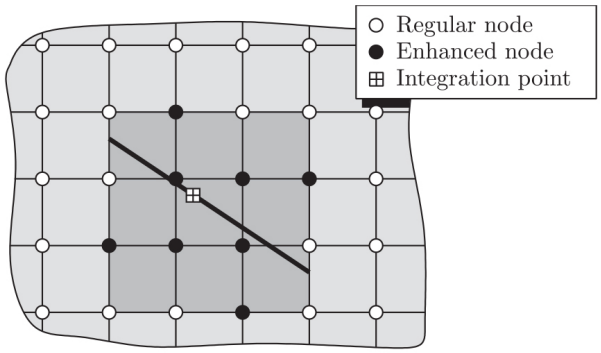

Fig. 9. Representation of a crack increment in the cohesive segments method by Remmers et al. [96]. A crack is introduced at the integration point when the failure criterion is satisfied and extends through three elements. Nodes in black are enhanced according to the partition of unity method to represent the displacement jump (Image from Remmers et al. [97]).

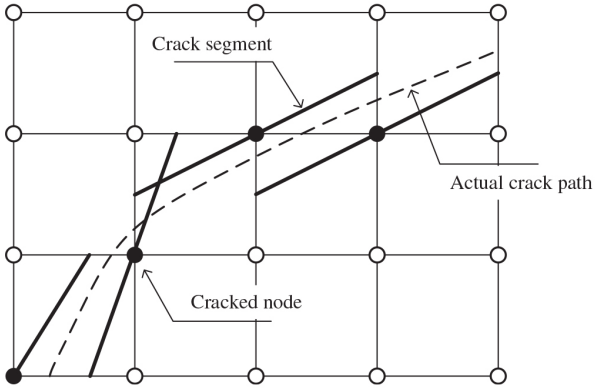

Fig. 10. Representation of a crack in the cracking node method by Song and Belytschko [98]. Nodes in black are enhanced according to the partition of unity method to represent the displacement jump. The dashed line represents the crack-path approximation. (Image from Song and Belytschko [98]).

ments are introduced to nodes and cross two adjacent elements (see Fig. 10).

During the last years, efforts to unify the design and the structural analysis resulted in the development of the *isogeometric analysis*. Fracture propagation using isogeometric analysis is still at its infancy, with the first approaches exploring the potential of the method using the partition of unity concept for modelling the cracks using the discrete crack approach [99, 100].

The above enriching approaches, either at elemental or nodal level, aim to capture strong discontinuities upon crack initiation by improving the kinematics of the finite elements. In this sense, they can be interpreted as a way to limit the discretization error in the non-linear range. In addition to that, directional mesh-bias independency is improved in many of these approaches through the use of tracking algorithms, which define explicitly the location of a propagating crack within the structure.

2.4 Smeared crack approaches

The Smeared Crack Approach (SCA) is the numerical counterpart of continuum solid mechanics. Contrary to discrete crack approaches, the effect of a crack is represented as smeared over a part of the finite element mesh, where the stress is reducing for an increasing strain according to a defined constitutive law (see Fig. 3e). This smeared representation of the material degradation matches well the diffused damage in reinforced concrete structures, and unsurprisingly the first application by Rashid [24] dealt with the simulation of cracking in prestressed concrete vessels.

In the years following Rashid's work, smeared crack approaches almost monopolized the simulation of cracking in quasi-brittle materials. The reason for this are two important practical advantages of the methodology compared to discrete crack approaches. Firstly, the fact that a crack is smeared within one or more elements poses no restriction on the orientation of the crack planes with respect to the directionality of the elements' sides. Secondly, their implementation in a conventional finite element code merely requires a subroutine with a constitutive model.

The popularity of the method dropped when it was realised that the dissipated energy was directly associated with the size of the used finite elements (e.g. [101, 102]). In the following years particular efforts were made to address the problem [103], leading to the crack-band approach by Bažant and Oh [5]. According to this, the traction-displacement relationship of the cohesive-zone model is adjusted to a stress-strain relationship considering equivalence of the dissipated energy. The regularization of the stress-strain relationship is possible considering the band over which the crack is smeared, h in Figs. 1b, 1d. In *local* smeared crack approaches this band is associated to the width of a single finite element (Fig. 3e). Constitutive models based on the local SCA are today part of almost every commercial finite element code, and are still the most favoured approach used by practitioners for crack propagation analysis in large- and small-scale structures.

As soon as the problem of the mesh-size dependency was successfully overcome, the trust over local smeared crack approaches was once more lessened due to the directional mesh-bias dependency. Considering the fact that well-aligned meshes, referring to meshes with the

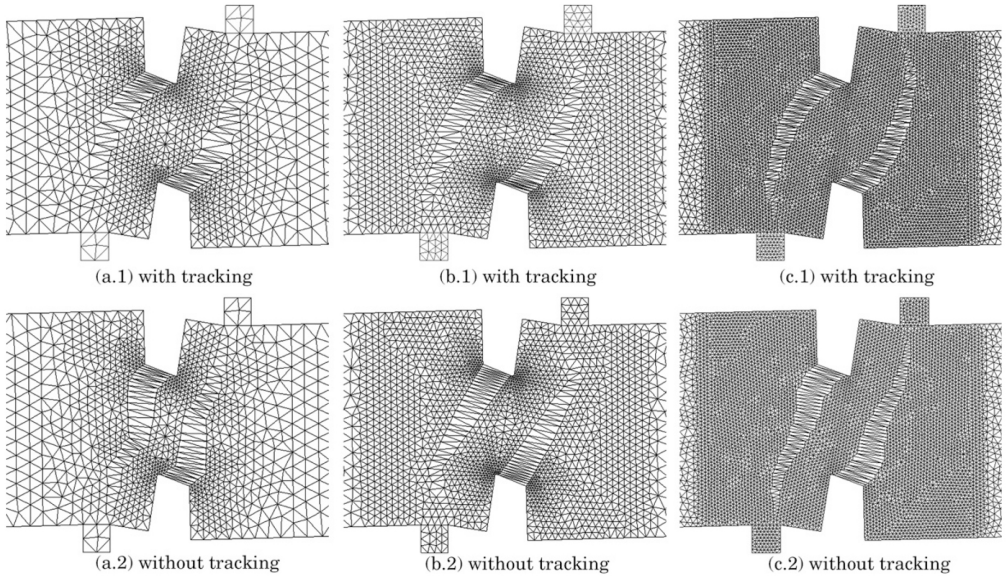

Fig. 11. Crack propagation analysis in a double-edge notched concrete specimen under four-point bending using meshes with increasing refinement from left to right. Analysis with an isotropic local damage model and a tracking algorithm (top) and without a tracking algorithm (bottom). (Image from Cervera and Chiumenti [28]).

element sides aligned to the crack propagation, produced good results, the first endeavoured remedy was once again the use of remeshing algorithms [104, 105] (Fig. 3f).

Along a different line, specific finite element formulations have been developed, within the context of local SCA, aiming to overcome the directional mesh-bias dependency through the limitation of the discretization error. To this aim, Ortiz et al. [106] and Belytschko et al. [107] proposed the enrichment of the strain field for the simulation of kinematic modes induced by a crack. This methodology was further elaborated by Simo et al. [108, 109] and resulted in the class of *Enhanced Assumed Strain (EAS)* finite elements (Fig. 3d). A more recent application of such an elemental enrichment in a smeared cracking context is the *mesh-corrected orthotropic damage model* [110, 111], being the smeared counterpart of the previously presented E-FEM.

The beneficial use of tracking algorithms in discrete crack approaches did not go unnoticed, and during the last decade tracking algorithms have also been used as an auxiliary device in local smeared crack approaches aiming to improve the directional mesh-bias independency. This strategy was introduced in a smeared cracking context by Cervera and Chiumenti [30, 28] aiming to define the location of cracks and restrict their evolution within a single row of finite elements (Fig. 11). Different formulations of tracking algorithms within smeared crack approaches have been presented in the last years in references [32, 112, 113, 114, 115, 116].

Mixed FE methods, introduced in the mid 1960s [118], offer another possibility for reducing the discretization error. The approach considers additional variables (such as the pressure, the stresses or the strains) to the nodal displacements as the primary unknowns of the boundary value problem under question. After their long use in computational fluid dynamics, due to their good performance in incompressible situations, mixed formulations were introduced during the last decade of the 20th century in strain localization problems by Zienkiewicz et al. [105] and Pastor et al. [119, 120]. In the last years, several mixed methods have been developed and applied to strain localization problems, including mixed pressure-displacement [121, 122, 29, 123, 124], stress-displacement [125, 31] and strain-displacement [125, 126, 127, 117, 128] finite elements (Fig. 12).

2.5 Regularized smeared crack approaches

In the 1990s, academic efforts focused on the development of new formulations that aimed to recover the well-posedness of the boundary value problem. The fruit of these efforts have been the so-called *regularised* smeared crack approaches, including *micropolar*, *non-local*, *gradient-enhanced* and *phase-field* models. In *micro-polar* or *Cosserat* models the underlying continuum description is enriched by adding rotational degrees-of-freedom to the conventional translational degrees-of-freedom [129, 26]. In *non-local* models

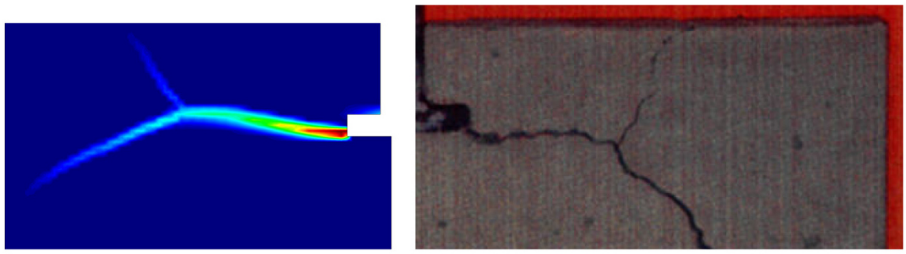

Fig. 12. Comparison between numerically obtained crack pattern using a mixed strain/displacement formulation by Benedetti et al. [117] and the experimental result of a pull-out test on a concrete specimen. (Image from Benedetti et al. [117]).

the local stress does not depend on the local strain but on an averaged strain computed over a defined area [130, 131]. A similar approach is followed in *gradient-enhanced* models, in which non-locality is considered by introducing higher order deformation gradients in the constitutive relationship [132, 133, 134]. For a comparison between non-local and gradient-enhanced models see Peerlings et al. [135] and between non-local models and X-FEM see Bobiński and Tejchman [136]. In the last years, Griffith's variational approach to fracture has been revived through the *phase-field* models [137, 138, 139, 140] (Fig. 13) (for a review see Ambati et al. [141]). Despite their different origin, de Borst and Verhoosel [142, 143] have presented recently the close mathematical relationship between gradient-enhanced and phase-field models. A common standpoint of the above models is the use of an internal characteristic length of physical nature, which acts as a localization limiter, as well as the use of highly refined meshes within this length to capture the material degradation [33].

Finally, strain-rate dependent *viscous-regularised* models [25, 144] have been considered as an alternative solution that recovers the well-posedness of the boundary value problem through the addition of viscous effects in the constitutive relationship. Obviously, the regularization effect vanishes with reducing viscosity.

2.6 Hybrid crack approaches

Apart from representing a crack exclusively with either a discrete or a smeared crack approach, there is also the possibility to combine both as shown in Fig. 14. In these hybrid strategies initial micro-cracking is simulated with the use of a smeared crack approach. At a second stage, in which material degradation has reached a defined threshold, the crack formation is simulated through the introduction of a strong discontinuity.

In the majority of these hybrid crack approaches, smeared cracking is simulated with a different kind of a regularised SCA model such as non-local [93, 145], viscous-regularised [146], or gradient-enhanced [147]. The use of a strong discontinuity at a later stage of damage evolution allows for the localized representation of cracking, which otherwise is smeared over a defined, and usually highly refined, region of the mesh due to the non-local definition (Fig. 14). An alternative approach to the use of regularised models for the smeared crack representation was adopted by Belytschko et al. [148], in which a transition between a local damage model and an X-FEM with cohesive enrichment is applied for the simulation of dynamic cracks. Aiming to a better estimation of the stress field prior to the introduction of a strong discontinuity, Oliver et al. [149] and Lloberas-Valls et al. [150] have recently proposed the use of mixed strain-displacement and enhanced assumed strains formulations, respectively.

3 Tracking algorithms

Tracking algorithms are an important part of many finite element approaches for the simulation of cracking. Their role is to identify the direction of the crack propagation, and designate the consolidated and extended crack-path within the discretized domain during the numerical simulation. According to the selected crack representation, a smeared or discrete crack approach is applied to the elements within the crack-path to simulate the effect of the crack in the material, while the rest of the elements outside the crack are usually prevented from failing.

Tracking algorithms can benefit the numerical solution at least in three ways [32]. Firstly, they aid the identification of the expected solution by minimizing the number of the potential ones. This is done through the use of a crack propagation criterion that defines the crack direction. Secondly, they result in a more realistic crack representation, especially in the case of mixed-mode problems with curved cracks. Finally, they minimize or limit the energy dissipation outside of the crack

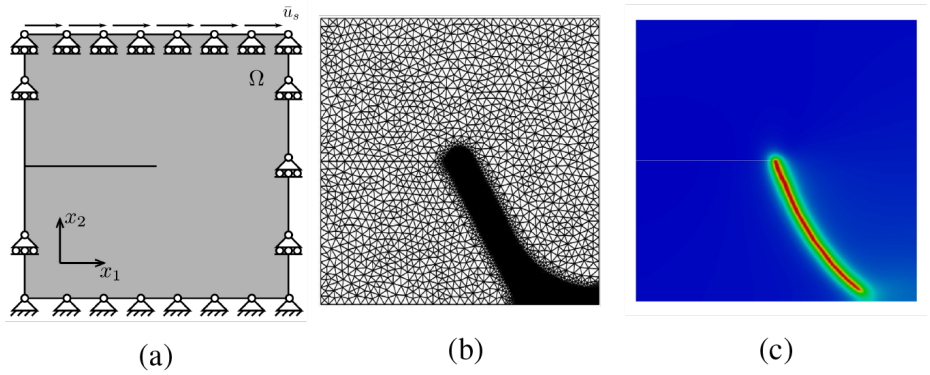

Fig. 13. (a) Single edge notched pure shear test setup, (b) used mesh, and (c) phase-field simulation by de Borst and Verhoosel [142]. (Collection of images from de Borst and Verhoosel [142]).

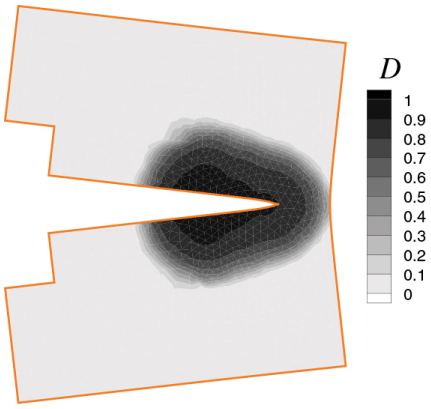

Fig. 14. Representation of a crack in a wedge splitting test combing a non-local damage model with X-FEM by Comi et al. [145]. D represents the value of the non-local damage variable. (Image from Comi et al. [145]).

band. The significance of the latter is to be emphasized since the stress-strain law in local smeared crack approaches is commonly regularised considering that each crack propagates within a single row of finite elements.

The long tradition of tracking algorithms in Discrete Crack Approaches (DCA) is justified for two more reasons. Firstly, they avoid numerical instabilities, since the kinematic enrichment is applied only to a narrow band within the mesh where the crack is expected to develop. Indiscriminate enrichment may not provide stable results. Secondly, they guarantee the crack-path continuity, improving in this way the robustness of the method. As discussed, crack-path continuity of the introduced strong discontinuities in discrete crack approaches is important to ensure compatibility between the deformation modes of adjacent elements, which if not guaranteed may result in spurious stress locking and mesh-dependent results [93, 95, 94].

The successful application of tracking algorithms in discrete crack approaches pointed to their potential benefits in a smeared cracking context, an approach which was introduced in [28, 30]. In the Smeared Crack Approach (SCA), tracking algorithms identify the elements crossed by the crack-path allowing them to damage according to the selected constitutive law, while preventing the ones outside of it from failing.

The following of this section outlines commonly used tracking algorithms in the available literature. First, a categorization of tracking algorithms is performed in terms of the information necessary for the definition and storage of the crack-path. According to this, four categories are defined and presented including: (i) local, (ii) global, (ii) partial domain tracking algorithms and (iv) tracking algorithms based on an underlying damage-related field. Following that, the crack propagation criteria, which can be used for most of the tracking algorithms independently of their category, are summarized.

3.1 Local algorithms

Local tracking algorithms identify the location of a crack within the mesh in an element-by-element manner. The crack propagation direction is computed locally, using information available at element level or within a restricted area surrounding it. Using this direction, the new crack segment within an element can be defined, as well as the locus of the crack edges in neighbouring elements. The same strategy is followed for each crack that may exist in the analysed structure, starting from the first element of the crack (called hereafter as *crack-root*) or the last element at the crack-front (called as *crack-tip* in two-dimensions or *crack-face* in three-dimensions).

The above general procedure, which is followed by a local tracking algorithm for constructing the crack-path, is illustrated in Fig. 15. The necessary ingredients

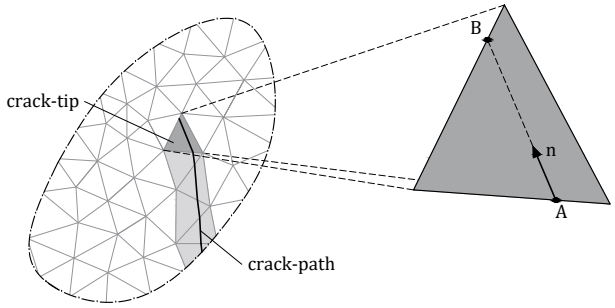

Fig. 15. Crack propagation in a part of the mesh using local tracking algorithms.

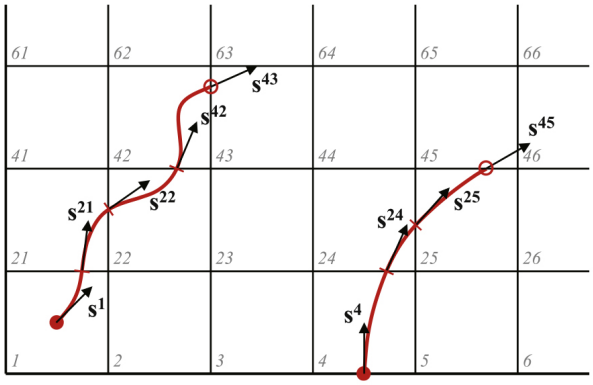

Fig. 16. C^1 continuous crack-path in the local tracking algorithm proposed by Slobbe et al. [112]. S^i denotes the crack propagation direction entry from the preceding element i. (Image from Slobbe et al. [112]).

are the crack propagation direction **n** and the crack-entry coordinates. Starting from the crack-entry point (Point A in Fig. 15), the exit point of the crack at the crack-tip element is easily identified as the intersection between the extension of the vector **n** and one of the element's sides (Point B in Fig. 15). The shared side with one of the neighbouring elements and the intersection point define the next crack-tip element and the position of its crack-entry point, respectively.

Owing to their quite simple strategy, local tracking algorithms have been used in various discrete and smeared crack approaches. Their implementation is likewise straightforward, needing a strategy for the calculation of the crack propagation direction, as in all tracking algorithms, and a side-connectivity array indicating the elements sharing a side with a given one. On the one hand, the latter can be easily constructed at the beginning of the analysis and stored for the rest of it (provided that no remeshing is used). The propagation direction, on the other hand, is continuously updated at the crack-tip element of each crack.

Despite the intrinsic simplicity of the above procedure, the literature riddles with diverse formulations of local tracking algorithms. The reason for this lies on their strong dependence on the finite element technology used. As it will be shown in the following, the crack propagation path within an element may vary depending to the interpolation strategy used, while the procedure followed for identifying the crack-entry/exit points depends on the shape of the used finite elements (triangles, quadrilaterals, tetrahedra, hexahedra etc.).

Local tracking algorithms were the first used for the simulation of propagating cracks in finite element applications. Their role was to define the direction and length of a new crack segment, which was then simulated through remeshing and nodal separation techniques [151, 47] or later with the introduction of cohesive interface elements [48].

A common characteristic of local tracking algorithms is the construction of a continuous crack-path (see Fig. 15). This intrinsic crack-path continuity of the method is a key feature for the limitation of stress locking in approaches with embedded strong discontinuities. In that sense, local tracking algorithms blend very well with E-FEM and numerous implementations exist in the literature [152, 153, 154, 67, 155, 156]. The first applications of X-FEM employed, likewise, local tracking algorithms for recognizing the crack-path and enriching accordingly the nodes of the elements crossed by it [70, 71]. It is noted that in X-FEM the crack-tip can be located at any point within the element, contrary to E-FEM in which the actual location is usually not defined within the element.

Complementary to their long tradition in discrete crack approaches, the use of local tracking algorithms in a smeared cracking context was proposed relatively recently in [157, 158, 159, 32]. In those applications, material degradation was simulated in the elements within the crack-path through the use of local continuum damage mechanics models, while the rest maintained a linear elastic stress-strain behaviour. Pelà et al. [160, 161] extended this tracking algorithm for the simulation of cracking in orthotropic materials such as masonry and wood.

In most local tracking algorithms, the crack propagation direction is updated at each new element and kept fixed during its propagation through it. This choice naturally gives a C^0 continuous crack-path constructed by piecewise linear segments. Slobbe et al. [112, 162] have recently proposed a local tracking algorithm in a SCA context, which can provide C^1 crack continuity among elements (see Fig. 16). This is achieved by constructing the crack propagation field within a crack-tip

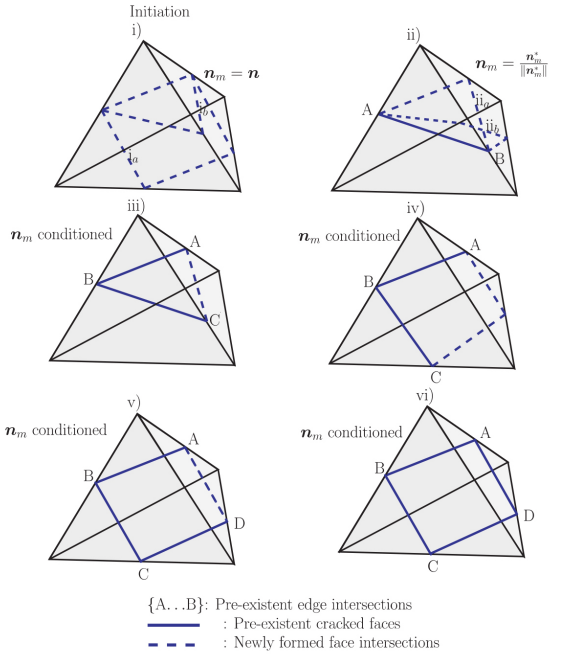

Fig. 17. Local tracking algorithm for the definition of a new crack surface in Areias and Belytschko [163]. $\boldsymbol{n}$ denotes the defined crack propagation direction according to the propagation criterion and $\boldsymbol{n}_m$ the modified one computed respecting pre-existing crack faces in adjacent elements. (Image from Areias and Belytschko [163]).

element considering the propagation directions at its integration points and the crack-entry direction from the previous element. The method needs the assignment of crack propagation directions at the corner nodes through a weighted linear least squares approximation using the known propagation directions at the crack-entry point and the integration points. Then the crack-path field can be interpolated at any location within the element using its shape functions.

In the case of planar cracks the extension of local tracking algorithms to three dimensions is straightforward (see [164]). Difficulties, however, may arise for representing the crack surface in non-planar cracks and an adequate strategy is necessary to ensure crack-path continuity. To this aim, several approaches have been proposed. In Areias and Belytschko [163], the new crack surface in the crack-tip element is defined considering a modified crack propagation direction. This depends on the local crack direction computed at element level and the pre-existing crack faces (i.e. the intersecting facets of neighbouring cracks with the current element) in neighbouring elements (see Fig. 17). Jäger et al. [165] report that it may be impossible using the above approach to construct a new crack plane in the case that the crack faces of adjacent elements do not

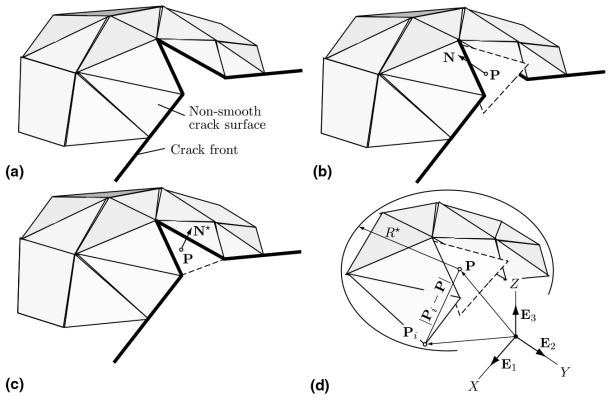

Fig. 18. Local tracking algorithm for the definition of a new crack surface (shown by the dashed triangles) in Gasser and Holzapfel [167]. $\boldsymbol{N}$ denotes the defined crack propagation direction according to the propagation criterion, $\boldsymbol{N}^\star$ the modified one and $\boldsymbol{P}$ a point used for the definition of the new crack surface. (a) Existing non-smooth crack surface and crack-front, (b) prediction of the new crack surface using $\boldsymbol{N}$ and $\boldsymbol{P}$, (c) correction of the new crack surface using $\boldsymbol{N}^\star$ and $\boldsymbol{P}$, (d) patch of elements used for the definition of $\boldsymbol{N}^\star$. (Image from Gasser and Holzapfel [167]).

lie within one plane at the crack-tip element. Gasser and Holzapfel proposed two alternatives to overcome the above problem by relaxing the requirement of a crack-path continuity among the different crack faces. In their first proposal [166], a new crack surface can be uniquely defined by its normal vector and a single point located at the crack. The first is computed considering the underlying stress field, while the definition of the latter depends on the adjacent crack-edges. The authors, however, observed that in some cases this approach may result in very irregular crack surfaces which may lead to (unphysical) crack bifurcations [167]. As a solution to this shortcoming, they proposed the addition of a corrector phase that follows the first prediction of the crack surface with the above procedure [167]. The corrector phase adjusts the predicted crack plane to fit the neighbouring cracks surfaces such that patch-wise linear or quadratic crack representations are possible (see Fig. 18). Jäger et al. [165] present a comparison between the tracking algorithm proposed by Areias and Belytschko [163] and the one by Gasser and Holzapfel [167].

3.2 Global algorithms

Contrary to local methods, global tracking algorithms compute simultaneously all the potential crack-paths at each step of the analysis. This is achieved through the solution of a linear boundary value problem defined in the whole analysed domain. The approach was pro-

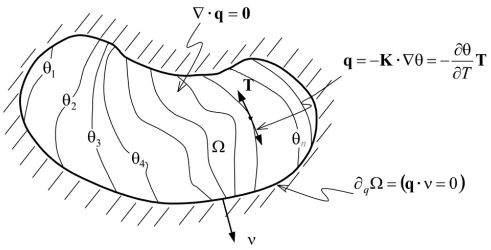

Fig. 19. The heat conduction problem used for the computation of the thermal isolines representing potential crack-paths in the global tracking algorithm proposed by Oliver et al. [168, 169]. (Image from Oliver and Huespe [169]).

posed by Oliver and co-workers [168, 169] and since then has been applied in various contexts for the propagation of two-dimensional (2D) and three-dimensional (3D) cracks.

The basic idea of the global tracking algorithm is to construct a scalar function θ whose isolines represent the crack propagation directions within the analysed structure. The procedure is presented in the following keeping the notation used in [168, 169] to facilitate the comparison with Fig. 19.

The scalar function θ, used for the definition of the potential crack-paths, is computed through the solution of an anisotropic heat conduction-like boundary value problem which can be defined as

$$\nabla \cdot \mathbf{q} = 0 \quad \text{in} \quad \Omega \tag{1a}$$

$$\mathbf{q} = -\mathbb{K} \cdot \nabla \theta = -\mathbf{T} \frac{\partial \theta}{\partial \mathrm{T}} - \left[\mathbf{S} \frac{\partial \theta}{\partial \mathrm{S}} \right] \quad \text{in} \quad \Omega \tag{1b}$$

$$\mathbf{q} \cdot \mathbf{v} = -(\mathbf{v} \cdot \mathbf{T}) \frac{\partial \theta}{\partial \mathrm{T}} - \left[(\mathbf{v} \cdot \mathbf{S}) \frac{\partial \theta}{\partial \mathrm{S}} \right] = \mathbf{0} \quad \text{on} \quad \partial\Omega. \tag{1c}$$

In the above equations $\mathbf{q}$ is the heat flux, $\mathbf{v}$ is the outnormal to the boundary $\partial\Omega$, $\mathbf{S}$ and $\mathbf{T}$ are arbitrary unit vectors having the direction of the failure plane. $\mathbb{K}$ is an anisotropic conductivity-like tensor defined as

$$\mathbb{K} = \mathbf{T} \otimes \mathbf{T} + [\mathbf{S} \otimes \mathbf{S}] + \varepsilon \, \mathbf{I}. \tag{2}$$

where $\mathbf{I}$ represents the unit tensor and ε is a small perturbation parameter introduced to avoid the singularity of $\mathbb{K}$. The effect of this perturbation parameter was studied in [170]. In the above equations, the terms within the brackets are necessary for the use of the tracking algorithm in 3D problems and have to be considered null in 2D ones.

Adopting a finite element discretization, the above boundary value problem is solved through a system of linear algebraic equations

$$[\mathbf{K}] \{\boldsymbol{\theta}\} = \{\mathbf{0}\} \tag{3}$$

with $[\mathbf{K}]$ being the stiffness matrix of the heat conduction-like finite element problem and $\{\boldsymbol{\theta}\}$ the vector of temperature-like nodal unknowns [168]. The solution of the problem needs the definition of the $\mathbf{T}$ and $\mathbf{S}$ vectors. If a vector $\mathbf{N}$ represents the crack propagation direction, computed according to the selected propagation criterion, the $\mathbf{T}$ and $\mathbf{S}$ are selected as orthogonal to $\mathbf{N}$. Finally, in order to provide a non-uniform field for θ, two arbitrary values for θ need to be prescribed, at least, in two nodes.

As soon as the failure condition is reached at an element i, its corresponding value $\theta_i = \theta_0$ is computed. The crack-path can then be identified by constructing the isoline corresponding to this value θ_i, starting from the centroid of the crack root element. Fracture is simulated by applying the chosen crack representation approach at the elements crossed by the θ_i isoline. In the original approach by Oliver et al. [168, 169] this was done by introducing strong discontinuities. Later, Huespe et al. [171, 172] followed the same approach for the simulation of ductile failure, whereas Dumstorff and Meschke [90] used this global tracking algorithm in the context of X-FEM. Cervera and Chiumenti [28, 30] implemented the same algorithm in a smeared cracking context, and cracks were simulated through the use of an isotropic continuum damage model in the elements crossed by the crack-path.

Recently, Riccardi et al. [173] have further elaborated the global tracking algorithm by proposing an alternative mathematical formulation for the construction of the θ scalar field. The motivation behind their work is the eradication of the user-defined perturbation parameter used for the definition of $\mathbb{K}$ in Eq. (2). This approach has shown to increase the stability of the global tracking algorithm, albeit the precision seems to reduce for coarse meshes [173] compared to the original one. In the same work, the authors propose the update of the crack-root at each numerical step and to construct the isoline of an existing crack considering the θ value of the crack-tip. This strategy seems to alleviate problems associated with the loss of crack-path continuity.

Global tracking algorithms are in general more demanding from the computational point of view [165] and more code invasive compared to local ones [32, 149]. This is because the tangent field to the crack $\boldsymbol{T}$ (and $\boldsymbol{S}$ in 3D) is computed for the whole domain, even at locations away from cracks and the global problem needs to be solved for each step. An additional limitation rises from their inability to handle merging, intersecting or branching cracks. Contrarily, one important advantage, evidenced from Eqs. (3), is the straightforward extension to 3D problems as shown in Oliver et al. [168],

Chaves [174] and Jäger et al. [175]. In addition to that, there is no strong dependence on the finite element technology, as with local tracking algorithms.

3.3 Partial-domain algorithms

Partial-domain tracking algorithms are a compromise between local and global ones. In these approaches, the crack is tracked through the solution of a boundary value problem at each numerical step within a subdomain rather than in the whole structure.

The most famous partial-domain tracking algorithm is the level set method. Originally, it was proposed by Osher and Sethian [176] for the representation of the motion of interfaces as the zero of a function, called the level set function. Much later, Belytschko et al. [177] and Stolarska et al. [178] introduced the use of level set methods for crack representation within the context of X-FEM.

A level set function is any continuous function dividing a domain into two parts and taking negative values in one, and positive in the other. The zero level set of this function defines the location of the interface of interest. Contrary to the original approach [176, 179], which focused on the motion of closed interfaces, cracks are open ones. Consequently, their representation necessitates one level set for representing the signed distance to the crack surface, and an additional one for each crack-tip representing the signed distance from it (see Fig. 20).

The necessary components for the tracking of cracks with the level set method are: (i) the level set functions for each crack, (ii) an update algorithm for these level set functions, (iii) the crack propagation direction, which normally is based on local criteria and the computation of the stress intensity factors and (iv) the crack propagation velocity or crack increment size which is used for the extension of the crack during one step and can be defined according to mechanical laws (e.g. [177, 180, 181, 182]) or explicitly by the user (e.g. [183, 184]).

At the beginning of the numerical analysis, a crack is introduced and a function ψ is constructed using the signed distance function from the crack

$$\psi(\boldsymbol{x}, t=0) = \pm \min ||\boldsymbol{x} - \boldsymbol{x}_{\gamma_0}|| \tag{4}$$

while the additional functions for each crack-tip $\varphi_{1,2}$ are defined as

$$\varphi_i(\boldsymbol{x}, t=0) = (\boldsymbol{x} - \boldsymbol{x}_i) \cdot \hat{\boldsymbol{t}}_i. \tag{5}$$

In the above equations, $\boldsymbol{x}$ represents the location of a point within the structure, $\boldsymbol{x}_{\gamma_0}$ is the location of a point belonging to the initially defined crack γ_0, $\boldsymbol{x}_i$ is the location of the ith crack-tip and $\hat{\boldsymbol{t}}_i$ is a unit vector tangent to the crack at its tip i. The sign of the minimum distance in Eq. (4) depends on which side of the crack a point $\boldsymbol{x}$ is located. As can be seen in Fig. 20 with these definitions the crack locus can be defined as

$$\gamma_t = \{\boldsymbol{x} : \psi(\boldsymbol{x}, t) = 0 \cap \varphi(\boldsymbol{x}, t) \leq 0)\} \tag{6}$$

where

$$\varphi(\boldsymbol{x}, t) = \max_i(\varphi_i). \tag{7}$$

In the level set method, the crack is represented in an implicit way. The location of the crack is identified through interpolation of the level set values, which are stored at the nodes, using the same shape functions of the displacements. Hence, the crack representation depends on the interpolation strategy of the chosen finite elements. Aiming to reduce the high computational cost and storage requirements, a partial domain around the crack is usually considered for the computation, update and storage of the level sets at the nodes of elements within it [178].

Having defined the initial level set functions for each crack, its location and propagation is monitored with the update of its level sets during the numerical analysis. To this end, several proposals exist to update the level set functions, which can be defined through geometrical evolutions and non-differential equations [178, 181, 183, 185], fast marching algorithms [186, 187, 188],

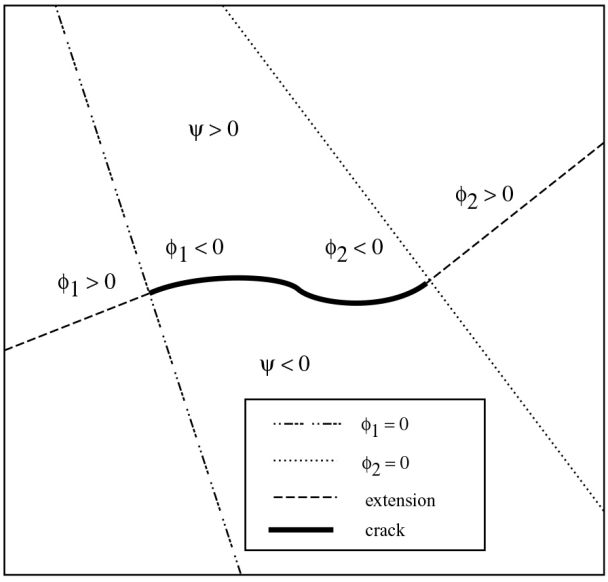

Fig. 20. Level set functions for the representation of a crack in Stolarska et al. [178]. ψ is the signed distance function from the crack and $\varphi_{1,2}$ are the signed distances from the normal to each crack-tip. (Image from Stolarska et al. [178]).

partial differential equations [180] or mixed approaches based on both geometrical and differential equation approaches [189, 182]. Fries and Baydoun [184] proposed an alternative approach for the crack extension. In their work, cracks are represented by level set functions but the crack extension is made with the use of a local tracking procedure starting from the crack-tip. When the crack-extension is identified, then the level sets are updated to include the new crack-path. Similar approaches have been recently presented by Holl et al. [190] and Sadeghirad et al. [191].

The proper update of the level set functions is very important for the accuracy of the numerical solution in X-FEM. This is due to the multiple roles that level sets have within X-FEM methods, the most important of which is the proper identification of the crack propagation and, thus, the nodal enrichment of the elements that are crossed by the crack, as well as those surrounding the crack-tip. Additionally, level sets are important for the calculation of auxiliary variables, such as the near-tip displacement and stress field and the stress-intensity factors, which in turn define the propagation direction. Duflot [189] gives an excellent review of different level set update methods and their role within X-FEM. The generality of some of the update schemes as well of the definitions for the level set functions allows their almost straightforward extension to 3D problems (e.g. [192, 193, 185, 194, 195]).

In finite element crack modelling, level set methods have been used almost exclusively in X-FEM applications. This is due to the fact that the propagation depends heavily on the crack-tip stresses, which can be accurately computed with the use of the enrichment functions. Contrariwise, in E-FEM the stresses can be far from accurate in the crack-tip because a crack propagates from one element to the other [66]. For this reason, level set methods cannot be applied in E-FEM without important elaboration at the crack-tip stress field [66], with recent developments in this direction presented in [196].

Another partial-domain tracking algorithm can be considered the one presented by Feist and Hofstetter [94, 197]. This approach is based on the global tracking algorithm presented in the previous Section 3.2, with the main difference that the scalar field θ is constructed only within a partial domain of the whole structure. This domain is occupied by elements already or potentially crossed by the crack. The approach is, similarly to the global tracking algorithm, easily extended to 3D cases [198], see also [199]. A comparison of the partial-domain and the global tracking algorithms is available in [94].

3.4 Algorithms based on an underlying damage-related field

In the last years a new class of tracking algorithms has emerged, in which the crack-path is identified considering an underlying scalar field representing material degradation in a smeared manner. These tracking algorithms are used in hybrid discontinuity approaches, presented in Section 2.6, and their aim is to monitor the evolution of the material degradation modelled with a smeared crack approach, and define the location where a strong discontinuity will be inserted to simulate the localized jump of the displacements. The use of tracking algorithms within these approaches aims to enhance the localization process and the correct representation of the crack kinematics rather than the enhancement of the mesh-objectivity, which was essentially the purpose of the algorithms presented in the previous sections. The latter is achieved, as discussed in Section 2.6, through the use of alternative smeared crack approaches such as regularised models, mixed formulations or finite elements with embedded weak discontinuities.

One of the first tracking algorithms in this category can be found in the work of Comi et al. [145], where a non-local damage model is used as the underlying field for the tracking of the crack. In this approach, the tracking algorithm monitors the non-local damage at the elements ahead of the crack-tip. As soon as this exceeds a defined threshold, a cohesive crack is inserted to the element directly connected to the crack-tip. The initial direction of the crack is set as equal to the direction of the already formed damage band of the non-local damage field.

The recently proposed *crack-path-field* tracking algorithm by Dias et al. [201, 202] and Oliver et al. [149] determines the position of a discrete crack considering a diffuse strain localization field α^h (see Fig. 21), which is obtained by non-linear local constitutive models with strain softening. The crack-path-field is defined as the location where the selected scalar field α^h takes its maximum value. The procedure for defining the crack-path is composed of four steps including the computation of: (i) the smooth continuous approximation of variable α^h denoted as ψ^h, (ii) its directional derivative $\partial\psi^h/\partial x$, (iii) a smooth continuous approximation of this directional derivative μ^h and (iv) its zero level set Γ. The above fields are illustrated in Fig. 21 for an one-dimensional case. The crack-path-field algorithm is used in the last part of a kinematic enhancement series employed for the mesh-objective localization of fracture. The first kinematic enhancement is applied to elements in which material bifurcation is about to occur

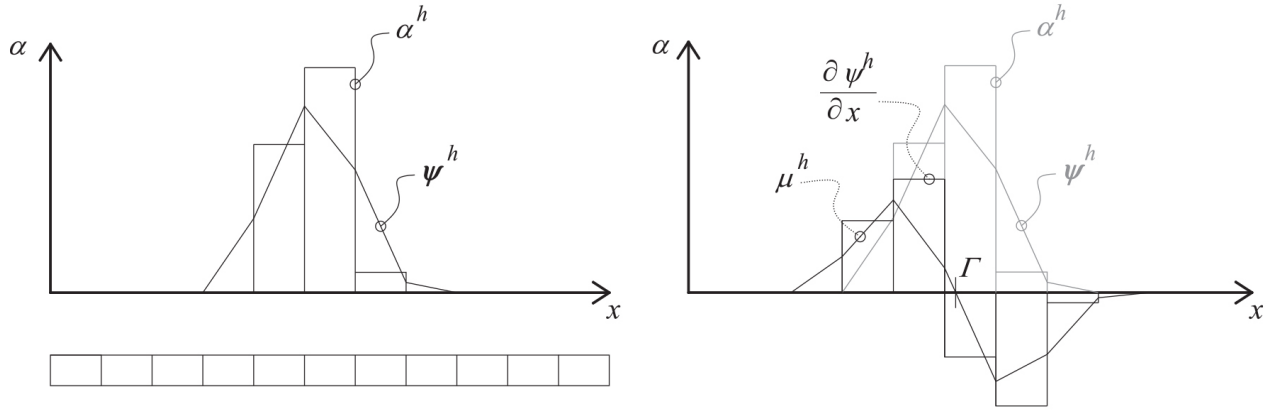

Fig. 21. One dimensional illustration of the strain localization field α^h and its directional derivative ψ^h (left) and the crack-path-field Γ as the zero level of μ^h, which is the continuous approximation of ψ^h (right). (Image from Dias et al. [200]).

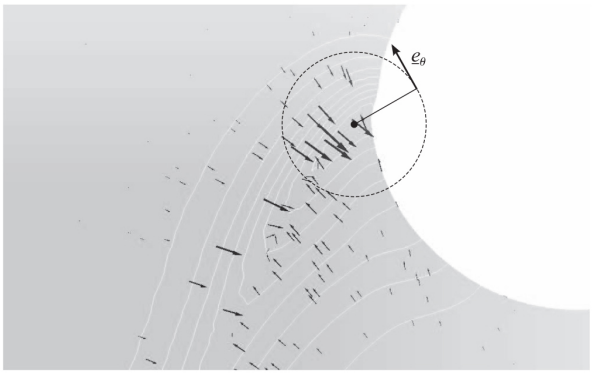

Fig. 22. Damage gradient vectors and an orthoradial vector $\underline{e}_\theta$ at the crack-tip of a potential crack in the marching ridges algorithm of Feld-Payet et al. [55]. (Image from Feld-Payet et al. [55]).

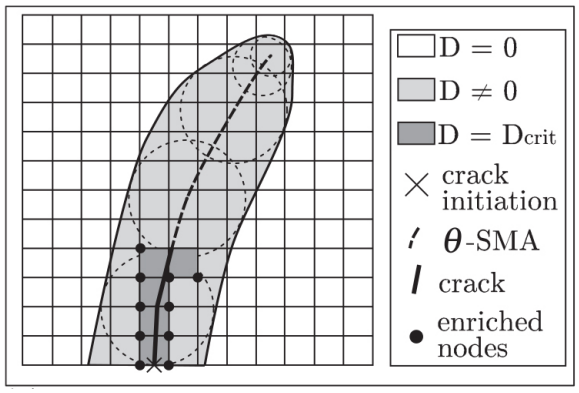

Fig. 23. Geometrical tracking algorithm proposed by Tamayo-Mas and Rodríquez-Ferran [204] for the calculation of the crack-path as the simplified medial axis (θ-SMA) of bi-tangent interior circles to a regularised damage field. (Image from Tamayo-Mas and Rodríquez-Ferran [204]).

[150] or has already occurred [149, 200]. This enhancement provides a better approximation of field α^h in potential locations of strain localization. Then, at an a-priori defined stage of the localisation process, a strong discontinuity is inserted at the aforementioned elements that are already enhanced in a weak manner and are crossed by the zero level set of the crack-path-field Γ. The algorithm has been used in two-dimensional simulations of quasi-static [149, 203, 200] and dynamic crack propagation [150].

Feld-Payet et al. [55] recently proposed a tracking algorithm to similar the crack-path-field. The so-called *marching ridges* tracking algorithm is based on the identification of the crack-path as the zero level set of a scalar product involving the gradient of a regularised degradation-related field and an orthoradial vector $\underline{e}_\theta$ defined on a polar grid centred on the crack-tip or crack origin (see Fig. 22). The algorithm has been used for both 2D and 3D problems.

In the continuous-discontinuous approach of Tamayo-Mas and Rodríguez-Ferran [205, 206] the transition between regularised and discrete damage is through the use of a geometrical tracking algorithm. The crack-path is constructed as the simplified medial axis (denoted as θ-SMA in Fig. 23) of an area where regularised damage overpasses a defined damage threshold. The θ-SMA is the loci of centres of bi-tangent interior circles to the aforementioned damaged area (see Fig. 23). In 3D, a damaged volume is considered instead of an area and the crack is defined in a similar way by its medial surface. The algorithm has been used as a transition between a gradient-enhanced damage model and traction-free cracks in [204] or cohesive cracks in [206].

3.5 Crack propagation direction in tracking algorithms

The crack propagation criterion is a vital part of a tracking algorithm. This criterion is usually based on the theory of Fracture Mechanics, empirical or physical considerations. In the following, a summary of the most used propagation criteria within tracking algorithms is given. Comparative studies between different propagation criteria used in tracking algorithms have been presented by Bouchard et al. [207], Dumstorff and Meschke [90] and Unger et al. [208].

3.5.1 Linear Elastic Fracture Mechanics criteria

Linear Elastic Fracture Mechanics (LEFM) provides three criteria with significant use in tracking algorithms: (i) the maximum circumferential (or maximum hoop/tangential) stress, (ii) the minimum strain energy density, and (iii) the maximum energy release criteria.

The *maximum circumferential stress* criterion, proposed by Erdogan and Sih [209], states that a crack propagates from its tip at a polar angle θ_c in which the circumferential stress $\sigma_{\theta\theta}$ reaches its maximum. As the circumferential stress in the crack propagation direction is a principal stress, the angle θ_c can be determined analytically by equating the shear circumferential stress $\sigma_{r\theta}$ to zero

$$\sigma_{r\theta} = \frac{1}{2\,\pi\,r}\,\cos(\theta/2) \left(\frac{1}{2}\,K_I\,\sin\theta + \frac{1}{2}\,K_{II}(3\cos\theta - 1)\right) = 0 \quad (8)$$

where θ and r are the local polar coordinates at the crack-tip and K_I, K_{II} are the stress intensity factors under mode I and mode II loading, respectively. The solution of the above equation gives

$$\theta_c = 2\,\arctan\left[\frac{1}{4}\left(K_I/K_{II} \pm \sqrt{(K_I/K_{II})^2 + 8}\right)\right]. \quad (9)$$

The crack propagation angle θ_c is the one corresponding to the maximum $\sigma_{\theta\theta}$ between the two possible ones given by Eq. (9). The extension of the maximum circumferential stress criterion to 3D has been presented by Shöllmann et al. [210].

Instead of considering stresses, the coeval *minimum strain energy density* criterion [211, 212, 213] looks at the strain energy density distribution around the crack-tip for the definition of the crack propagation direction. Here, crack propagation takes place when the strain-energy density factor S reaches a critical value S_c (assumed to be a material property) at a neighbourhood of the crack-tip and in a direction defined by the angle θ_c corresponding to the local minimum of S

$$\left.\frac{\partial S}{\partial \theta}\right|_{\theta=\theta_c} = 0 \quad (10a)$$

$$\left.\frac{\partial^2 S}{\partial \theta^2}\right|_{\theta=\theta_c} \geq 0. \quad (10b)$$

The strain energy density is defined as [211, 212, 213]

$$S = \alpha_{11}\,K_I^2 + 2\,\alpha_{12}\,K_I\,K_{II} + \alpha_{22}\,K_{II}^2 + \alpha_{33}\,K_{III}^2 \quad (11)$$

where

$$\alpha_{11} = \frac{1}{16\,G}\,[(\kappa - \cos\theta)(1 + \cos\theta)] \quad (12)$$

$$\alpha_{12} = \frac{1}{16\,G}\,\sin\theta\,[2\cos\theta - (\kappa - 1)] \quad (13)$$

$$\alpha_{22} = \frac{1}{16\,G}\,[(\kappa + 1)(1 - \cos\theta) + (1 + \cos\theta)(3\cos\theta - 1)] \quad (14)$$

$$\alpha_{33} = \frac{1}{4\,G} \quad (15)$$

with ν being the Poisson ratio and G the shear modulus. Finally, κ is defined as

$$\kappa = \begin{cases} 3 - 4\,\nu & \text{for plane strain} \\ (3 - \nu)/(1 + \nu) & \text{for plane stress.} \end{cases} \quad (16)$$

As can be seen from Eqs. (9) and (11), the use of the maximum stress and the minimum strain energy density criteria necessitates the computation of the stress intensity factors. In the first applications of these local propagation criteria [151, 214, 47], the stress intensity factors were computed with the use of special singular finite elements around the crack-tip (e.g. [215, 216, 217]). An alternative to these elements was the use of isoparametric quadratic elements with simple modifications on the position of the internal nodes [218, 219], such that the singular stress fields near a crack-tip could be reproduced [220]. Considering recent applications, the maximum circumferential stress criterion is very popular within the X-FEM. In this context, the stress intensity factors are calculated using domain forms of the interaction integrals over a selected area circumscribed by a radius r_d, which is normally defined as a factor of the finite element characteristic length (see Fig. 24). Applications of the maximum circumferential stress criterion in the context of the partition of unity methods can be found in [70, 71, 221, 222, 223, 185, 224] among others.

The *maximum release energy* criterion stems from the original Griffith's energy release theory concept [225, 226] and was later reconsidered in [209, 227, 228]. Contrary to the above criteria, which depend on a local

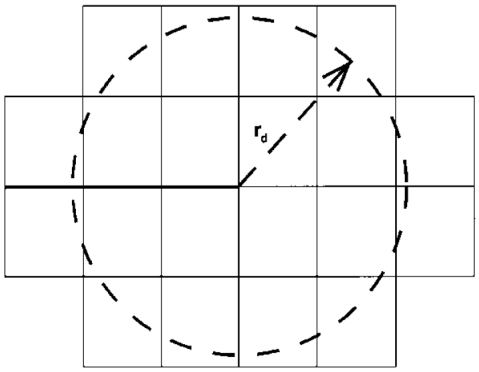

Fig. 24. Selected elements surrounding the crack-tip for the calculation of the interaction integral in the computation of the crack propagation direction within X-FEM. (Image from Moës et al. [71]).

near-tip variable (i.e. the stress or strain energy density), the maximum release energy criterion depends on a global energy state. In particular, a crack propagates from the crack-tip along a direction defined by the polar angle θ_c, which maximizes the global released energy of the structure G_e. This can be stated by the following conditions

$$\frac{\partial G_e}{\partial \theta}\Big|_{\theta=\theta_c} = 0 \tag{17a}$$

$$\frac{\partial^2 G_e}{\partial \theta^2}\Big|_{\theta=\theta_c} \leq 0. \tag{17b}$$

Propagation is initiated when the released energy G_e reaches a critical value G_c, which is a material property.

Early applications of the maximum energy release criterion in the context of the finite element method can be found in [151, 229]. Much later, Meschke and Dumstorff [230, 90] used the maximum energy release criterion in the context of X-FEM. In their formulation, the crack propagation direction as well as its extension length are introduced as global unknowns to the problem, which is then solved enforcing a minimization of the total energy of the body. Similar criteria have been used afterwards by Unger et al. [208] and Zhang et al. [66]. In the latter approaches, an iterative procedure is used and the global energy of the structure is computed for different angles and crack extensions. The angle minimizing the global energy is finally selected for the new increment. This iterative procedure increases importantly the computational cost of these methods [208].

In their first applications in the context of FEM the above LEFM criteria were commonly implemented in the same code and used for comparative studies using remeshing and nodal separation methods (see for instance [151, 48]). The same procedure was followed later by Bouchard et al. [207]. A common outcome of these studies was the similar performance of the maximum circumferential stress and the maximum release energy criteria, while the use of the minimum strain energy density criterion yielded less accurate results regarding the expected crack propagation [151, 207].

3.5.2 Maximum Principal Stress criterion

When resisting forces are assumed to apply at the crack surfaces, either through a cohesive-traction separation law or from a stress-strain continuum model, the singularity at the crack-tip considered in linear elastic fracture mechanics disappears [222]. In such cases, the use of the presented propagation criteria of LEFM need some further modifications. One very common modification concerns the maximum circumferential stress criterion, which turns into the *maximum principal stress* criterion.

The maximum principal stress criterion states that a crack will propagate in a direction orthogonal to the maximum principal stresses. Due to its straightforward implementation, as well as the good accuracy for straight and slightly curved cracks, this criterion has been one of the most used for crack propagation in both discrete [51, 39, 231, 232, 233, 234] and smeared crack approaches [158, 32, 161, 112, 115, 113].

A common practice used for the improvement of the reliability of the stresses in the vicinity of the crack is to use an average stress tensor, which is computed using smoothing/averaging techniques around the crack-tip (e.g. [235, 231, 236, 198, 97, 67]) or nonlocal stress/strain tensors [93] (see Fig. 25).

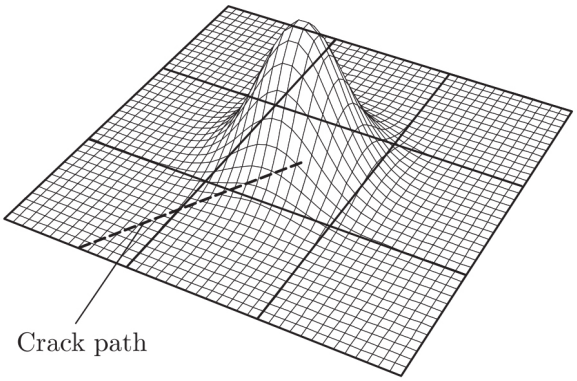

Fig. 25. Computation of the crack propagation considering an averaged value of stresses of the crack-tip and neighbouring elements through Gaussian weight function in Dumstorff and Meschke [90].

3.5.3 Discontinuous material bifurcation analysis

Discontinuous material bifurcation analysis is frequently used for the computation of the propagation direction. The method dates back to the work of Hill [237] who associated the strong ellipticity character of the acoustic (or localization) tensor $\boldsymbol{Q}$ to the existence of discontinuous acceleration waves. In subsequent works the loss of the elliptic (or hyperbolic in dynamics) character of the governing equations was linked likewise to the strain localization in an elastic-plastic [238, 239, 240] or a softening solid [60, 241, 242].

The criterion for loss of the material stability and therefore onset of strain localization can be defined as

$$\det\left[\boldsymbol{Q}(\mathbf{n})\right] \leq 0 \tag{18}$$

where the acoustic/localization tensor $\boldsymbol{Q}$ is a function of the constitutive tangent matrix $\boldsymbol{C}$ and the normal vector to the material discontinuity $\mathbf{n}$

$$\boldsymbol{Q} = \mathbf{n} \cdot \boldsymbol{C} \cdot \mathbf{n}. \tag{19}$$

The above equations define that the material loses its stability (or, in other words, the material bifurcates) when the determinant of the acoustic tensors ceases to be positive in a direction defined by a vector $\mathbf{n}$. Inversely, the crack propagation direction can be computed by finding the normal vector $\mathbf{n}$ which gives the minimum determinant of $\boldsymbol{Q}$ and checking whether the inequality of Eq. (18) is satisfied.

For simple cases, analytical derivations are possible for the discontinuous material bifurcation analysis [237, 243, 244, 245, 169], while more general cases necessitate the numerical solution of the problem with proper algorithms [106, 246, 247]. Recent contributions on analytical strain localization analyses have been presented by Wu and Cervera [248, 19] for constitutive models based on associative plasticity and damage formulations.

The solution of the local analytical problem normally gives two possible directions for material bifurcation [249, 247, 35, 250]. In these cases, the selection of the propagation direction necessitates the use of an additional criterion. Rabczuk and Belytschko chose the propagation plane as the one with the normal closest to the direction of the principal tensile stress [251] or the direction corresponding to the maximum displacement gradient in the localization direction [252]. Similar criteria considering the gradient of the instantaneous (or the rate of the) displacement field have been considered by Oliver et al. [33] and Weed et al. [253]. In [114] an energetic approach is used to selecting among the two potential crack planes given by the Mohr Coulomb theory of fracture. According to this, the selected crack plane is the one that maximizes the energy release. This direction is selected as the one along which the accumulated strain energy density before crack propagation is higher.

3.5.4 Crack branching

Crack branching refers to the splitting of a crack at its crack-tip into two or more cracks (branches) during its propagation within a solid. The phenomenon commonly occurs under dynamic loading, although crack branching has been observed also under quasi-static loading.

The simulation of crack branching with tracking algorithms is not a trivial task, as it necessitates two additional criteria that specify the moment of the crack-branching and the direction of the new branches. Today, a robust predictive theory that can give answers to the above conditions is missing. As a consequence, the criteria used in tracking algorithms for the definition of crack branching are heuristic or empirical based on experimental evidence.

Belytschko et al. [148] allow a crack to branch when the propagation directions at elements ahead of the crack-tip, obtained with a discontinuous material bifurcation analysis, are no longer constant but present a significant variation among them. The same criterion was used by Song et al. [75], with the difference that in this case the crack propagation directions are computed with a maximum principal stress criterion. A similar criterion was used later by Song and Belytschko [98] in the context of the cracking nodes method, allowing new cracks to initiate next to existing ones when their propagation direction makes an angle with the existing crack direction greater than a defined threshold.

In Linder and Armero [154] (see also [254]) the crack branching is associated with the Rayleigh wave speed. In particular, a crack is allowed to branch as soon as the propagation velocity at the crack tip reaches a critical value, expressed as a fraction of the Rayleigh wave speed. The approach is implemented in quadrilateral elements and as soon as the branching criterion is satisfied the two elements that fall out of the crack propagation direction at the crack-tip are selected as the new crack-tips (see Fig. 26). From them, the crack propagates following the direction of the maximum principal stress.

Fig. 26 demonstrates another implication that needs to be considered in the modelling of crack branching with strong discontinuity methods. This is the special construction of the branching elements, which is necessary to ensure compatibility of the kinematics of discontinuities in the neighbouring elements at the crack branches. Implementations of these elements in the con-

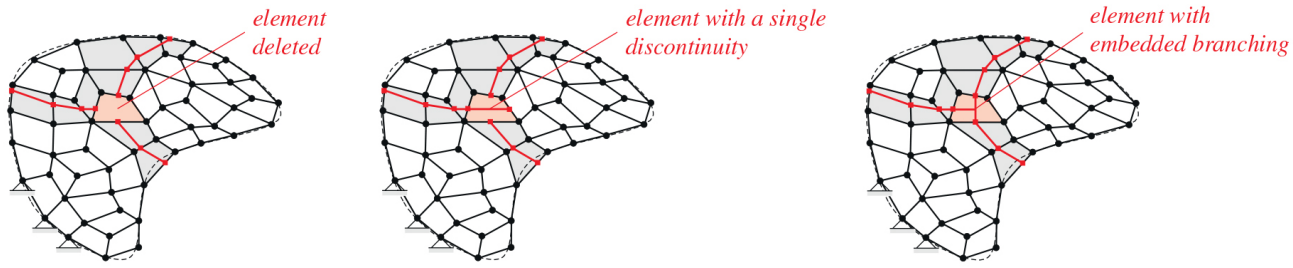

Fig. 26. Branching of a crack in Linder and Armero [154] and different strategies for the branching element: element deletion (left), element with a single discontinuity (middle) and element with embedded branching (right). (Image from Linder and Armero [154]).

text of the partition of unity methods can be found in [255, 256], and for embedded strong discontinuities in [154, 150].

4 Local tracking algorithm - Monotonic loading

This section focuses on the different aspects involved in the development of tracking algorithms for the simulation of propagating cracks under monotonic loading. To this aim, a local tracking algorithm [32, 114, 115, 257, 116] is outlined, focusing on the methodology used for the crack initiation and propagation, as well as crack-path continuity, in a smeared damage framework. The presented tracking algorithm is implemented within the finite element program COMET [258] developed at the International Centre for Numerical Methods in Engineering (CIMNE), in Barcelona, and is used for all the numerical analysis of Sections 5,7,8. Pre- and post-processing is carried-out with GiD [259] also developed in CIMNE.

As discussed in Section 3, the purpose of a tracking algorithm is to limit the strain localization to crack-paths composed of a series of consecutive finite elements. This is performed through the execution of a sequence of tasks at each solution step including the identification of new cracks and the definition of their propagation, in addition to the propagation of existing ones that have consolidated in previous steps.

As soon as the crack paths are defined, a labelling system is used to categorize the elements falling within or outside of them. In this work, the elements within a crack respond according to the constitutive law presented in [260] and summarized in Appendix A. The rest of the elements maintain a linear elastic stress-strain relationship.

The presented tracking algorithm is devised for triangular constant strain finite elements. Despite their known limitations, these elements ensure a straightforward implementation in any finite element code and allow for the easier meshing of irregular geometries. The extension of this approach to other element typologies is possible as in [112, 113].

4.1 Crack nucleation - Fixed-directional tracking

4.1.1 Crack-roots

The first task of a tracking algorithm is to define where and when new cracks appear, which is done through the use of a crack nucleation criterion. This criterion commonly coincides with the satisfaction of a failure condition under tensile or shear stress states. An exception to this strategy are tracking algorithms based on an underlying damage-related field, as those presented in Section 3.4.

In the following, the nucleation of a new crack at a new numerical step $n+1$ is associated with the satisfaction of the tensile failure criterion of a continuum damage model (see Appendix A). This criterion has the form

$$\Phi^{+}_{n+1} = \tau^{+}_{n+1} - r^{+}_{n+1} = 0 \tag{20}$$

where τ^{+} is a norm termed as the equivalent stress and r^{+} is the stress threshold. The simulation of arbitrary cracking from any location of the analysed structure, without their a-priori definition by the analyst, implies that the crack nucleation criterion should be checked all over the simulated domain. Therefore, this condition is checked for all the existing undamaged elements of the mesh, and the ones fulfilling it are temporarily labelled as *potential crack-root* elements.

The control of the damage dispersion over a small part of the discretized domain, and thus the simulation of separate and individual cracks, is possible with the use of an *exclusion radius criterion*. This criterion, introduced in [157, 158], states that a new crack can originate at an element which is located in an area in

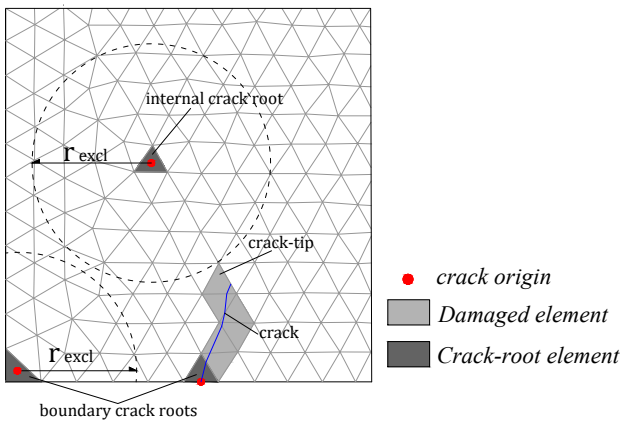

Fig. 27. Illustration of some basic elements of the presented local tracking algorithm. Crack-roots are the origin elements of the cracks, crack-tips are the last elements at the propagating front and crack-origins refer to the location within an element where a crack begins.

which no other cracks exist. This area is circumscribed by the *exclusion radius* r_{excl}, which is defined by the user (see Fig. 27). The definition of an exclusion radius averts the initiation of secondary spurious cracking surrounding existing cracks, a pathology that may spoil the correct damage localization in later steps of the simulation [168, 98]. Similar criteria have been used by Oliver et al. [168] and Song & Belytschko [98], where the equivalent exclusion area (named as shielding zone in [168]) is defined as a multiple of the finite element size. Note that the exclusion radius here controls only the nucleation of new cracks at a certain distance to existing ones and does not preclude the propagation of cracks close to others as in [168]. A similar use of the exclusion radius to the one presented in this work is possible in the tracking algorithm proposed by Slobbe et al. [112], whereas in Alfaiate et al. [153] the exclusion radius prevents the initiation of new cracks only around the crack-tip.

Apart from its aforementioned numerical purpose, the exclusion radius has a second functionality when a composite material, such as masonry, is simulated. More specifically, r_{excl} can be defined according to the average distance between the weak zones of the composite, heterogeneous material. For many masonry typologies, the weak zones are the interfaces between the mortar and the units due to the contact of two different materials, or the mortar joints themselves, and consequently the distance between cracks is determined by the size of the brick or stone units [261, 262]. In such cases, the staggering of the masonry can be considered using an exclusion radius equivalent to the unit's size.

With the above definitions, a potential crack-root element without any existing crack within the area circumscribed by the exclusion radius is defined as a *crack-root element*. Crack-root elements with one or more sides on the boundary of the mesh are referred to as *boundary crack-root* elements, while those with no sides on the boundary of the mesh are *internal crack-root* elements. If more than one finite elements are defined as potential crack-roots at the same increment, and the distance between them is less than the exclusion radius, the one with the highest value of the tensile equivalent stress τ^+ (see Eq. (A.6) in Appendix A) is selected as a crack-root. A similar approach for selecting the crack-root among many elements satisfying the crack initiation criterion in the same analysis step has been recently used by Wu et al. [156]. Figure 27 presents an example of boundary and internal crack-roots.

4.2 Crack-origin coordinates

Following the identification of the new crack-roots, the coordinates of the *crack-origin* points are defined and stored. For cracks initiating at corner or at internal elements, the centroid of the triangular element is selected as the crack-origin. In case of cracks initiating at an element with one side over the boundary, the midpoint of this side is selected as the crack-origin. Figure 27 presents examples for crack-origins at corner, boundary and internal elements.

4.3 Crack propagation

The propagation of new and existing cracks at each step of the numerical analysis starts from the *crack-root* and *crack-tip* elements, respectively. A crack-tip is the last damaged element at the propagating front of a crack that has already formed in a previous step of the analysis (see Fig. 27). The possibility of simulating crack propagation along one or two directions depending on the position of the crack-root element is considered. Cracks originating from elements at the boundary (i.e. boundary crack-roots) can propagate along one direction, while those originating from an internal element (i.e. internal crack-roots) can propagate along two opposite directions. The procedure for each case is presented in the following.

4.3.1 Propagation along one direction

The crack propagation from boundary crack-root and crack-tip elements is illustrated in Fig. 28. For each

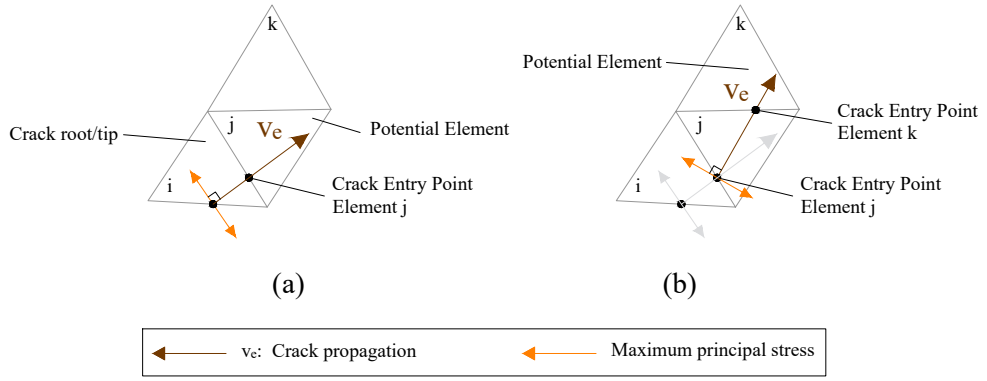

Fig. 28. Procedure for crack propagation from a *crack-tip* or from a *boundary crack-root* (picture adapted from [159]).

boundary crack-root element, a vector is defined, starting from the crack-origin location, with a direction orthogonal to the one given by the maximum principal effective stress. This direction is calculated using a stress tensor constructed from the average values of the effective stresses at the nodes of each element. The use of smoothed values of stresses is a common practice in local tracking algorithms aiming to increase the reliability of the stress directions at the crack-tip (see for instance [231, 236, 232, 97, 67]). The intersection of this vector with the neighbouring element defines the exit point and the next *potential element* of the crack (Fig. 28a). Similarly, starting from this point the following potential elements of the crack are recognised (Fig. 28b). The same procedure is followed for identifying the propagation path of consolidated cracks from the crack-tip elements. In this case the crack-origin point is the exit point of the crack at the previous cracked element.

4.3.2 Propagation along two directions

Contrary to cracking starting from the boundary, other cracks, such as shear ones, initiate from the interior and propagate along two opposite directions. The numerical procedure for modelling internal crack propagation is presented in Fig. 29 and is detailed in the following.

Starting from the crack-origin of the internal crack-root element, two vectors $(v_{e,1})$ and $(v_{e,2})$ are defined, having a direction orthogonal to that of the maximum principal effective stress but opposing orientations (Fig. 29a). Following this, the crack path is recognized in two stages. First, the elements pertaining to the path defined by the orientation of vector $(v_{e,1})$ are identified starting from the crack-origin point and following the same process as described above for the boundary crack-root and crack-tip elements (Fig. 29b). Upon concluding the labelling towards that side of the crack, the elements lying at the opposite face can be recognised starting again from the crack-origin point of the internal crack-root, but using the orientation of vector $(v_{e,2})$ (Fig. 29c).

4.4 End of the labelling procedure

The labelling procedure for a crack stops at a numerical step when at least one of the following criteria are satisfied:

(i) *Boundary criterion*: a crack reaches the mesh boundary and at least one of the elements in the wake of the crack with a distance from the crack-tip smaller than the exclusion radius does not have sides or nodes on the boundary of the mesh.

(ii) *Stress-threshold criterion*: the stress-state of a *potential element* is lower than a pre-defined threshold. This threshold can be conveniently defined in terms of the tensile equivalent stress and previous works [157, 159, 32, 160] have demonstrated that labelling can be completed when the inequality $\tau^+ < 0.75 f^+$ holds, where f^+ is the tensile strength. This is a common strategy in tracking algorithms that limits the computational cost, since it allows the termination of the labelling procedure during a numerical step before the crack meets the boundary.

A common local mechanism of unreinforced masonry structures is the rocking of piers due to the formation of flexural cracks at their supports. A similar case is illustrated in Fig. 30a, where cracks originate from the corners and propagate towards the interior of a masonry wall analysed under horizontal loading at its top. A close-up of the principal stress directions at the region of the crack-tip during the loading, shown in Fig. 31, reveals that these are not parallel to the boundary. This is due to the adopted boundary conditions at the top and bottom of the wall. Under these conditions,

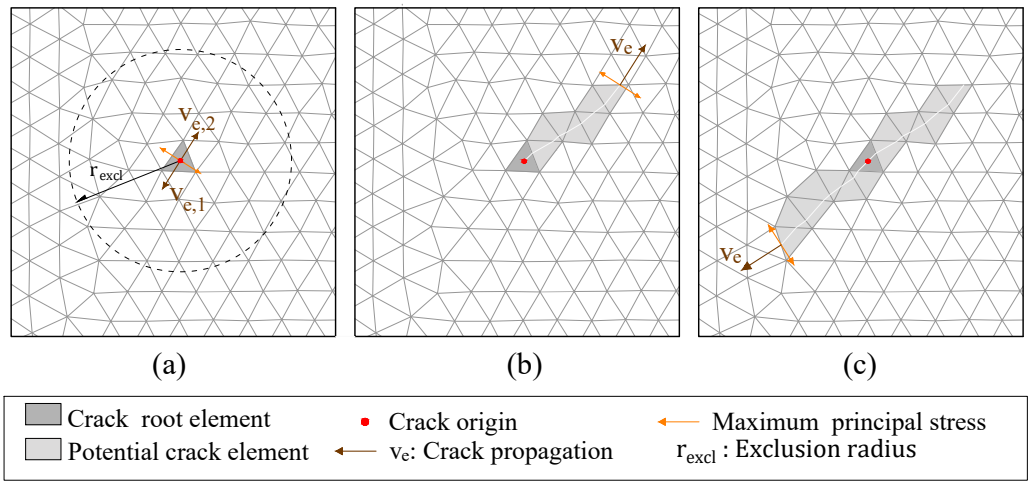

Fig. 29. Simulation of internal cracking with the tracking algorithm: (a) *internal crack-root* element with the two opposite vectors ($v_{e,1}$ and $v_{e,2}$) of the crack propagation, (b) labelling of the *potential crack* elements towards the first side of the crack, (c) labelling of the *potential crack* elements towards the second side of the crack.

it is possible that the crack originating from the corner of the wall (element A in Fig. 31) exits the mesh at its lower boundary (element B in Fig. 31). The presented definition of *boundary criterion*, addresses this unrealistic end of the crack propagation. In this way, if a crack reaches the boundary but condition (i) is not fulfilled, the crack direction is corrected and defined as parallel to the boundary of the mesh where the crack exits. The labelling process in this case ends when this crack reaches again another boundary of the mesh, as for instance the vertical end of the wall for the case of Fig. 30. As will be shown through the structural applications included in this paper, the above definition succeeds in identifying correctly complete or incomplete cracks that propagate across the boundary of the analysed structure. Instead, the improper definition of the *boundary criterion* would lead to the result of Fig. 30b, where the two cracks stop as soon as the crack fronts reach the boundary of the mesh, resulting in an improper identification of the collapse mechanism and the load capacity.

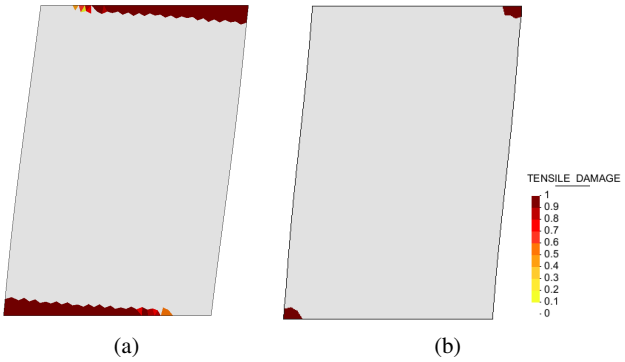

Fig. 30. Flexural crack propagation on top and bottom of a shear wall for a top displacement of $\delta = 2\,mm$: (a) with and (b) without proper definition of the *boundary criterion*.

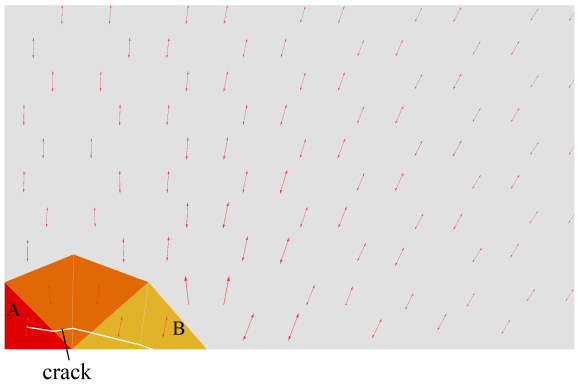

Fig. 31. Flexural crack at the bottom of a shear wall exiting the mesh.

4.5 Element labelling and crack-path continuity

4.5.1 Element labelling

As soon as the propagation of all the cracks has been defined, each element of the mesh is labelled with a flag representing its *element-state* for the current step of the analysis. The following three element-states are defined:

– *Intact element, outside a crack*: element outside of a crack-path. Its stress-strain relationship will remain linear elastic for the current analysis step.

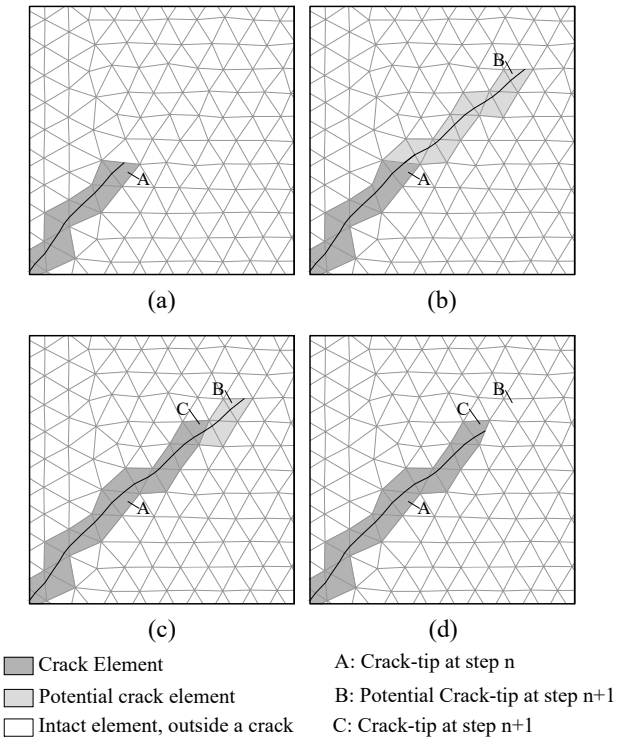

Fig. 32. Assigned flags to the elements of the mesh for a propagating crack: (a) consolidated crack prior to crack propagation at the end of step n, (b) potential crack path at step $n+1$, (c) consolidated crack after convergence of step $n+1$, (d) labelling element-state at the end of step $n+1$.

- *Potential crack element*: undamaged element falling within a crack-path. If it satisfies the damage criterion, its stress-strain relationship will be defined according to the selected constitutive model (see Appendix A).
- *Crack element*: element that is a part of a consolidated crack and has experienced damage at a previous analysis step. Its stress-strain relationship is characterized by the selected constitutive model.

The above categorization of elements can be visualised in Fig. 32, which illustrates the propagation of a crack and the labelling procedure during a step of the numerical analysis. Figure 32a presents the consolidated part of the crack, which has propagated up to element A in the previous analysis step n. In the new step $n+1$, the tracking algorithm identifies that the crack can potentially propagate up to element B (see Fig. 32b), which is the last one satisfying the *stress threshold criterion* presented in Section 4.4. A flag is assigned to all the elements between A and B categorizing them as *potential crack elements*. This flag activates the selected non-linear constitutive law for these *potential crack elements*, while the rest will maintain a linear elastic stress-strain relationship. Fig. 32c shows the updated labelling of the elements in the crack at the end of the iterations of step $n+1$, when convergence is attained. All the elements up to element C have damaged, while the rest potential elements did not satisfy the failure criterion and therefore remained linear elastic. Before proceeding to the new analysis step, the tracking algorithm is called to update the element-state for a last time. The element-state of all potential elements that remained intact is initialized to *Intact element, outside a crack* as shown in Fig. 32d. This ensures that during the next analysis step, the crack will propagate starting from element C, with a crack propagation direction according to the new converged stress state.

4.5.2 Crack path continuity

Let us now consider the same case of the single propagating crack, but assuming that two elements D and E, prior to element C, have not damaged after convergence of the analysis at step $n+1$ even if they had been identified as *potential crack elements* at the beginning of the step (see Fig. 33a). If no further consideration is made, the element-state of elements D and E would be set to *intact element, outside a crack* at the end of the step, and the crack loses its continuity breaking in more than one parts. This is avoided with the implementation of a *crack path continuity* procedure. According to this, the damage state of all the elements of the crack is inspected after convergence starting from the potential crack-tip elements and going backwards towards the crack-tip at the beginning of the step. For the current example, this means starting from element B and going backwards up to element A. As soon as, a damaged element is found, in this case element C, the rest of the status of all the preceding elements is changed to *Crack element* (Fig. 33b). The procedure continues up to the crack-tip element at the beginning of the current step, which is element A in Fig. 33.

The above procedure implies that the algorithm stores for each crack the crack-tip of the consolidated crack (e.g. element A in Fig. 33) and the potential crack-tip at the end of the labelling procedure (e.g. element B in Fig. 33). Additionally, each element is associated with the crack(s) it belongs to. In this way, the crack-path of each crack can be recovered at any moment, starting from the (potential) crack-tip and going backwards considering elements belonging to the same crack.

4.6 Maximum curvature criterion

The definition of the crack nucleation and propagation, considering the stress/strain values at a restricted area

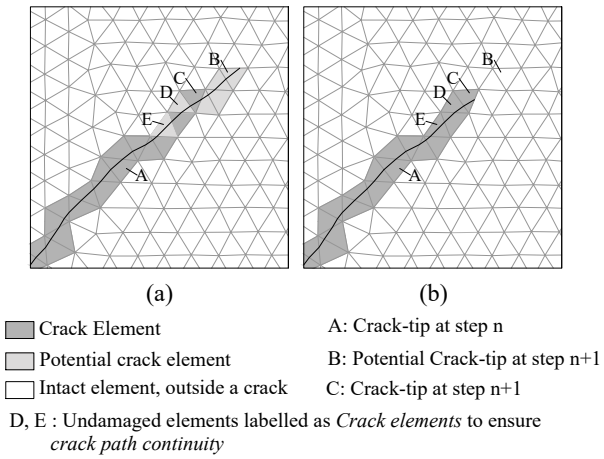

Fig. 33. Assigned flags to the elements of the mesh for a propagating crack (a) before and (b) after the application of the *crack path continuity* procedure.

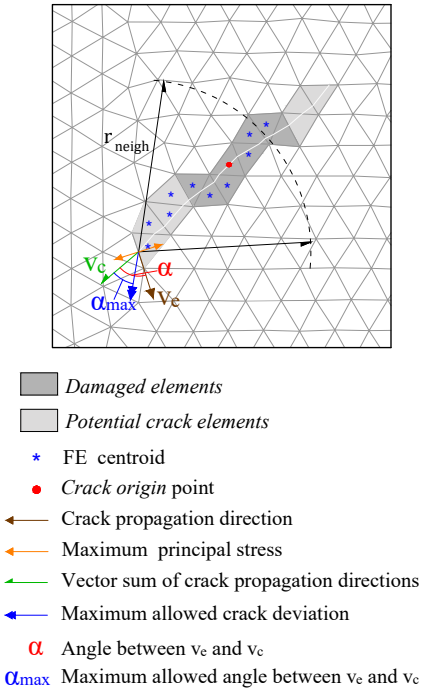

Fig. 34. Illustration of the *maximum curvature criterion* used for the correction of the crack propagation direction during the propagation of an internal crack.

around each element, justifies the "local" nature of the presented tracking algorithm. This choice is very convenient for handling cases with multiple cracks and in terms of computational efficiency compared to global tracking algorithms [32]. Nevertheless, local tracking algorithms can encounter some difficulties under bending stress states, when the local calculation of the principal stress directions at the crack-tip may be relatively poor due to high stress-gradients, resulting in spurious changes in the crack direction.

To avoid such non-realistic result, Clemente et al. [157, 158, 32] proposed the enhancement of the tracking algorithm with a procedure for the apropos correction of the crack propagation. This procedure, termed as *maximum curvature criterion*, is activated at each element at the propagating front of the crack (i.e. the crack-tip elements) before the selection of the *next potential element*. The idea is to compare the crack propagation direction defined at the crack-tip element (v_e), with the vector sum of the crack directions (v_c) of both the potential and the damaged elements within a neighbourhood of radius r_{neigh} (see Fig. 34). If the relative angle among them is greater than a threshold angle α_{max}, the vector v_c is used for the definition of the crack direction instead of the vector v_e. This is formalised as

$$|v_c \cdot v_e| \begin{cases} \geq \cos(\alpha_{max}) \text{ crack propagates using } v_e \\ < \cos(\alpha_{max}) \text{ crack propagates using } v_c \end{cases} \quad (21)$$

The parameters involved in the use of the maximum curvature criterion are the r_{neigh} radius and the α_{max} angle. As presented in [159, 32], the proper choice of the radius r_{neigh}, and thus the selection of the number of elements considered in the definition of the vectorial sum v_c, is important in cases with curved cracks. Contrariwise, the effect of r_{neigh} is limited for cracks which are straight or exhibit small curvature.

The use of similar criteria for preventing sudden turns in propagating cracks is common in tracking algorithms. For instance, Jäger et al. [165] use the same criterion in a 3D local tracking algorithm and allow a deviation angle of a new crack segment between $\pi/6$ and $\pi/4$. In Zhang et al. [66] the new crack direction in the crack-tip is defined using the consolidated crack direction at the previous element and the mean value of the crack directions of the following two new crack elements. This smoothing strategy alleviates sudden turns in the crack direction (see [263, 66]).

An alternative to the explicit control of the crack diverging angle has been presented by Slobbe et al. [112, 162] also in the context of local tracking algorithms. The main concept is to postpone the crack path fixation up to the moment that a certain level of damage is reached at an element crossed by a potential crack (denoted as the *damage path*). The idea resembles closely the strategy used by Jirásek and Zimmerman [93] and Sancho et al. [65, 91] for the adaptation of embedded strong discontinuities until a certain crack width is reached, which is usually defined according to the material parameters. Similar assumptions are common also in continuous-discontinuous models, in which

a strong discontinuity is inserted, at a later stage of damage localization, to represent the displacement discontinuity of the crack (e.g. [206, 55]). Despite the potentiality of this method demonstrated in the context of an embedded crack model [65, 91, 264, 234], Slobbe et al. [112, 162] show that delayed crack path fixation may provide ambiguous results concerning the appearance of spurious crack tortuosity, while the criteria for the proper definition of the parameter controlling the moment of crack path fixation (damage/crack-width limit) are still under research. In Slobbe et al. [112, 162], the preclusion of the crack overturning is also achieved by adopting a C^1 continuous crack representation, in which the crack-entry direction is considered in the definition of the new propagation direction at a new element of the crack.

5 Applications of the tracking algorithm under monotonic loading

This section includes two applications of the presented tracking algorithm to the simulation of cracking in concrete and masonry structures under monotonic loading. The first case considers the tensile splitting test on concrete cylinders. This is used as a benchmark test for the simulation of a dominant internal crack, starting from the interior of the discretized domain and propagating towards two directions. The second application considers a real-scale masonry frame under in-plane horizontal loading. This case assesses the capacity of the presented tracking algorithm to model multiple internal and boundary cracking.

5.1 Internal cracking - Tensile splitting test

The tensile splitting strength of geomaterials, such as concrete and rocks, is experimentally obtained with a standardized test method carried-out on cylinder specimens [265, 266]. The test consists in applying diametric compressive loading along the two sides of the tested specimen, as shown in Fig. 35. This loading results in the failure of the cylinder due to cracking, which starts from the interior and propagates vertically towards the locations of the applied load. The tensile splitting strength f_{sp} of the tested material is obtained through the following expression [265, 266]

$$f_{sp} = \frac{2\,F}{\pi\,D\,L} \tag{22}$$

where F is the maximum measured load, L is the length of the cylinder and D its diameter (see Fig. 35).

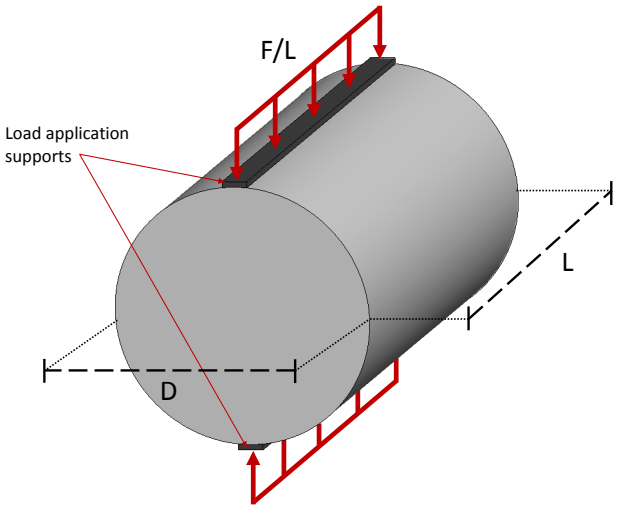

Fig. 35. Geometry and load configuration for the tensile splitting test.

The numerical simulation considers an experimental test carried-out by Malárics et al. [267, 268] on a cylindrical concrete specimen with diameter $D = 150\,mm$ and length $L = 300\,mm$. The compressive load was applied through two steel plates of $10\,mm$ width and length equal to the specimen's length.

Figure 36 presents the crack propagation for one of the tested high strength gravel concrete specimens, measured with the use of a series of conducting silver plates denoted with LS1-7. For a detailed description of the experimental set-up and results the reader is referred to Malárics et al. [268, 267].

The numerical model was prepared based on the material properties reported in [267] for the tested specimen HK-1 made of high strength gravel concrete. These are $E = 36.4\,GPa$, $v = 0.20$, $f^+ = 5.6\,MPa$, $f^- = 78.5\,MPa$, $G_f^+ = 151.7\,J/m^2$, $\rho = 2400\,kg/m^2$. The failure criterion is the one proposed by Lubliner et al. [15] and is obtained by setting $\kappa_1 = 1.0$ in Eq. (A.10). The value of the compressive fracture energy was not given in [267] and has been defined equal to $G_f^- = 250 G_f^+ = 37925\,J/m^2$ according to [269, 270]. It is noted that the sensitivity of the strength capacity of the specimen to the compressive fracture energy is minimal. The numerical parameters used in the tracking algorithm are $r_{excl} = 50\,mm$, $\alpha_{max} = \pi/4$ and $r_{neigh} = 50\,mm$.

The experiment has been simulated by applying a vertical displacement at the top of the specimen through a steel plate of $10\,mm$ width. The horizontal displacement at both top and bottom supports is restrained. At each step of the analysis, the corresponding non-linear equations are solved with the use of a secant (Picard's) method along with a line-search procedure.

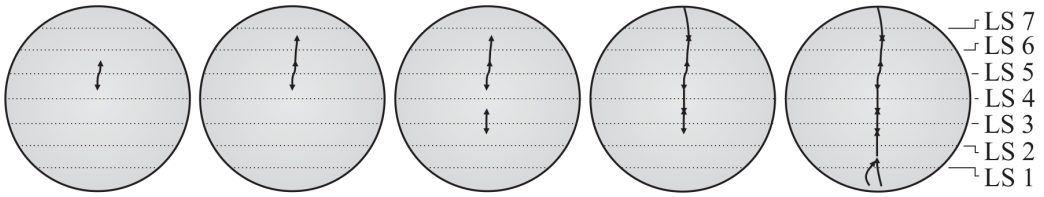

Fig. 36. Cracking sequence in the splitting tensile test of a high strength gravel concrete specimen tested by Malárics [268]. (Image from Malárics [268]).

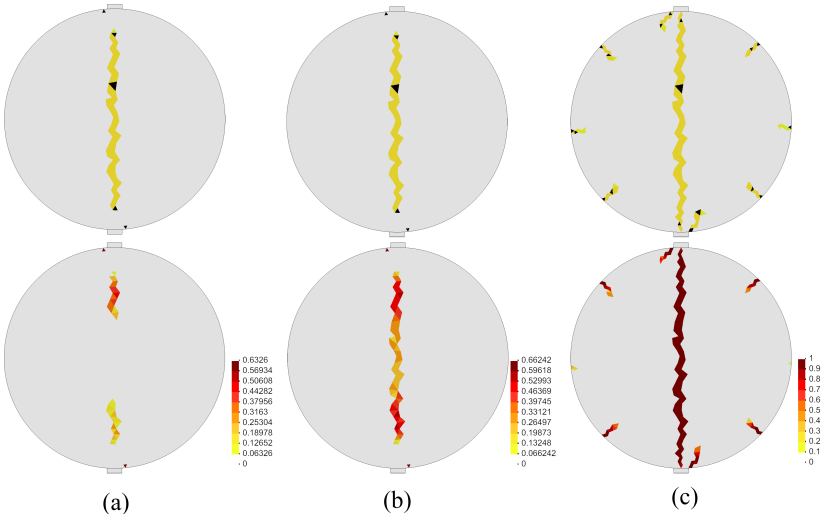

Fig. 37. First row: labelling of the tracking algorithm with elements in black representing crack origins or crack-tips. Second row: tensile damage contour. Vertical displacement at the top equal to: (a) $-0.115\,mm$, (b) $-0.120\,mm$, (c) $-0.130\,mm$.

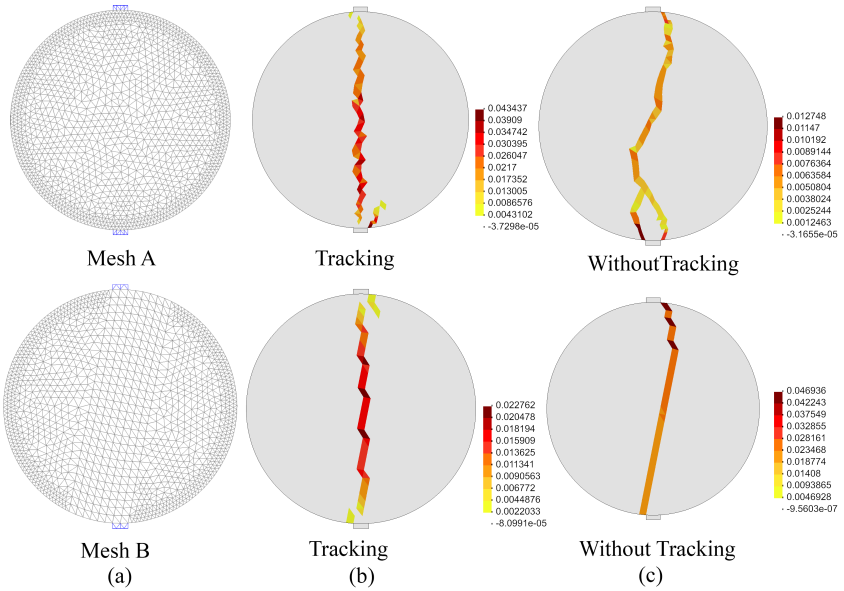

Fig. 38. (a) Finite element meshes and maximum principal strains (b) with and (c) without the tracking algorithm. First row: Mesh A. Second row: Mesh B.

Convergence of an increment is attained when the ratio between the iterative residual forces and the norm of the total external forces is lower than 10^{-3} (0.1%).

Fig. 37 shows the results of the analysis using an unstructured mesh of 2856 constant strain triangles (1525 nodes) under plane strain conditions. The first

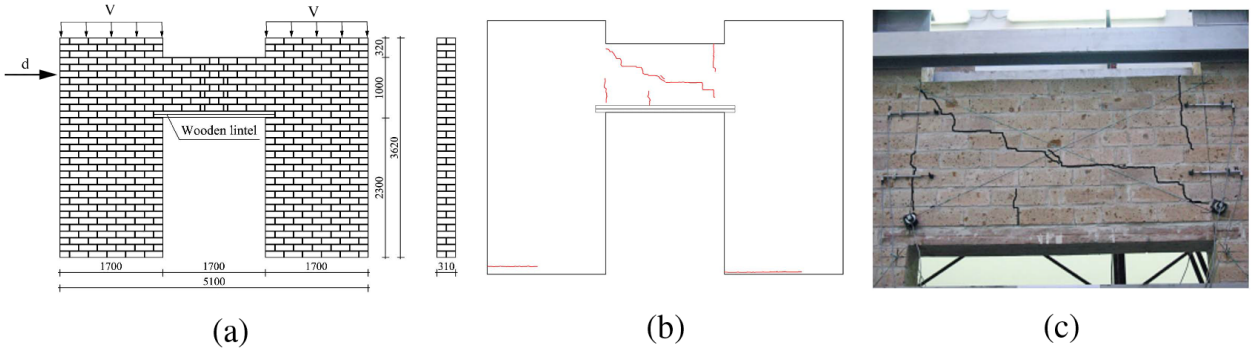

Fig. 39. (a) Geometry (values in mm) and load configuration of the experiment on a real scale unreinforced masonry frame. Cracking at the end of the experiment of (b) the whole frame and (c) the spandrel. (Picture adapted from Augenti et al. [271]).

row presents the labelling of the tracking system, while the second one the tensile damage contour. For a vertical displacement of 0.115 mm an internal crack, starting at around the 2/3 of the specimens height, propagated very fast towards the two load supports (Fig. 37a). Damage initially concentrated at the two tips of the crack, and for increasing displacement extended to its central part (Fig. 37b). The final capacity of the specimen was determined by the propagation of this crack up to the boundaries of the specimen. As soon as that happened, some additional cracking appeared around the locations of the load application and the external boundaries. The numerically predicted splitting strength of the specimen, measured with Eq. (22), was 5.18 MPa. This value is almost identical to the mean of the experimentally predicted from the various tested specimens of the same concrete typology, which was measured equal to 5.20 MPa with a coefficient of variation of 0.10.

The directional mesh-bias dependency of the numerical solution is investigated in Fig. 38, where the results obtained with two different meshes with and without the tracking algorithm are presented in terms of maximum principal strains. Mesh A is the unstructured mesh used for the results shown in Fig. 37. Mesh B is composed of 2530 constant strain triangles (1356 nodes), and its central part is discretized with a structured pattern that is slanted by 13° with respect to the vertical axis. The obtained results illustrate the way that tracking algorithms can improve the directional mesh-bias dependency of the classical smeared crack approach. As can be seen in the middle row of Fig. 37, the use of the tracking algorithm results in a vertical crack for both meshes, and no sensitivity on the used mesh is observed. On the contrary, when the tracking algorithm is not used a different strain localization is obtained, which depends strongly on the directionality of the mesh.

5.2 Multiple internal and boundary cracking - Masonry frame

An important challenge of tracking algorithms is the simulation of multiple arbitrary cracking. This is a common pathology of unreinforced masonry structures, with flexural cracks starting at the boundaries of openings, and shear internal cracks affecting wall and spandrel elements. The capacity of tracking algorithms to simulate such failure patterns was investigated by the authors in [115, 272] and is outlined in the following.

This structural application considers a real-scale masonry frame with a door opening, with its geometry presented in Fig. 39a. The structure was tested by Augenti et al. [271] under in-plane horizontal monotonic loading applied at the top left corner. A vertical load of 200 kN was maintained constant during the experiment at the top of the piers, simulating the gravitational effect of additional floors. Figures 39b-c illustrate the obtained damage pattern at the end of the experiment. The spandrel above the timber lintel was the most damaged element, with flexural vertical cracks at its two ends, and a shear crack crossing it diagonally through its whole length. Regarding the piers, two horizontal flexural cracks formed at their lower ends (Fig. 39b).

The structure was analysed under plane stress conditions using an unstructured mesh composed of 20728 constant-strain triangles (10678 nodes). Three different materials, presented in Table 1 were used for simulating the masonry, the timber lintel above the door and the interface between these two. Non-linear behaviour was assumed for the masonry and for the interface between masonry and the lintel, while elastic properties have been attributed to the timber lintel. The selection of the properties and their influence on the numerical result are discussed in [272, 260]. The numerical parameters for the tracking algorithm are $r_{excl} = 300\ mm$

(equal to the length of the bricks), $\alpha_{max} = \pi/4$ and $r_{neigh} = 200\ mm$.

The experimental test was simulated by applying a horizontal displacement d at the left top part of the structure for a constant vertical force of $V = 200\,kN$ at the top of the piers (see Fig. 39a). Similar to the splitting tensile test, a secant (Picard's) method has been used for solving the non-linear equilibrium equations at each numerical step of the analysis along with a line search procedure. Convergence of a numerical step is attained when the ratio between the iterative residual forces and the norm of the total external forces is lower than 10^{-2} (1%).

Figure 40 shows the evolution of the tensile damage at five stages of the analysis. The first damage affecting the structure are two vertical cracks at the corners of the spandrel (Fig. 40a). With increasing horizontal displacement two horizontal cracks form at the base of the piers (Fig. 40b), facilitating a rocking behaviour. Following this, internal cracking starts to appear within the spandrel (Fig. 40c-d). For a horizontal displacement around 21 mm, this crack rapidly extends through the whole length of the spandrel, inducing secondary flexural cracks at the top and bottom of the spandrel (Fig. 40e). The formation of this diagonal crack results in the sudden drop of the structural capacity, similarly to the experimental result, as can be appreciated in the numerical and experimental graphs presented in Fig. 41.

A comparison between the experimentally obtained damage (Figs. 39b-c) and the open cracks at the end of the analysis, presented in Fig. 40f with the contour of the maximum principal strains, shows that the numerical model could resemble very closely the experimentally obtained damage pattern. Moreover, the simulation of the changes in the structural capacity due to the evolution of different cracks within the structure, shown in the graph of Fig. 41, demonstrates the ability of the numerical model to account for the sudden changes in the stress distribution within the structure following the appearance of each crack. This is an important aspect for assessing the stability and displacement capacity of existing masonry structures.

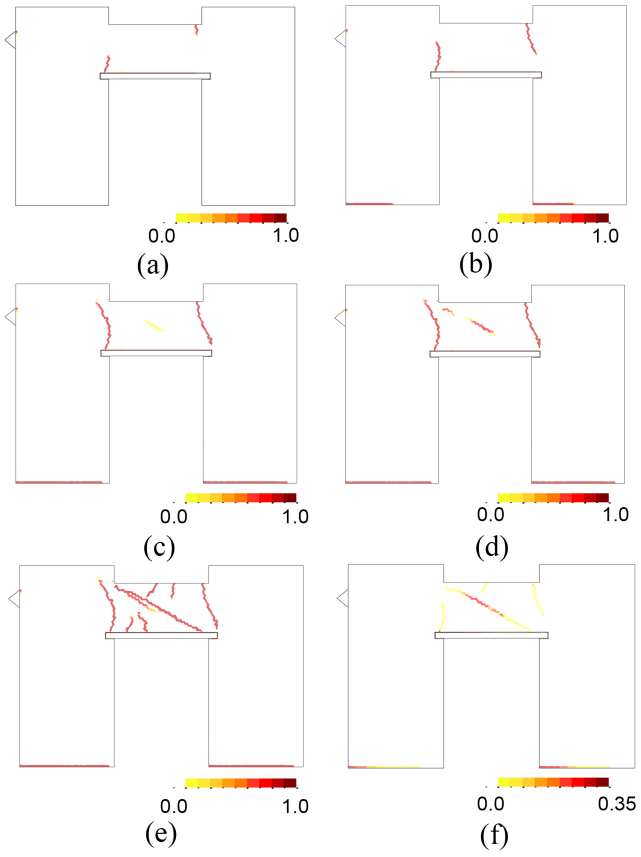

Fig. 40. Tensile damage contour for an horizontal displacement of: (a) $d = 1.5\ mm$, (b) $d = 3.3\ mm$, (c) $d = 12.3\ mm$, (d) $d = 17.3\ mm$, (e) $d = 20.7\ mm$. (f) Maximum principal strains contour for $d = 20.7\ mm$.

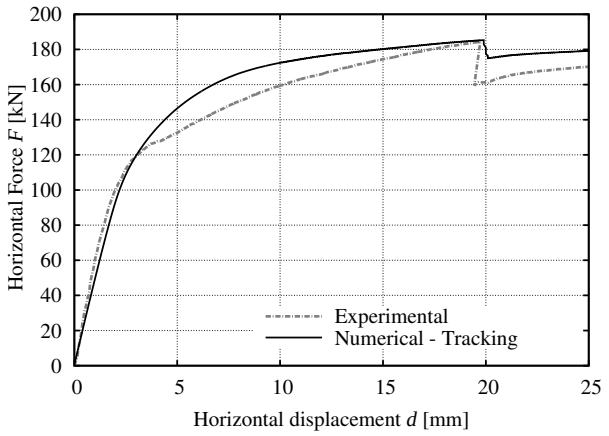

Fig. 41. Load-displacement graph of the experimental test and the numerical analysis of the masonry frame.

Cracking in masonry structures commonly appears in the weakest zones, which are the brick-mortar interface or the mortar joints in case of low strength historical mortars. The studied experiment presents an analogous behaviour. The flexural cracks start at the joints, before splitting the bricks met along their vertical propagation, while similarly the diagonal crack in the spandrel propagates mostly through the masonry joints. The higher fragility of the brick-mortar interface makes the size of the bricks as the determinant parameter for defining the distance between the cracks. This role is played by the exclusion radius in

Table 1. Material parameters adopted in the simulation of the masonry frame wall.

Material	f^+ $[MPa]$	f^- $[MPa]$	G_f^+ $[J/m^2]$	G_f^- $[J/m^2]$	E $[GPa]$	ρ $[kg/m^3]$	v $[-]$
Masonry	0.13	3.9	15	35000	1.54	1200	0.2
Interface	0.01	3.9	5	35000	0.02	1200	0.2
Timber	-	-	-	-	15	500	0.2

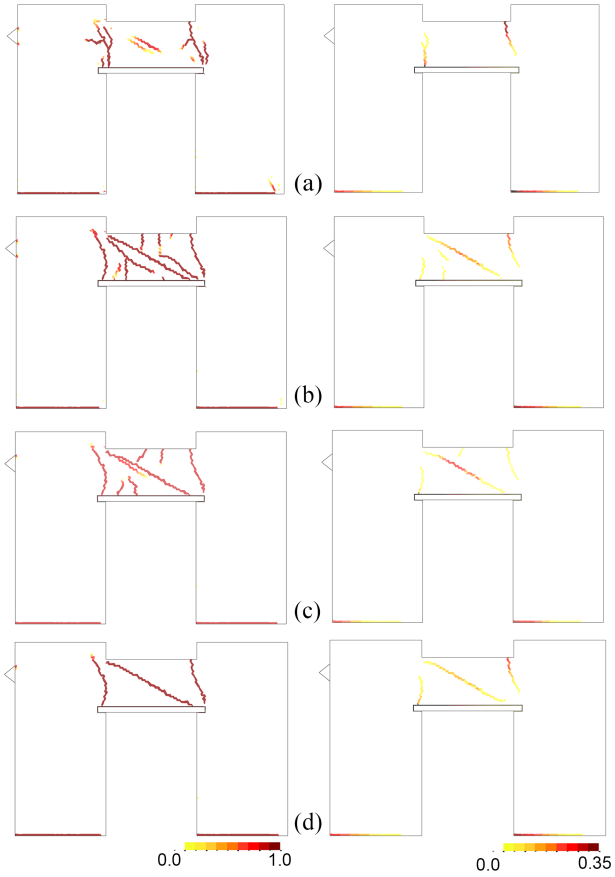

Fig. 42. Contour of tensile damage (left) and maximum principal strains (right): (a) $r_{excl} = 100\ mm$, (b) $r_{excl} = 200\ mm$, (c) $r_{excl} = 300\ mm$, (d) $r_{excl} = 500\ mm$ (horizontal displacement $d = 0.21\ m$).

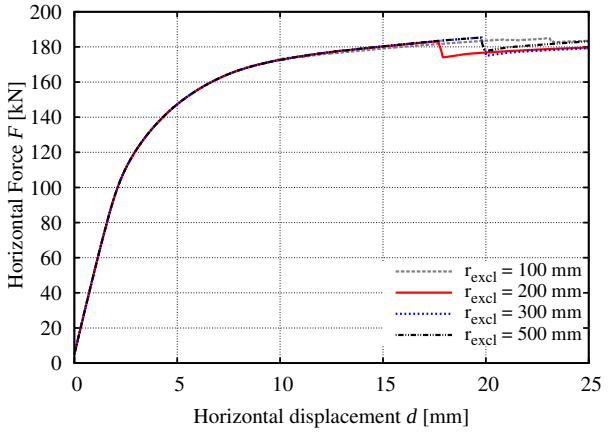

Fig. 43. Load-displacement graphs obtained from the simulation of the masonry frame with different values of r_{excl}.

the presented numerical model. This can be visualised in Fig. 42 presenting the tensile damage distribution obtained for four different values of the exclusion radius $r_{excl} = 100\,mm; 200\,mm; 300\,mm; 500\,mm$. A value of the exclusion radius equal to $100\,mm$ does not take into account the internal micro-structure of masonry defined by the size of the brick (i.e. $150 \times 300 \times 100\,mm^3$), resulting in a denser cracking at the two corners of the spandrel, which did not occur in the experiment. This flexural cracking affects the structural response, as can be appreciated in the respective load vs displacement graph of Fig. 43, where for $r_{excl} = 100\ mm$ the typical graph for a rocking failure mode is obtained, without the drop in the capacity associated with the shear damage in the spandrel. Contrariwise, for values of the exclusion radius of $200\,mm$ and above, the numerical model reproduces the experimentally obtained structural response in terms of cracking (Fig. 42b-d), strength and ductility (Fig. 43).

6 Local tracking algorithm - Cyclic loading

Despite their substantial differences in crack representation, crack propagation and nucleation criteria, a common standpoint of many algorithms in the literature (e.g. [153, 168, 32, 112, 113, 156]) is the assumption that the propagation of a crack stops when it meets another one. The various successful applications of these tracking algorithms show that this choice can be valid, or a least not detrimental, for structural applications under monotonic loading. Contrariwise, the experience of past earthquakes demonstrates that cyclic loading of concrete and masonry structures may cause complex cracking and situations including crack opening and closing as well as crack intersection. This section deals with the application of tracking algorithms to cases with cyclic loads, and outlines the algorithmic issues that have to be addressed for modelling the aforementioned cracking phenomena.

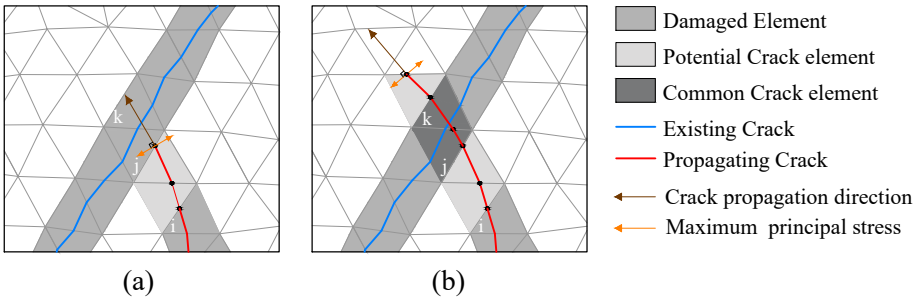

Fig. 44. Illustration of a case (a) prior and (b) after the intersection of two cracks as modelled by the local tracking algorithm.

6.1 Crack intersection

The modelling of cracking using the smeared crack approach allows the straightforward extension of the crack propagation strategy presented in Section 4.3 for simulating crack intersection. The procedure is presented in Fig. 44, where a propagating crack (in red) starting from the crack-tip element "i" meets an existing crack (in blue) towards its propagation. As shown in Fig. 44a, the crack propagation direction at the current crack-tip element "j", which is a part of the existing crack, is defined in the same way as for intact elements. Note that the crack propagation direction is computed considering the values of the effective stresses, which makes possible its definition even if the common element is completely damaged. In the same manner, the crack continues its propagation through the existing crack as shown in Fig. 44b, with the elements "j" and "k" being common crack elements now.

As it can be seen from the above procedure, the modelling of crack intersection can be easily pursued in the context of a smeared crack approach. On the contrary, in discrete crack approaches the simulation of crack intersection requires changes at nodal or elemental level (see [255, 154]) to enable the modelling of the different kinematics induced by the intersecting cracks. Another challenge in discrete crack approaches concerns the proper calculation of the stress intensity factors and, consequently, the computation of the propagation direction, which may necessitate the mesh refinement in the crack-tip zone [86]. Nevertheless, it should be noted that in smeared crack approaches the correct crack propagation relies on the accurate strain localization, which depends strongly on the kinematics of the chosen finite elements. In the presented tracking algorithm, local errors in the crack propagation direction can be potentially corrected through the maximum curvature criterion (see Section 4.6).

As soon as cracks can intersect, an element may belong to more than one crack, implying that it will have as many crack-entry points as the number of the cracks crossing it. It is recalled that the storage of the crack-entry point is necessary for three functions. The first one is when the element is the crack-tip of a crack and thus the crack-entry coordinates are necessary to identify the starting point for the crack propagation. The second one is to check crack path continuity (Section 4.5.2), while the third function concerns the use of the maximum curvature criterion (Section 4.6). In the maximum curvature criterion, the crack-entry points at elements on the wake of the crack-tip are recovered in order to opportunely correct the propagation of the crack. To this aim, a proper matrix is implemented to save the potential crack-entry coordinates for each side of the element. In the case that more than one cracks enter from the same side, two options are possible: (i) to add elements in the matrix corresponding to each new crack-entry coordinates, (ii) to use an average crack-entry point for that side. The first choice favours accuracy, but increases the numerical cost since there is the need for dynamically allocating memory, as well as the use of additional arrays to associate the crack-entry point with the number of each crack. Due to the above, the second choice has been selected in this work in favour of computer memory usage and robustness, which are necessary for the analysis of structures with a large number of cracks.

6.2 Crack nucleation - Multi-directional tracking

The criteria for crack initiation, presented in Section 4.1, define that new cracks can start at a certain distance from existing ones, which is determined by the exclusion radius r_{excl}. As shown in Section 5, this procedure is robust for structural cases with monotonic loading, where the crack directions do not show sudden changes during the loading history (see also other applications in [32, 160, 273, 274, 114, 275]). However, cyclic loading (e.g. due to earthquakes) may induce *multi-directional cracking* with cracks initiating at the same region of existing cracks but with a different propagat-

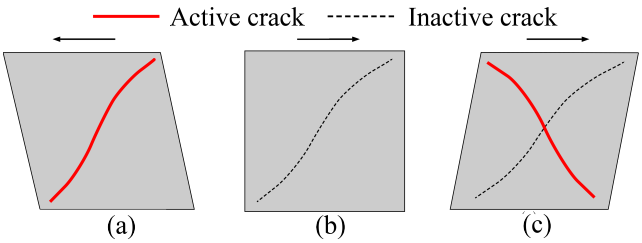

Fig. 45. Example of cracking under the shear loading of a wall: (a) opening of a crack during the loading towards the left, (b) closing of the crack when returning to the initial configuration and (c) opening of a second crack, diagonal to the first during the reverse loading.

ing direction. This phenomenon is illustrated in Fig. 45, showing a masonry wall under the effect of cyclic shear loading at its top (restraining the rotation). The top displacement towards the left produces a diagonal shear crack, starting from the middle of the wall and propagating towards its two opposite corners (Fig. 45a). Unloading finds the wall at its initial configuration with the crack closed, illustrated in Fig. 45b. Loading towards the right results in the opening of a new crack at the centre of the wall that propagates diagonally producing the common X-crack pattern of unreinforced masonry walls (Fig. 45c).

The simulation of such cases needs a different approach for crack initiation compared to the one presented in Section 4.1. For instance, in the specific case of the shear wall of Fig. 45, the crack initiation criterion should allow the initiation of the second crack at the finite element that satisfies the failure criterion after the reversal of the loading cycle, without considering if this lies within the exclusion radius area of the first crack.

For the simulation of cases involving the nucleation of cracks due to different stress-states at a region of existing cracks, the authors have proposed the categorization of cracks into *active* and *inactive* [116]. To this aim, two versors are used:

- *Crack direction* ($\hat{v}_{cr}$)*:* is a versor denoting the average direction of a consolidated crack. The crack direction of a crack is calculated using the coordinates of its two ends. These are the coordinates of the crack origin and the crack-tip for single-direction propagating cracks (with a boundary crack-root), and the coordinates of the two crack-tips for double-direction propagating cracks (with an internal crack-root).
- *Crack closure direction* ($\hat{v}_{cl}$): is a versor denoting the average direction orthogonal to the maximum principal effective stress (or strains) of all the elements within the crack. It is equivalent to an average crack propagation direction obtained considering the effective stress state of all the elements within a crack.

The *crack direction* and *crack closure direction* versors are updated at the end of each analysis step for all the consolidated cracks. A crack i is defined as *active* if the angle between its crack direction versor $\hat{v}^i_{cr}$ and its crack closure direction versor $\hat{v}^i_{cl}$ is lower than a predefined limit angle α_{lim}. The crack status can be formally expressed through the use of the following function

$$H^i[|\hat{v}^i_{cr} \cdot \hat{v}^i_{cl}| - cos(\alpha_{lim})] = \begin{cases} 0 : \text{Inactive crack} \\ 1 : \text{Active crack} \end{cases} \tag{23}$$

where $(\cdot)$ is the dot product, the subscript $i = 1, N_{cr}$ is used to denote the versor values for each crack of the total existing cracks N_{cr} and $H[\bullet]$ is the Heaviside step function

$$H[x] = \begin{cases} 0 & \text{for} \quad x < 0 \\ 1 & \text{for} \quad x \geq 0 \end{cases} \tag{24}$$

Following the above, an element is a crack-root when all of the following criteria are satisfied:

(i) The failure condition, as defined by the constitutive model (Eq. 20), is satisfied.
(ii) There is no *active* crack within an area defined by the exclusion radius r_{excl}.
(iii) There is no crack within an area defined by the exclusion radius r_{excl} with a crack direction making an angle with the crack propagation direction of the crack-root lower than the limit angle α_{lim}.

The first two conditions imply that new cracks can initiate at locations where the current stress-state has resulted in the closing of the pre-existing cracks. The third one prevents the presence of spurious cracking with similar direction to consolidated neighbouring cracks.

To illustrate this, Fig. 46 presents how the algorithm models the two shear cracks at the middle of the wall for the example of Fig. 45. Fig. 46a shows the stress-state within the crack at the moment of the opening of the crack during the movement towards the left. The two versors of the crack ($\hat{v}_{cr}$ and $\hat{v}_{cl}$, shown in one of the two crack-tips of the crack) coincide, as the crack direction has been defined according to the crack-propagation direction of each element within it. The crack is active and can continue its propagation. Figure 46b presents the stress state for a step during the reversal of the cycle. The wall now is deforming towards the right and the existing crack is closed. This can be seen looking at the directions of the principal stresses which have rotated compared to when the crack was open. The crack closure ($\hat{v}_{cr}$) and crack direction versors ($\hat{v}_{cl}$) form an angle

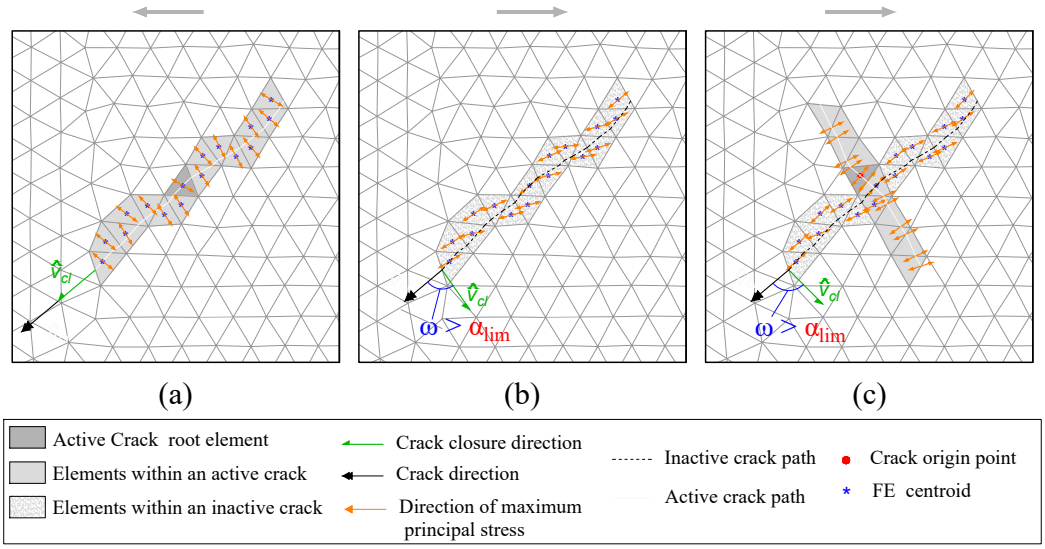

Fig. 46. Crack propagation in the middle of a shear wall: (a) propagation of a shear crack for the loading towards the left, (b) deactivation of the crack due to the change in the stress state, (c) initiation and propagation of a second crack next to the inactive one.

which is greater than the limit angle α_{lim}. The existing crack is therefore identified as inactive, and new cracks are allowed to open. This happens at a later instance, shown in Fig. 46c, when a crack initiates very close to the existing crack and propagates thereafter.

The use of a limit angle as a way to identify the closure of existing cracks and the possibility of new ones to open, was introduced at constitutive level in the smeared crack models by de Borst & Nauta [20]. Similarly, Song & Belytschko employed a threshold angle for allowing the initiation of crack branching in propagating cracks [98] under dynamic fracture.

7 Structural application under cyclic loading

This section presents an application (detailed in [116, 260]) of the presented tracking algorithm to a case with intersecting cracking under cyclic loading. This an unreinforced masonry wall that was tested under quasi-static in-plane cyclic shear loading by Anthoine et al. [276, 277].

The experimental set-up is presented in Fig. 47. The wall was built in an English bond pattern with unit dimensions of $55 \times 120 \times 250\ mm^3$ and $10\ mm$ mortar joint thickness, resulting in a specimen with width of $d = 1.00\,m$, height $h = 1.35\,m$ and thickness $w = 0.25\,m$. The effect of an earthquake action on the wall was investigated through the application of a horizontal displacement at the top in a cyclic fashion with increasing magnitude. During the whole experiment a constant vertical load of $150\ kN$ was applied at the top of the wall, while proper boundary conditions were used to avoid its top and bottom rotation.

The wall is discretized using 5470 constant strain triangles (2836 nodes) and analysed under plane stress conditions. The material parameters are presented in Table 2 and have been selected according to the available experimental data on stack bond prisms reported in [278, 279]. The not available data have been defined according to the discussion presented in [116, 260] for calibrating the shear response of the constitutive model. Regarding the tracking parameters, the exclusion radius has been set equal to $r_{excl} = 200\,mm$, which is a value between the length and the width of the bricks, while the parameters for the maximum curvature criterion are $\alpha_{max} = 25°$, $r_{neigh} = 600\ mm$. The limit angle used for the activation-deactivation of the cracks under the cyclic loading is $\alpha_{lim} = 40°$.

Figure 48 presents the numerical results in terms of tensile and compressive damage, as well as the maximum principal strains at the end of the analysis. The contour of the tensile damage in Fig. 48a reveals that important cracking has affected the structure during the loading history, with horizontal cracks at the bottom and top ends and the left and right sides of the wall, and diagonal shear cracks in the middle. Nevertheless, the compressive damage and maximum principal strains contours (Figs. 48b,c) reveal that the main degradation of the wall is due to a X-crack pattern, which typically characterizes unreinforced masonry walls under seismic loading. This dominating shear failure is depicted in the force-displacement graph

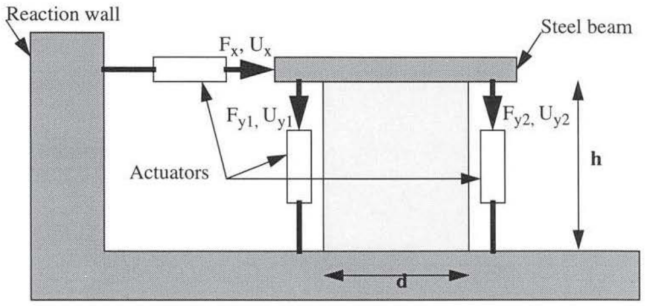

Fig. 47. Experimental set-up of the tested masonry wall. (Image from Anthoine [277]).

Table 2. Material parameters adopted in the simulation of the masonry shear wall.

f^+	f^-	G_f^+	G_f^-	E	ρ	υ	β	κ_1
$[MPa]$	$[MPa]$	$[J/m^2]$	$[J/m^2]$	$[MPa]$	$[kg/m^3]$	$[-]$	$[-]$	$[-]$
0.15	6.2	80.0	14000	1490	1750	0.2	0.95	0.15

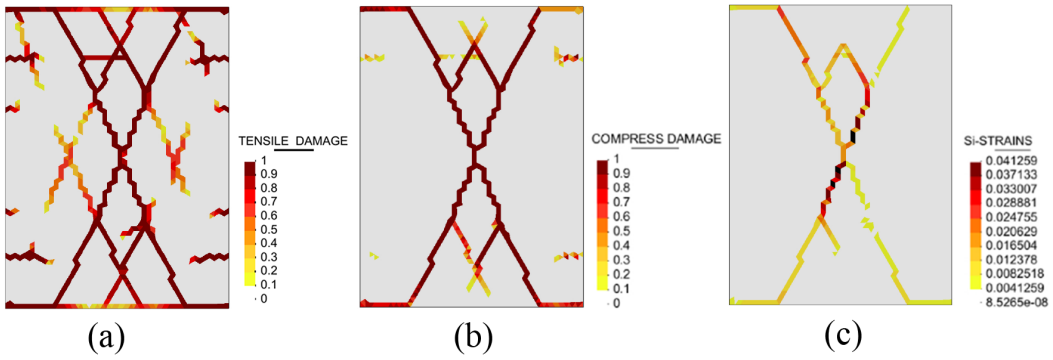

Fig. 48. Contours of: (a) tensile damage d^+, (b) compressive damage d^-, and (c) the maximum principal strains at the end of the analysis.

of Fig. 49. The structural response is characterized by a softening behaviour with appreciable energy dissipation after reaching the maximum capacity for a displacement of 3 mm.

The performance of the proposed approach for the crack-activation and deactivation can be appreciated in Figs. 50, 51, which present the crack state and the damage pattern at different instances of the loading history. During the first cycle, shown in Fig. 50, the loading towards the right produces three cracks, one at the top right and lower left corners and an internal crack starting from the middle of the wall. These cracks progressively close during the load reversal, and are recognized as inactive by the tracking algorithm. Their deactivation allows new ones to appear at the boundaries and centre of the wall. Fig. 51 shows the crack state and the cracking of the wall for the cycle with $\pm 3.0\,mm$ maximum top displacement. Despite the important cracking, the tracking algorithm can capture correctly the changes in the stress state within the wall and recog-

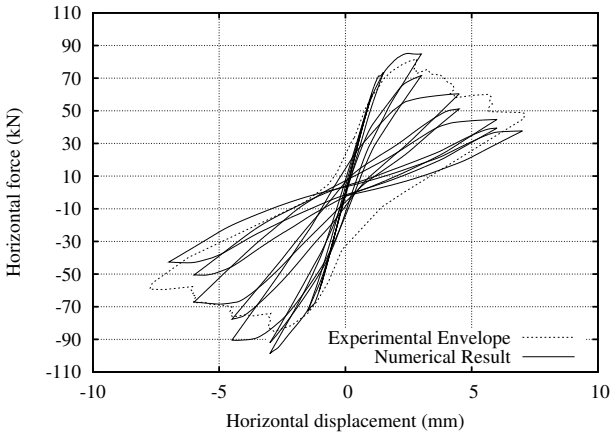

Fig. 49. Force against horizontal displacement graphs for the masonry shear wall obtained through the numerical analysis.

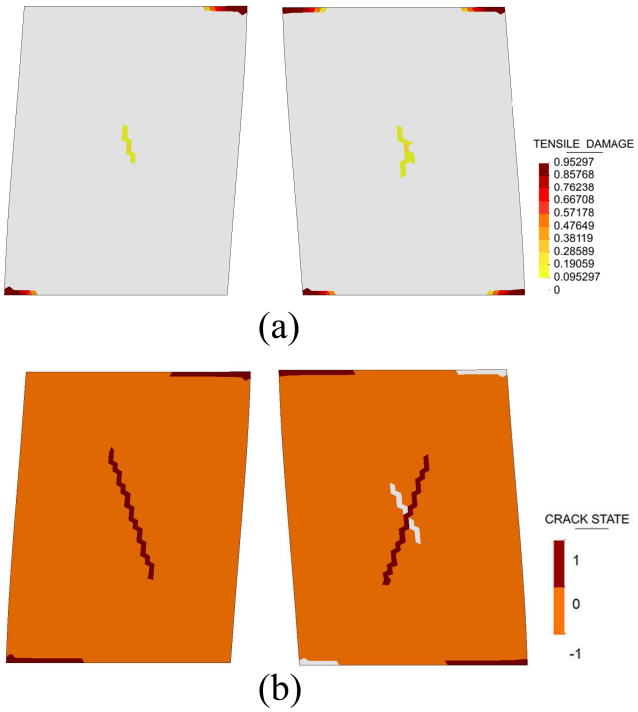

Fig. 50. (a) Tensile damage contour d^+ and (b) crack state during the first loading cycle for the maximum displacement towards the right (left column) and the maximum displacement towards the left (right column) (deformed mesh $\times 100$).

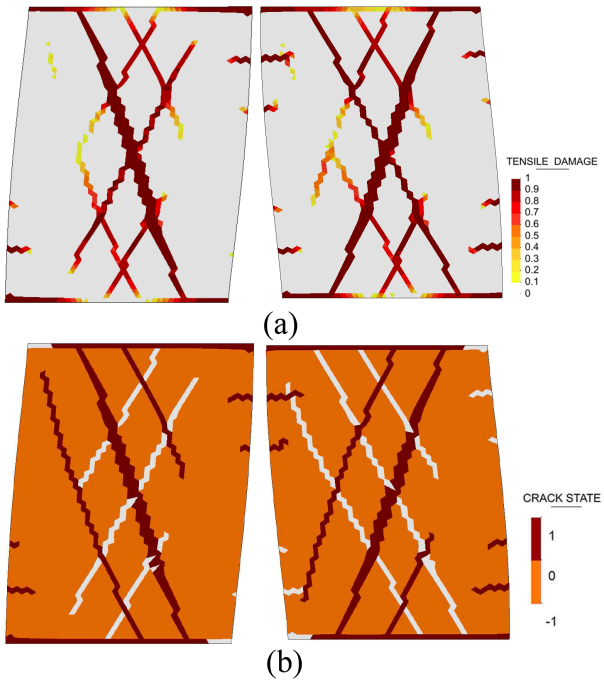

Fig. 51. (a) Tensile damage contour d^+ and (b) crack state for a maximum displacement of $+3.00\,mm$ (left column) and $-3.00\,mm$ (right column) (deformed mesh $\times 50$).

nize correctly the active and inactive cracks according to the loading direction and their open or close configuration respectively. During this cycle, the diagonal shear cracking at the middle of the wall reaches the top and bottom ends, and results in the drop in the structural capacity as shown in Fig. 49.

8 Large-Scale structural application

Large-scale problems with extensive cracking are a big challenge for tracking algorithms. Such cases necessitate numerical models that are capable of handling multiple and arbitrary crack initiation and propagation, allowing for crack intersection and showing the necessary robustness and efficiency. This section outlines a relative application of the tracking algorithm to a large-scale structure presented in [257].

The structural application deals with the pushover analysis of an interior structural wall of an unreinforced masonry building situated in Via Martoglio, Catania Italy [280]. This is a well-known case study in the literature, analysed with diverse numerical tools oriented to the simulation of masonry structures (e.g. [280, 281, 282]).

Figure 52 illustrates the geometry of the analysed structure and the distinguishing structural elements.

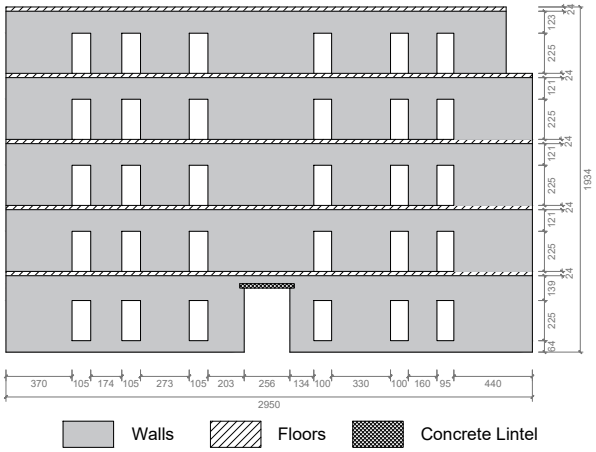

Fig. 52. Geometry (in cm) and material distribution of the analysed wall.

Table 3. Materials assigned to the different structural elements of Model-A and Model-B.

Material	Model A	Model B
A	Walls & Floors	Walls
B	Lintel	Floors & Lintel

The floors are constructed with clay brick vaults supported on concrete girders, while the roof is a timber structure. Since no information is available regarding

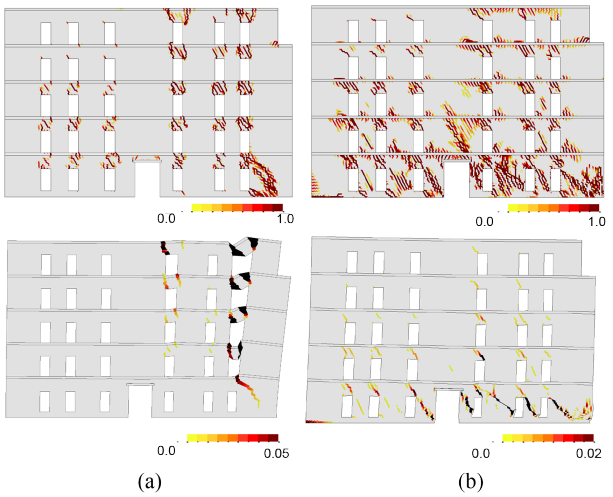

Fig. 53. Tensile damage (first row) and maximum principal strains (second row) at the end of the analysis for (a) Model A and (b) Model B.

the floor's rigidity, two models are considered with different material properties for the floors (see Table 3). The first one (denoted hereafter as Model A) adopts the existence of a flexible diaphragm and is prepared using the same material parameters for both masonry walls and floors (Material A in Table 4). The second model (denoted hereafter as Model B) intents to simulate the effect of a stiff diaphragm and the floors are modelled as linear elastic having the double stiffness of masonry's one (Material B in Table 4). In both models the concrete lintel above the central opening at the ground floor has been simulated also as linear elastic. A value of 0.45 is assigned to κ_1 parameter resulting in a shear strength of 0.15 MPa, which is the value used in [280, 281]. As the previous case study (Section 5), the exclusion radius is defined equal to the bricks length $r_{excl} = 250\,mm$, while the rest of the tracking parameters are $\alpha_{max} = \pi/4$ and $r_{neigh} = 500\,mm$. Multi-directional crack initiation is not considered for this case, due to the monotonic nature of the applied loading.

The structure is discretized using an unstructured mesh with 51052 constant strain triangles (26538 nodes) and plane stress conditions are adopted. The effect of an earthquake is simulated by means of a non-linear equivalent static analysis (pushover analysis), which is carried-out in two stages. In the first one, the self-weight of the walls and floors is applied, as well as the live load as defined in [280]. In the second stage, horizontal forces are applied at the level of each floor. This loading pattern is proportional to the height and the vertical loading of each floor as suggested in [283].

Figure 53 shows the results obtained with the two models in terms of tensile damage (first row) and maximum principal strains (second row). The different assumptions regarding the floor parameters result in distinct structural responses by the two models. In Model A, the spandrels above the openings are the most severely damaged elements, exhibiting important vertical cracking. The absence of the consolidating action from a stiff diaphragm allows the free rotation of the piers as soon as the cracks in the spandrels are completely open. As a result, the last three vertical piers of the right side rotate as cantilevers around their base with almost no interaction among them. Failure of the structure is eventually determined by the collapse of the right side, as shown in the second row of Fig. 53a. Contrary to Model A, the modelling of a stiff linear elastic floor in Model B mobilises the shear response of both spandrels and walls. This is demonstrated by the diagonal cracking experienced by these elements in Fig. 53b (first row). Collapse in this case is due to the shear failure of the piers at the base of the structure (see second row of Fig 53b).

The above results illustrate the capacity of tracking algorithms to handle cases with an extensive number of cracks. The numerical stability can be appreciated in Fig. 54, which presents the obtained base shear against horizontal displacement graphs for Model A and B. In both cases, the complete loading history with an important part of the post-peak response could be reproduced. Moreover, the numerical model is capable of reproducing the change in structural response according to the adopted assumption on the floors rigidity of the two models.

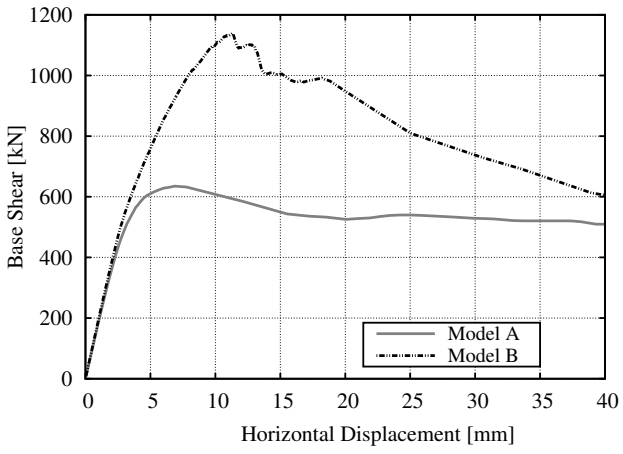

Fig. 54. Base shear versus horizontal displacement at the top right corner of the structure for the flexible diaphragm case (Model A) and for the stiff diaphragm case (Model B).

Table 4. Material parameters adopted in the numerical simulations of the large-scale structural wall.

Material	f^+ $[MPa]$	f^- $[MPa]$	G_f^+ $[J/m^2]$	G_f^- $[J/m^2]$	E $[GPa]$	ρ $[kg/m^3]$	v $[-]$
A	0.10	3.0	100	50000	2.5	1700	0.2
B	[-]	[-]	[-]	[-]	5.0	1700	0.2

The effect of directional mesh-bias dependency is also investigated in this large-scale application. To this aim Model A is analysed with two different mesh typologies, presented in Fig. 55. The results without and with the tracking algorithm are shown in Fig. 56 and Fig. 57, respectively. It can be appreciated in Fig. 56 that the solutions without the tracking algorithm are severely biased by the mesh-directionality. For the structured mesh vertical cracking affects the spandrel, while for the unstructured one the cracks in the spandrels are mainly diagonal. The tracking algorithm alleviates significantly the mesh-bias dependency as can be appreciated in Fig. 57. For both cases, the same vertical flexural cracking is predicted in the spandrels, which is the expected damage due to the absence of a stiff diaphragm. This effect is also shown in the graphs of Fig. 58. The mesh-bias dependency in the analyses without the tracking algorithm gives an important difference in the capacity and post-peak response. On the contrary, the analyses performed using the tracking algorithm are consistent among them.

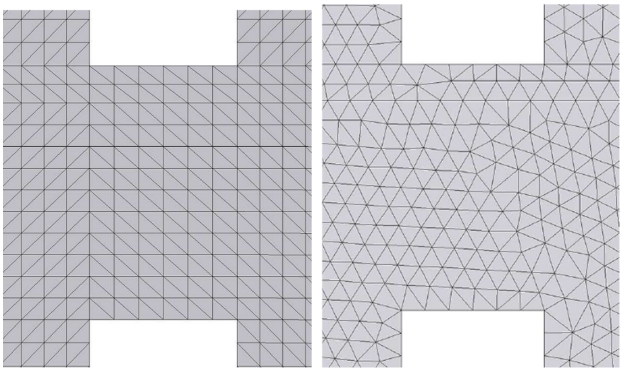

Fig. 55. Close-up of the two meshes used for the analysis of Model A: (a) structured, (b) unstructured.

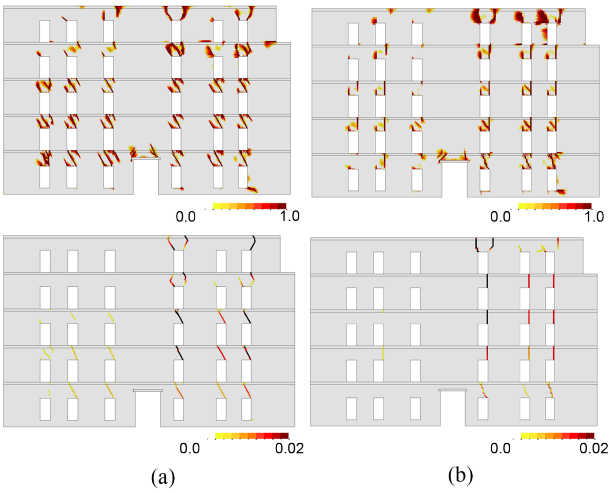

Fig. 56. Simulation of Model A using the classical smeared crack approach without the tracking algorithm. Tensile damage (first row) and maximum principal strains (second row). (a) Unstructured mesh for a horizontal displacement of 15.4 mm (Point A in Fig. 58). (b) Structured mesh for a horizontal displacement of 15.5 mm (Point B in Fig. 58).

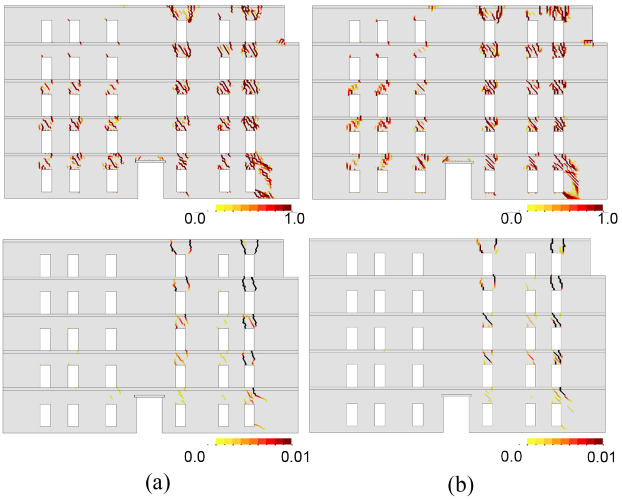

Fig. 57. Simulation of Model A using the proposed tracking algorithm. Tensile damage (first row) and maximum principal strains (second row). (a) Unstructured mesh for a horizontal displacement of 20.9 mm (Point C in Fig. 58). (b) Structured mesh for a horizontal displacement of 21.2 mm (Point D in Fig. 58).

9 Conclusions

Finite element modelling of cracking in quasi-brittle materials counts almost six decades of applications. During this period, a wide range of numerical strategies have been proposed with different levels of accuracy in crack representation and associated computational

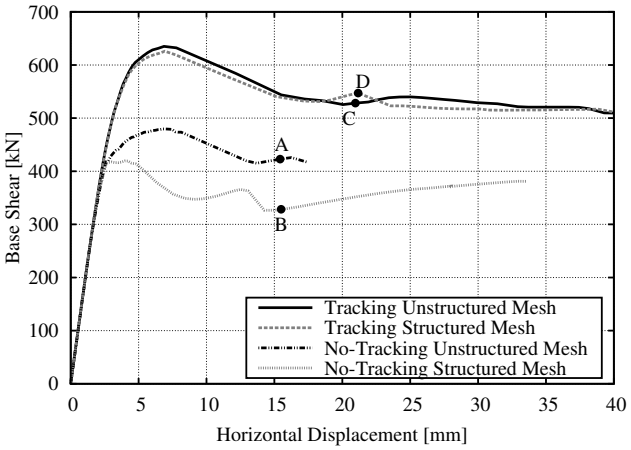

Fig. 58. Base shear versus horizontal displacement at the top right corner of the structure using two different meshes (structured and unstructured), with and without the proposed tracking algorithm.

cost. Despite the obtained experience, the realistic simulation of cracking is still a challenging issue.

Today there exist both numerical and physical challenges that need to be addressed for the finite element simulation of propagating cracks. On the one hand, probably the most important numerical challenge is the overcoming of the directional mesh-bias sensitivity of finite element solutions. This pathology has been the driving force behind the development of different strain localization techniques during the last three decades. In addition to this, an important issue is the limitation of the computational cost such that the developed numerical strategy can be used by both researchers and practitioners for the analysis of large-scale structures with multiple cracks. On the other hand, physical challenges include, among others, the understanding of phenomena associated with multiple crack nucleation, crack-opening and closing, crack intersection, definition of crack propagation direction and crack branching.

The available numerical approaches for the simulation of propagating cracks can be categorized with respect to the choice of the crack representation. This is possible using a strong discontinuity (discrete crack approach), weak ones (smeared crack approach), or a combination of both (hybrid crack approaches). Despite their differences, many of these approaches have as a common standpoint the use of tracking algorithms. These are numerical procedures used to define the zones within the structure that cracking is expected to occur. In this way, the discrete or smeared crack modelling of cracking is applied in a limited zone within the investigated structure. One of the most important benefits of using tracking algorithms is the improvement of the directional mesh-bias independency, experienced by both discrete and smeared crack approaches, due to the explicit definition of the crack location according to a selected a-priori crack propagation strategy.

Tracking algorithms have seen many advances in the last two decades. Considering the information necessary for defining and storing the crack path, tracking algorithms can be categorized as local, global and partial-domain ones, while a special category are the ones based on an underlying damage-related field.

An important part of every tracking algorithm is the criterion used for selecting the crack propagation direction. This can be based on linear elastic fracture mechanics criteria, material bifurcation analysis or empirical criteria. The topic is certainly not exhausted and a wide variety of crack propagation criteria are used today.

Contrary to monotonic loading, cyclic response is a relatively unexplored territory for tracking algorithms. Cases with cyclic loads necessitate to account for crack-opening and closing, as well as crack intersection phenomena. These phenomena are easier to simulate with tracking algorithms based on a smeared crack approach than with a discrete crack framework.

Some of the identified challenges for modelling cracking with tracking algorithms have been addressed in this paper through the presentation of a local tracking algorithm. Strategies for modelling arbitrary internal and boundary cracking, crack-path continuity, crack intersection, crack opening and closing, as well as multi-directional cracking have been detailed. The validity of these strategies has been demonstrated through the presentation of four case studies with monotonic and cyclic loading.

Acknowledgements This research has received the financial support from the MINECO (Ministerio de Economia y Competitividad of the Spanish Government) and the ERDF (European Regional Development Fund) through the MULTIMAS project (Multiscale techniques for the experimental and numerical analysis of the reliability of masonry structures, ref. num. BIA2015-63882-P) and the EACY project (Enhanced accuracy computational and experimental framework for strain localization and failure mechanisms, ref. MAT2013-48624-C2-1-P).

Compliance with ethical standards

Conflict of interest The authors declare that they have no conflict of interest.

Appendix A Continuum damage mechanics model

A.1 Constitutive equation

The constitutive model used in this work is a continuum damage model that distinguishes between tensile (d^+) and compressive damage (d^-). The constitutive equation is

$$\boldsymbol{\sigma} = (1 - d^+)\,\bar{\boldsymbol{\sigma}}^+ + (1 - d^-)\,\bar{\boldsymbol{\sigma}}^-. \tag{A.1}$$

The effective stresses ($\bar{\boldsymbol{\sigma}}$) are computed adopting a strain equivalent hypothesis [284, 285] as

$$\bar{\boldsymbol{\sigma}} = \boldsymbol{C_0} : \boldsymbol{\varepsilon}^e \tag{A.2}$$

$$\boldsymbol{\varepsilon}^e = \boldsymbol{\varepsilon} - \boldsymbol{\varepsilon}^i \tag{A.3}$$

where $\boldsymbol{C_0}$ is the 4th order isotropic elastic constitutive tensor, while $\boldsymbol{\varepsilon}$, $\boldsymbol{\varepsilon}^e$ and $\boldsymbol{\varepsilon}^i$ are second order tensors representing the total, the elastic and the irreversible strains, respectively. The split of the effective stress tensor into a positive ($\bar{\boldsymbol{\sigma}}^+$) and a negative part ($\bar{\boldsymbol{\sigma}}^-$) is performed according to Faria et al. [286, 13] as

$$\bar{\boldsymbol{\sigma}}^+ = \sum_{j=1}^{3} \langle \bar{\sigma}_j \rangle \, \mathbf{p_j} \otimes \mathbf{p_j} \tag{A.4}$$

$$\bar{\boldsymbol{\sigma}}^- = \bar{\boldsymbol{\sigma}} - \bar{\boldsymbol{\sigma}}^+. \tag{A.5}$$

In the above equations, $\bar{\sigma}_j$ is the principal effective stress corresponding to the eigenvector $\mathbf{p_j}$ of the effective stress tensor and the symbols $\langle \cdot \rangle$ are the Macaulay brackets ($\langle x \rangle = x$, if $x \geq 0$,$\langle x \rangle = 0$, if $x < 0$).

A.2 Damage criteria

Loading, unloading and reloading conditions are distinguished with the use of two scalar positive quantities, one for tension τ^+ and a second for compression τ^-, termed as equivalent stresses. Their values are defined according to the following functions proposed by Petracca et al. [287, 288]

$$\tau^+ = H_0\left[\bar{\sigma}_{max}\right]\left[\frac{1}{1-a}\left(a\bar{I}_1 + \sqrt{3\bar{J}_2} + b\langle\bar{\sigma}_{max}\rangle\right)\frac{f^+}{f^-}\right] \tag{A.6}$$

$$\tau^- = H_0\left[-\bar{\sigma}_{min}\right]\left[\frac{1}{1-a}\left(a\bar{I}_1 + \sqrt{3\bar{J}_2} + \kappa_1 b\langle\bar{\sigma}_{max}\rangle\right)\right] \tag{A.7}$$

$$a = \frac{\left(f_b^-/f^-\right) - 1}{2\left(f_b^-/f^-\right) - 1} \tag{A.8}$$

$$b = (1-a)\,f^-/f^+ - (1+a)\,. \tag{A.9}$$

In the above, f^+ and f^- stand for the tensile and compressive uniaxial strengths, respectively, and f_b^- for the biaxial compressive strength. $\bar{I}_1$ is the first invariant of the effective stress tensor and $\bar{J}_2$ the second invariant of the deviatoric effective stress tensor. The κ_1 variable in Eq. (A.7) was introduced in [287, 288] as a way to control the shape of the compressive damage surface in the shear quadrants, and through this the dilatant behaviour of the material under shear stress states. Its value varies between 0 (i.e. the Drucker-Prager criterion) and 1 (i.e. the criterion proposed by Lubliner et al. [15]). Finally, $\bar{\sigma}_{max}$ and $\bar{\sigma}_{min}$ designate the maximum and minimum principal effective stresses respectively, whereas H_0 is the specific Heaviside function ($H_0[x] = 1$ for $x > 0$ and $H_0[x] = 0$ for $x \leq 0$). The evolution of tensile and compressive damage is controlled with two damage criteria ($\Phi^\pm$), which are defined as

$$\Phi^\pm(r^\pm, \tau^\pm) = \tau^\pm - r^\pm \leq 0. \tag{A.10}$$

The stress thresholds ($r^\pm$) are internal stress-like variables representing the current damage threshold. Their initial values are equal to the uniaxial tensile and compressive strength at the moment of damage initiation $r_0^\pm = f^\pm$. After damage is triggered, both thresholds become equal to the maximum attained values by the equivalent stresses and can be explicitly computed for a generic time instant t as

$$r_t^\pm = \max\left[r_0^\pm, \max_{i\,\in\,(0,t)}\left(\tau_i^\pm\right)\right]. \tag{A.11}$$

A.3 Irreversible strains

The irreversible strains are considered as an internal variable with the following evolution law proposed in [116]

$$\Delta\boldsymbol{\varepsilon}^i_{n+1} = \beta\,\frac{r(\tilde{\bar{\boldsymbol{\sigma}}}_{n+1}) - r_n}{r_{n+1}}\,\boldsymbol{\varepsilon}^e_{n+1}. \tag{A.12}$$

where $\tilde{\bar{\boldsymbol{\sigma}}}_{n+1}$ are the trial effective stresses and $r(\tilde{\bar{\boldsymbol{\sigma}}}_{n+1})$ the equivalent stress threshold computed as

$$\tilde{\bar{\boldsymbol{\sigma}}}_{n+1} = (\bar{\boldsymbol{\sigma}}|_{\Delta\boldsymbol{\varepsilon}^i=0})_{n+1} = \bar{\boldsymbol{\sigma}}_n + \boldsymbol{C_0} : \Delta\boldsymbol{\varepsilon}_{n+1} \tag{A.13}$$

$$r(\tilde{\bar{\boldsymbol{\sigma}}}_{n+1}) = \max\left[r_n, \tau(\tilde{\bar{\boldsymbol{\sigma}}}_{n+1})\right]. \tag{A.14}$$

The parameter $\beta = [0, 1]$ is used to determine the magnitude of the incremental irreversible strains. For $\beta = 0$ no increment of irreversible strains is considered, while for $\beta = 1$ the total strain increment is irreversible. Numerically, the effect of the irreversible strains is consid-

ered through the update of the effective stresses according to the following expressions (see [116, 260])

$$\bar{\boldsymbol{\sigma}}_{n+1} = \lambda\, \tilde{\bar{\boldsymbol{\sigma}}}_{n+1} \tag{A.15}$$

$$\lambda = 1 - \beta \left(1 - \frac{r_n}{r(\tilde{\bar{\boldsymbol{\sigma}}}_{n+1})}\right). \tag{A.16}$$

A.4 Damage variables

The damage variables are defined according to the exponential softening law proposed in [289]

$$d^{\pm} = 1 - \frac{r_0^{\pm}}{r^{\pm}} \exp\left\{2H_d^{\pm}\left(\frac{r_0^{\pm} - r^{\pm}}{r_0^{\pm}}\right)\right\} \qquad r^{\pm} \geq r_0^{\pm}. \tag{A.17}$$

Tension and compression evolution laws consider the positive G_f^+ and negative G_f^- fracture energies, respectively, as well as the characteristic finite element width l_{dis} through the corresponding discrete softening parameter $H_d^{\pm}$ ensuring mesh-size independent energy dissipation according to the crack-band theory [5]. For the case of tension this is

$$H_d^+ = \frac{l_{dis}}{l_{mat}^+ - l_{dis}} \tag{A.18}$$

For the case of compressive damage, the expression proposed in [116, 260] is used to compute the discrete softening parameter H_d^-

$$H_d^- = \frac{1}{1-\beta}\left(\frac{l_{dis}}{l_{mat}^- - l_{dis}}\right) \tag{A.19}$$

The above definition is consistent with the crack bandwidth approach yielding objective results for different values of β by considering the contributions to the dissipated energy due to the evolutions of the irreversible strains and the compressive damage. In the above, the material characteristic length $l_{mat}^{\pm}$ for tension and compression is

$$l_{mat}^{\pm} = \frac{2EG_f^{\pm}}{(f^{\pm})^2}. \tag{A.20}$$

The current work considers the use of constant strain triangles for which the characteristic finite element length has been considered as $l_{dis} = \sqrt{2A_{fe}}$, with A_{fe} representing the area of the finite element. This is a standard procedure that can be refined to consider the crack direction and the finite element size according to references [290, 110, 291].

References

1. Felippa, C. A. A historical outline of matrix structural analysis: A play in three acts. *Computers and Structures*, 79(14):1313–1324, 2001.
2. Barenblatt, G. I. The Mathematical Theory of Equilibrium of Crack in Brittle Fracture. *Adv. Appl. Mech.*, 7: 55–129, 1962.
3. Dugdale, D. S. Yielding of steel sheets containing slits. *Journal of the Mechanics and Physics of Solids*, 8(2): 100–104, 1960.
4. Hillerborg, A. and Modéer, M. and Petersson, P. E. Analysis of crack formation and crack growth in concrete by means of fracture mechanics and finite elements. *Cement and Concrete Research*, 6(6):773–781, 1976.
5. Bažant, Z. P. and Oh, B. Crack band theory for fracture of concrete. *Materials and Structures*, 16:155–177, 1983.
6. Chen, W. F. *Plasticity in reinforced concrete*. McGraw-Hill, 1982. ISBN 1932159746. 474 pp.
7. Simo, J.C. and Hughes, T.J.R. *Computational Inelasticity*, volume 7. Springer, 1998. ISBN 4420767936. 392 pp.
8. Feenstra, P. H. and de Borst, R. A composite plasticity model for concrete. *International Journal of Solids and Structures*, 33(5):707–730, 1996.
9. Oñate, E. and Oller, S. and Oliver, J. and Lubliner, J. A constitutive model for cracking of concrete based on the incremental theory of plasticity, 1988. ISSN 0264-4401.
10. Mazars, J. and Pijaudier-Cabot, G. Continuum damage theory - application to concrete. *Journal of Engineering Mechanics*, 115(2):345–365, 1989.
11. Oliver, J. and Cervera, M. and Oller, S. H. and Lubliner, J. Isotropic damage models and smeared crack analysis of concrete. In *Proc. SCI-C Computer Aided Analysis and Design of Concrete Structures*, number February, pages 945–957, 1990.
12. Cervera, M. and Oliver, J. and Faria, R. Seismic evaluation of concrete dams via continuum damage models. *Earthquake Engineering & Structural Dynamics*, 24(9): 1225–1245, 1995.
13. Faria, R. and Oliver, J. and Cervera, M. A strain-based plastic viscous-damage model for massive concrete structures. *International Journal of Solids and Structures*, 35(14):1533–1558, 1998.
14. Mazars, J. and Hamon, F. and Grange, S. A new 3D damage model for concrete under monotonic, cyclic and dynamic loadings. *Materials and Structures*, pages 3779–3793, 2014.
15. Lubliner, J. and Oliver, J. and Oller, S. and Oñate, E. A plastic-damage model for concrete. *International Journal of Solids and Structures*, 25(3):299–326, 1989.
16. Lee, J. and Fenves, G. L. Plastic-Damage Model for Cyclic Loading of Concrete Structures. *Journal of Engineering Mechanics*, 124(8):892–900, 1998.
17. Armero, Francisco and Oller, Sergio. A general framework for continuum damage models. I. Infinitesimal plastic damage models in stress space. *International Journal of Solids and Structures*, 37:7409–7436, 2000.
18. Voyiadjis, George Z. and Taqieddin, Ziad N. and Kattan, Peter I. Anisotropic damage-plasticity model for concrete. *International Journal of Plasticity*, 24(10): 1946–1965, 2008.
19. Wu, Jian Ying and Cervera, Miguel. A thermodynamically consistent plastic-damage framework for localized failure in quasi-brittle solids: Material model and strain

localization analysis. *International Journal of Solids and Structures*, 88-89:227–247, 2015.
20. de Borst, R. and Nauta, P. Non-orthogonal cracks in a smeared finite element model. *Engineering Computations*, 2(1):35–46, 1985.
21. Rots, J. G. and Nauta, P. and Kusters, G. M a and Blaauwendraad, J. Smeared Crack Approach and Fracture Localization in Concrete. *Heron*, 30(1), 1985.
22. Ngo, D. and Scordelis, C. Finite Element Analysis of Reinforced Concrete Beams. *ACI Journal*, 64(3):152–163, 1967.
23. Nilson, Arthur H. Nonlinear analysis of reinforced concrete by the finite element method. *ACI Journal Proceedings*, 65(9):757–766, 1968.
24. Rashid, Y.R. Ultimate strength analysis of prestressed concrete pressure vessels. *Nuclear Engineering and Design*, 7(4):334–344, 1968.
25. Needleman, A. Material rate dependence and mesh sensitivity in localization problems. *Computer Methods in Applied Mechanics and Engineering*, 67(1):69–85, 1988.
26. de Borst, R. Simulation of Strain Localization: a Reappraisal of the Cosserat Continuum. *Engineering Computations*, 8(4):317–332, 1991.
27. de Borst, R. and Sluys, L.J. and Mühlhaus, H.-B. and Pamin, J. Fundamental issues in Finite Element Analyses of localization of deformation. *Engineering Computations*, 10(2):99–121, 1993.
28. Cervera, M. and Chiumenti, M. Smeared crack approach: back to the original track. *International Journal for Numerical and Analytical Methods in Geomechanics*, 30(12):1173–1199, 2006.
29. Cervera, M. and Chiumenti, M. and Agelet de Saracibar, C. Shear band localization via local J2 continuum damage mechanics. *Computer Methods in Applied Mechanics and Engineering*, 193(9-11):849–880, 2004.
30. Cervera, M. and Chiumenti, M. Mesh objective tensile cracking via a local continuum damage model and a crack tracking technique. *Computer Methods in Applied Mechanics and Engineering*, 196(1-3):304–320, 2006.
31. Cervera, M. and Chiumenti, M. and Codina, R. Mixed stabilized finite element methods in nonlinear solid mechanics. Part II: Strain localization. *Computer Methods in Applied Mechanics and Engineering*, 199(37-40): 2571–2589, 2010.
32. Cervera, Miguel and Pelà, Luca and Clemente, Roberto and Roca, Pere. A crack-tracking technique for localized damage in quasi-brittle materials. *Engineering Fracture Mechanics*, 77(13):2431–2450, 2010.
33. Oliver, J. and Huespe, a. E. and Dias, I. F. Strain localization, strong discontinuities and material fracture: Matches and mismatches. *Computer Methods in Applied Mechanics and Engineering*, 241-244:323–336, 2012.
34. Jirásek, Milan and Grassl, Peter. Evaluation of directional mesh bias in concrete fracture simulations using continuum damage models. *Engineering Fracture Mechanics*, 75(8):1921–1943, 2008.
35. Rabczuk, T. Computational Methods for Fracture in Brittle and Quasi-Brittle Solids : State-of-the-art Review and Future Perspectives. *ISRN Applied Mathematics*, 2013:1–61, 2012.
36. Nilson, Arthur H. Nonlinear Analysis of Reinforced Concrete by the Finite Element Method. *ACI Journal*, 65(9):757–766, 1968.
37. Goodman, R.E. and Taylor, R.L. and Brekke, T.L. A model for the mechanics of jointed rock. *Journal of Soil Mechanics & Foundations Div*, 94(3):637–659,, 1968.
38. Rots, J.G. *Computational modeling of concrete fracture*. PhD thesis, Delft University of Technology, 1988.
39. Cendón, D. A. and Gálvez, J. C. and Elices, M. and Planas, J. Modelling the fracture of concrete under mixed loading. *International journal of fracture*, 103 (3):293–310, 2000.
40. Gálvez, J. C. and Červenka, J. and Cendón, D. A. and Saouma, V. A discrete crack approach to normal/shear cracking of concrete. *Cement and Concrete Research*, 32(10):1567–1585, 2002.
41. Page, Adrian W. A Model for the In-Plane Behaviour of Masonry and a Sensitivity Analysis of its CriticaI Parameters. In *5th International Brick Masonry Conference*, pages 262–267, 1979.
42. Lotfi, H R and Shing B.P. Interface model applied to fracture of masonry structures. *Journal of Structural Engineering*, 120(1):63–80, 1994.
43. Lourenço, P. B. and Rots, J. G. Multisurface Interface Model for Analysis of Masonry Structures. *Journal of Engineering Mechanics*, 123(7):660–668, 1997.
44. Gambarotta, L. and Lagomarsino, S. Damage models for the seismic response of brick masonry shear walls. Part I: The mortar joint model and its applications. *Earthquake Engineering & Structural Dynamics*, 26(4): 423–439, apr 1997.
45. Macorini, L. and Izzuddin, B. A. A non-linear interface element for 3D mesoscale analysis of brick-masonry structures. *International Journal for Numerical Methods in Engineering*, 85(12):1584–1608, 2011.
46. Petracca, Massimo and Pelà, Luca and Rossi, Riccardo and Zaghi, Stefano and Camata, Guido and Spacone, Enrico. Micro-scale continuous and discrete numerical models for nonlinear analysis of masonry shear walls. *Construction and Building Materials*, 149:296–314, 2017.
47. Saouma, V. E. and Zatz, I. J. An automated finite element procedure for fatigue crack propagation analyses. *Engineering Fracture Mechanics*, 20(2):321–333, 1984.
48. Ingraffea, A. R. and Saouma, V. Numerical modeling of discrete crack propagation in reinforced and plain concrete. In *Fracture mechanics of concrete: Structural application and numerical calculation*, pages 171–225. Springer Netherlands, Dordrecht, 1985. ISBN 978-94-009-6152-4.
49. Shephard, Mark S. and Yehia, Nabil A B and Burd, Gary S. and Weidner, Theodore J. Automatic crack propagation tracking. *Computers and Structures*, 20(1-3):211–223, 1985.
50. Wawrzynek, P. A. and Ingraffea, A. R. Interactive finite element analysis of fracture processes: An integrated approach. *Theoretical and Applied Fracture Mechanics*, 8 (2):137–150, 1987.
51. Bocca, Pietro and Carpinteri, Alberto and Valente, Silvio. Mixed mode fracture of concrete. *International Journal of solids and structures*, 27(9):1139–1153, 1991.
52. Swenson, D V and Ingraffea, A.R. Modeling mixed-mode dynamic crack propagation using finite elements: Theory and applications. *Computational Mechanics*, 3: 381–397, 1988.
53. Martha, Lf and Wawrzynek, Pa and Ingraffea, Ar. Arbitrary crack representation using solid modeling. *Engineering with Computers*, pages 63–82, 1993.
54. Schrefler, Bernhard A. and Secchi, Stefano and Simoni, Luciano. On adaptive refinement techniques in multifield problems including cohesive fracture. *Computer*

Methods in Applied Mechanics and Engineering, 195(4-6):444–461, 2006.
55. Feld-Payet, S. and Chiaruttini, V. and Besson, J. and Feyel, F. A new marching ridges algorithm for crack path tracking in regularized media. *International Journal of Solids and Structures*, 71:57–69, 2015.
56. Areias, P. and Reinoso, J. and Camanho, P. and Rabczuk, T. A constitutive-based element-by-element crack propagation algorithm with local mesh refinement. *Computational Mechanics*, 56(2):291–315, 2015.
57. Johnson, C. and Scott, R. A Finite Element Method for Problems in Perfect Plasticity Using Discontinuous Trial Functions. In *Nonlinear Finite Element Analysis in Structural Mechanics*, pages 307–324. Springer Berlin Heidelberg, Berlin, Heidelberg, 1981.
58. Dvorkin, E. N. and Cuitiño, A. M. and Gioia, G. Finite elements with displacement interpolated embedded localization lines insensitive to mesh size and distortions. *International Journal for Numerical Methods in Engineering*, 30(3):541–564, 1990.
59. Klisinski, Marek and Runesson, Kenneth and Sture, Stein and Others. Finite element with inner softening band. *Journal of engineering mechanics*, 117(3):575, 1991.
60. Simo, J. C. and Oliver, J. and Armero, F. An analysis of strong discontinuities induced by strain-softening in rate-independent inelastic solids. *Computational Mechanics*, 12(5):277–296, 1993.
61. Larsson, Ragnar and Runesson, Kenneth and Ottosen, Niels Saabye. Discontinuous displacement approximation for capturing plastic localization. *International Journal for Numerical Methods in Engineering*, 36(12): 2087–2105, 1993.
62. Armero, Francisco and Garikipati, K. An analysis of strong discontinuities in multiplicative finite strain plasticity and their relation with the numerical simulation of strain localization in solids. *International Journal of Solids and Structures*, 33(20-22):2863–2885, 1996.
63. Oliver, J. Continuum modelling of strong discontinuities in solid mechanics using damage models. *Computational Mechanics*, 17(1-2):49–61, 1995.
64. Oliver, J and Cervera, M. and Manzoli, O. On the Use of Strain-Softening models for the Simulation of Strong Discontinuities in Solids. In R.de Borst and E. V. D.Giessen, editors, *Material Instabilities in Solids*, pages 104–123. John Wiley & Sons, Ltd, 1998.
65. Sancho, J M and Planas, J. and Gálvez, J. C. and Reyes, E. and Cendón, D. A. An embedded cohesive crack model for finite element analysis of mixed mode fracture of concrete. *Fatigue & Fracture of Engineering Materials & Structures*, 29(12):1056–1065, dec 2006.
66. Zhang, Yiming and Lackner, Roman and Zeiml, Matthias and Mang, Herbert a. Strong discontinuity embedded approach with standard SOS formulation: Element formulation, energy-based crack-tracking strategy, and validations. *Computer Methods in Applied Mechanics and Engineering*, 287:335–366, 2015.
67. Dias-da-Costa, D. and Alfaiate, J. and Sluys, L. J. and Júlio, E. Towards a generalization of a discrete strong discontinuity approach. *Computer Methods in Applied Mechanics and Engineering*, 198(47-48):3670–3681, 2009.
68. Jirásek, M. Comparative study on finite elements with embedded discontinuities. *Computer Methods in Applied Mechanics and Engineering*, 188(1-3):307–330, 2000.
69. Oliver, J. and Huespe, A. E. and Samaniego, E. A study on finite elements for capturing strong discontinuities. *International Journal for Numerical Methods in Engineering*, 56(14):2135–2161, 2003.
70. Belytschko, T. and Black, T. Elastic crack growth in finite elements with minimal remeshing. *International Journal for Numerical Methods in Engineering*, 45(5): 601–620, 1999.
71. Moës, Nicolas and Dolbow, John and Belytschko, Ted. A finite element method for crack growth without remeshing. *International Journal for Numerical Methods in Engineering*, 46(1):131–150, 1999.
72. Melenk, J.M. and Babuška, I. The partition of unity finite element method: Basic theory and applications. *Computer Methods in Applied Mechanics and Engineering*, 139(1-4):289–314, 1996.
73. Babuška, Ivo and Melenk, J. M. The partition of unity method. *International Journal for Numerical Methods in Engineering*, 40(4):727–758, 1997.
74. Hansbo, Anita and Hansbo, Peter. A finite element method for the simulation of strong and weak discontinuities in solid mechanics. *Computer Methods in Applied Mechanics and Engineering*, 193(33-35):3523–3540, 2004.
75. Song, Jeong Hoon and Areias, Pedro M A and Belytschko, Ted. A method for dynamic crack and shear band propagation with phantom nodes. *International Journal for Numerical Methods in Engineering*, 67(6): 868–893, 2006.
76. Chau-Dinh, Thanh and Zi, Goangseup and Lee, Phill Seung and Rabczuk, Timon and Song, Jeong Hoon. Phantom-node method for shell models with arbitrary cracks. *Computers and Structures*, 92-93:242–246, 2012.
77. Duarte, C.A. and Babuška, I. and Oden, J.T. Generalized finite element methods for three-dimensional structural mechanics problems. *Computers & Structures*, 77 (2):215–232, 2000.
78. Strouboulis, T. and Babuška, I. and Copps, K. The design and analysis of the Generalized Finite Element Method. *Computer Methods in Applied Mechanics and Engineering*, 181(1):43–69, 2000.
79. Strouboulis, T and Copps, K and Babuska, I. The generalized finite element method: an example of its implementation and illustration of its performance. *International Journal for Numerical Methods in Engineering*, (May 1999):1–16, 2000.
80. Strouboulis, T. and Copps, K. and Babuška, I. The generalized finite element method. *Computer Methods in Applied Mechanics and Engineering*, 190(32):4081–4193, 2001.
81. Garzon, J. and O'Hara, P. and Duarte, C. A. and Buttlar, W. G. Improvements of explicit crack surface representation and update within the generalized finite element method with application to three-dimensional crack coalescence. *International Journal for Numerical Methods in Engineering*, 97(4):231–273, 2014.
82. Karihaloo, B. L. and Xiao, Q. Z. Modelling of stationary and growing cracks in FE framework without remeshing: A state-of-the-art review. *Computers and Structures*, 81:119–129, 2003.
83. Abdelaziz, Yazid and Hamouine, Abdelmadjid. A survey of the extended finite element. *Computers and Structures*, 86(11-12):1141–1151, 2008.
84. Belytschko, Ted and Gracie, Robert and Ventura, Giulio. A review of extended/generalized finite element methods for material modeling. *Modelling and Simula-*

tion in Materials Science and Engineering, 17:043001, 2009.
85. Fries, Thomas-Peter and Belytschko, Ted. The extended/generalized finite element method: An overview of the method and its applications. *International Journal for Numerical Methods in Engineering*, 84(3):253–304, 2010.
86. Sukumar, N. and Dolbow, J. E. and Moës, N. Extended finite element method in computational fracture mechanics: a retrospective examination. *International Journal of Fracture*, 196(1-2):189–206, 2015.
87. Jirásek, Milan and Belytschko, Ted Bohdan. Computational resolution of strong discontinuities. In *Fifth world congress on computational mechanics*, pages 7–12, Vienna, 2002.
88. Oliver, J. and Huespe, A. E. and Sánchez, P. J. A comparative study on finite elements for capturing strong discontinuities: E-FEM vs X-FEM. *Computer Methods in Applied Mechanics and Engineering*, 195(37-40): 4732–4752, 2006.
89. Dias-Da-Costa, D. and Alfaiate, J. and Sluys, L. J. and Júlio, E. A comparative study on the modelling of discontinuous fracture by means of enriched nodal and element techniques and interface elements. *International Journal of Fracture*, 161(1):97–119, 2010.
90. Dumstorff, Peter and Meschke, Günther. Crack propagation criteria in the framework of X-FEM-based structural analyses. *International Journal for Numerical and Analytical Methods in Geomechanics*, 31(2):239–259, 2007.
91. Sancho, J. M. and Planas, J. and Cendón, D. A. and Reyes, E. and Gálvez, J. C. An embedded crack model for finite element analysis of concrete fracture. *Engineering Fracture Mechanics*, 74(1-2):75–86, 2007.
92. Zhang, Yiming and Zhuang, Xiaoying. A softening-healing law for self-healing quasi-brittle materials: Analyzing with strong discontinuity embedded approach. *Engineering Fracture Mechanics*, 192:290–306, 2018.
93. Jirásek, Milan and Zimmermann, Thomas. Embedded crack model. Part II. Combination with smeared cracks. *International Journal for Numerical Methods in Engineering*, 50(6):1291–1305, 2001.
94. Feist, Christian. *A numerical model for cracking of plain concrete based on the strong discontinuity approach*. PhD thesis, Universität Innsbruck, 2004.
95. Samaniego, Esteban. *Contributions to the continuum modelling of strong discontinuities in two-dimensional solids*. PhD thesis, Universitat Politècnica de Catalunya (UPC-BarcelonaTech), 2003.
96. Remmers, J. J C and de Borst, R. and Needleman, A. A cohesive segments method for the simulation of crack growth. *Computational Mechanics*, 31(1-2 SPEC.):69–77, 2003.
97. Remmers, Joris J C and de Borst, R. and Needleman, Alan. The simulation of dynamic crack propagation using the cohesive segments method. *Journal of the Mechanics and Physics of Solids*, 56(1):70–92, 2008.
98. Song, Jeong Hoon and Belytschko, Ted. Cracking node method for dynamic fracture with finite elements. *International Journal for Numerical Methods in Engineering*, 77(3):360–385, 2009.
99. Ghorashi, Seyed Shahram and Valizadeh, Navid and Mohammadi, Soheil. Extended isogeometric analysis for simulation of stationary and propagating cracks. *International Journal for Numerical Methods in Engineering*, 89(9):1069–1101, 2012.
100. Tambat, A. and Subbarayan, G. Isogeometric enriched field approximations. *Computer Methods in Applied Mechanics and Engineering*, 245-246:1–21, 2012.
101. Cedolin, Luigi and Bažant, Zdeněk P. Effect of finite element choice in blunt crack band analysis. *Computer Methods in Applied Mechanics and Engineering*, 24(3): 305–316, 1980.
102. Pietruszczak, S. and Mroz, Z. Numerical analysis of elastic-plastic compression of pillars accounting for material hardening and softening. *International Journal of Rock Mechanics and Mining Sciences and Geomechanics*, 17(4):199–207, 1980.
103. Pietruszczak, St. and Mróz, Z. Finite element analysis of deformation of strain-softening materials. *International Journal for Numerical Methods in Engineering*, 17(3): 327–334, 1981.
104. Zienkiewicz, O C and Huang, G C. A note on localization phenomena and adaptive finite-element analysis in forming processes. *Communications in Applied Numerical Methods*, 6(2):71–76, 1990.
105. Zienkiewicz, O. C. and Huang, Maosong and Pastor, M. Localization problems in plasticity using finite elements with adaptive remeshing. *International Journal for Numerical and Analytical Methods in Geomechanics*, 19(2):127–148, 1995.
106. Ortiz, Michael and Leroy, Yves and Needleman, Alan. A finite element method for localized failure analysis. *Computer Methods in Applied Mechanics and Engineering*, 61(2):189–214, 1987.
107. Belytschko, T. and Fish, J. and Engelmann, B. E. A finite element with embedded localization zones. *Computer Methods in Applied Mechanics and Engineering*, 70(1):59–89, 1988.
108. Simo, J. C. and Rifai, M. S. A class of mixed assumed strain methods and the method of incompatible modes. *International Journal for Numerical Methods in Engineering*, 29(8):1595–1638, 1990.
109. Simo, J. C. and Armero, F. Geometrically non-linear enhanced strain mixed methods and the method of incompatible modes. *International Journal for Numerical Methods in Engineering*, 33(7):1413–1449, 1992.
110. Cervera, M. An orthotropic mesh corrected crack model. *Computer Methods in Applied Mechanics and Engineering*, 197(17-18):1603–1619, 2008.
111. Cervera, Miguel. A smeared-embedded mesh-corrected damage model for tensile cracking. *International Journal for Numerical Methods in Engineering*, 76(July): 1930–1954, 2008.
112. Slobbe, A. T. and Hendriks, M. A N and Rots, J. G. Smoothing the propagation of smeared cracks. *Engineering Fracture Mechanics*, 132:147–168, 2014.
113. Burnett, Damon J. *A Mesh Objective Algorithm for Modeling Mode-I Cracks Using a Standard Finite Element Formulation*. PhD thesis, University of New Mexico, 2015.
114. Saloustros, Savvas and Pelà, Luca and Cervera, Miguel. A crack-tracking technique for localized cohesive-frictional damage. *Engineering Fracture Mechanics*, 150:96–114, 2015.
115. Saloustros, Savvas and Pelà, Luca and Cervera, Miguel and Roca, Pere. Finite element modelling of internal and multiple localized cracks. *Computational Mechanics*, 59 (2):299–316, 2016.
116. Saloustros, Savvas and Cervera, Miguel and Pelà, Luca. Tracking multi-directional intersecting cracks in numerical modelling of masonry shear walls under cyclic load-

ing. *Meccanica*, 53(7):1757–1776, 2018.
117. Benedetti, Lorenzo and Cervera, Miguel and Chiumenti, Michele. High-fidelity prediction of crack formation in 2D and 3D pullout tests. *Computers & Structures*, 172: 93–109, 2016.
118. Fraeijs de Veubeke, B. M. Displacement and equilibrium models. In O. C.Zienkiewicz and H.G., editors, *Stress Analysis*, pages 145–197. Wiley, London, 1965.
119. Pastor, M and Quecedo, M and Zienkiewicz, O C. A mixed displacement-pressure formulation for numerical analysis of plastic failure. *Computers & Structures*, 62 (1):13–23, 1997.
120. Pastor, M. and Li, T. and Liu, X. and Zienkiewicz, O. C. Stabilized low-order finite elements for failure and localization problems in undrained soils and foundations. *Computer Methods in Applied Mechanics and Engineering*, 174(1-2):219–234, 1999.
121. Chiumenti, M. and Valverde, Q. and Agelet de Saracibar, C. and Cervera, M. A stabilized formulation for incompressible elasticity using linear displacement and pressure interpolations. *Computer Methods in Applied Mechanics and Engineering*, 191(46):5253–5264, nov 2002.
122. Cervera, M. *Viscoelasticity and Rate-dependent Continuum Damage Models, Monography N-79*. CIMNE, Barcelona, 2003. ISBN 8495999374. 76 pp.
123. Chiumenti, M. and Valverde, Q. and Agelet de Saracibar, C. and Cervera, M. A stabilized formulation for incompressible plasticity using linear triangles and tetrahedra. *International Journal of Plasticity*, 20 (8-9):1487–1504, aug 2004.
124. Sánchez, P. J. and Sonzogni, V. E. and Huespe, A. E. Study of a stabilized mixed finite element with emphasis on its numerical performance for strain localization problems. *Communications in Numerical Methods in Engineering*, 24(4):297–320, 2007.
125. Cervera, M. and Chiumenti, M. and Codina, R. Mixed stabilized finite element methods in nonlinear solid mechanics. Part I: Formulation. *Computer Methods in Applied Mechanics and Engineering*, 199(37-40):2559–2570, 2010.
126. Cervera, M. and Chiumenti, M. and Benedetti, L. and Codina, R. Mixed stabilized finite element methods in nonlinear solid mechanics. Part III: Compressible and incompressible plasticity. *Computer Methods in Applied Mechanics and Engineering*, 285:752–775, 2015.
127. Benedetti, L. and Cervera, M. and Chiumenti, M. Stress-accurate Mixed FEM for soil failure under shallow foundations involving strain localization in plasticity. *Computers and Geotechnics*, 64:32–47, mar 2015.
128. Benedetti, Lorenzo. *Mixed finite element formulations for strain localization and failure in plasticity*. PhD thesis, Universitat Politècnica de Catalunya (UPC-BarcelonaTech), 2017.
129. Steinmann, P. and William, K. Localization within the framework of micropolar elasto-plasticity. In *Advances in Continuum Mechanics VI*, pages 293–313. Springer, 1991.
130. Bažant, Zdeněk P. and Lin, Feng B. Nonlocal Smeared Cracking Model for Concrete Fracture. *Journal of Structural Engineering*, 114(11):2493–2510, 1988.
131. Bažant, Zdeněk P. and Jirásek, Milan. Nonlocal Integral Formulations of Plasticity and Damage: Survey of Progress. *Journal of Engineering Mechanics*, 128(11): 1119–1149, 2002.
132. Vardoulakis, I. A gradient flow theory of plasticity for granular materials. *Acta Mechanica*, 87:197–217, 1991.
133. Muhlhaus, H. B. and Aifantis, E. C. The influence of microstructure-induced gradients on the localization of deformation in viscoplastic materials. *Acta Mechanica*, 89(1-4):217–231, 1991.
134. de Borst, R. and Mühlhaus, Hans-Bernd. Gradient-dependent plasticity: Formulation and algorithmic aspects. *International Journal for Numerical Methods in Engineering*, 35(3):521–539, 1992.
135. Peerlings, R. H J and Geers, M. G D and de Borst, R. and Brekelmans, W. A M. A critical comparison of nonlocal and gradient-enhanced softening continua. *International Journal of Solids and Structures*, 38(44-45):7723–7746, 2001.
136. Bobiński, Jerzy and Tejchman, Jacek. Comparison of continuous and discontinuous constitutive models to simulate concrete behaviour under mixed-mode failure conditions. *International Journal for Numerical and Analytical Methods in Geomechanics*, 40(3):406–435, 2016.
137. Francfort, G.A. and Marigo, J.-J. Revisiting brittle fracture as an energy minimization problem. *Journal of the Mechanics and Physics of Solids*, 46(8):1319–1342, 1998.
138. Bourdin, B. and Francfort, G. A. and Marigo, J. J. Numerical experiments in revisited brittle fracture. *Journal of the Mechanics and Physics of Solids*, 48(4):797–826, 2000.
139. Bourdin, Blaise and Francfort, Gilles A. and Marigo, Jean Jacques. *The variational approach to fracture*. Number April. Springer, 2008. ISBN 9781402063947. 1–164 pp.
140. Miehe, Christian and Hofacker, Martina and Welschinger, Fabian. A phase field model for rate-independent crack propagation: Robust algorithmic implementation based on operator splits. *Computer Methods in Applied Mechanics and Engineering*, 199 (45-48):2765–2778, 2010.
141. Ambati, Marreddy and Gerasimov, Tymofiy and De Lorenzis, Laura. A review on phase-field models of brittle fracture and a new fast hybrid formulation. *Computational Mechanics*, 55(2):383–405, 2014.
142. de Borst, R. and Verhoosel, Clemens V. Gradient damage vs phase-field approaches for fracture: Similarities and differences. *Computer Methods in Applied Mechanics and Engineering*, 312:78–94, 2016.
143. De Borst, René and Verhoosel, Clemens V. A discussion on gradient damage and phase-field models for brittle fracture. In *Advanced Structured Materials*, volume 60, pages 263–277. Springer Singapore, 2016. ISBN 978-981-10-0958-7.
144. Sluys, L. J. and de Borst, R. Wave propagation and localization in a rate-dependent cracked medium-model formulation and one-dimensional examples. *International Journal of Solids and Structures*, 29(23):2945–2958, 1992.
145. Comi, Claudia and Mariani, Stefano and Perego, Umberto. An extended FE strategy for transition from continuum damage to mode I cohesive crack propagation. *International Journal for Numerical and Analytical Methods in Geomechanics*, 31(2):213–238, 2007.
146. Wells, G. N. and Sluys, L. J. and de Borst, R. Simulating the propagation of displacement discontinuities in a regularized strain-softening medium. *International Journal for Numerical Methods in Engineering*, 53(5):

1235–1256, 2002.
147. Simone, A. and Wells, G. N. and Sluys, L. J. From continuous to discontinuous failure in a gradient-enhanced continuum damage model. *Computer Methods in Applied Mechanics and Engineering*, 192(41-42):4581–4607, 2003.
148. Belytschko, Ted and Chen, Hao and Xu, Jingxiao and Zi, Goangseup. Dynamic crack propagation based on loss of hyperbolicity and a new discontinuous enrichment. *International Journal for Numerical Methods in Engineering*, 58(12):1873–1905, 2003.
149. Oliver, J. and Dias, I. F. and Huespe, A. E. Crack-path field and strain-injection techniques in computational modeling of propagating material failure. *Computer Methods in Applied Mechanics and Engineering*, 274:289–348, 2014.
150. Lloberas-Valls, O. and Huespe, A. E. and Oliver, J. and Dias, I. F. Strain injection techniques in dynamic fracture modeling. *Computer Methods in Applied Mechanics and Engineering*, 308:499–534, 2016.
151. Ingraffea, Anthony R and Heuze, F. Finite element models for rock fracture mechanics. *International Journal for Numerical and Analytical Methods in Geomechanics*, 4(1):25–43, 1980.
152. Oliver, Javier. Modelling strong discontinuities in solid mechanics via strain softening constitutive equations. Part 2: Numerical simulation. *International Journal for Numerical Methods in Engineering*, 39(21):3601–3623, 1996.
153. Alfaiate, J. and Wells, G. N. and Sluys, L. J. On the use of embedded discontinuity elements with crack path continuity for mode-I and mixed-mode fracture. *Engineering Fracture Mechanics*, 69(6):661–686, 2002.
154. Linder, C. and Armero, F. Finite elements with embedded branching. *Finite Elements in Analysis and Design*, 45(4):280–293, 2009.
155. Manzoli, O. L. Predição de propagação de fissuras através de modelos constitutivos locais e técnica de construção progressiva da trajetória de descontinuidade. *Revista Internacional de Metodos Numericos para Calculo y Diseno en Ingenieria*, 27(3):180–188, 2011.
156. Wu, Jian Ying and Li, Feng Bo and Xu, Shi Lang. Extended embedded finite elements with continuous displacement jumps for the modeling of localized failure in solids. *Computer Methods in Applied Mechanics and Engineering*, 285:346–378, 2015.
157. Clemente, Roberto. *Análysis estructural de edificios históricos mediante modelos localizados de fisuración*. PhD thesis, Universitat Politècnica de Catalunya (UPC-BarcelonaTech), 2006.
158. Clemente, Roberto and Cervera, Miguel and Roca, Pere. Localized damage model applied to the analysis of masonry structures. *Revista Internacional de Métodos Numéricos para Cálculo y Diseño en Ingeniería*, 24(1):67–91, 2008.
159. Pelà, Luca. *Continuum Damage Model for Nonlinear Analysis of Masonry Structures*. PhD thesis, Universitat Politècnica de Catalunya (UPC-BarcelonaTech), 2009.
160. Pelà, L. and Cervera, M. and Roca, P. An orthotropic damage model for the analysis of masonry structures. *Construction and Building Materials*, 41:957–967, 2013.
161. Pelà, Luca and Cervera, Miguel and Oller, Sergio and Chiumenti, Michele. A localized mapped damage model for orthotropic materials. *Engineering Fracture Mechanics*, 124-125:196–216, 2014.
162. Slobbe, Arthur T. *Propagation and band width of smeared cracks*. PhD thesis, Delft University of Technology, 2015.
163. Areias, Pedro M A and Belytschko, Ted. Analysis of three-dimensional crack initiation and propagation using the extended finite element method. *International Journal for Numerical Methods in Engineering*, 63(5):760–788, 2005.
164. Mergheim, J. and Kuhl, E. and Steinmann, P. Towards the algorithmic treatment of 3D strong discontinuities. *Communications in Numerical Methods in Engineering*, 23(2):97–108, 2006.
165. Jäger, Philippe and Steinmann, Paul and Kuhl, Ellen. On local tracking algorithms for the simulation of three-dimensional discontinuities. *Computational Mechanics*, 42(3):395–406, 2008.
166. Gasser, Thomas C. and Holzapfel, Gerhard A. Modeling 3D crack propagation in unreinforced concrete using PUFEM. *Computer Methods in Applied Mechanics and Engineering*, 194(25-26):2859–2896, 2005.
167. Gasser, Thomas C. and Holzapfel, Gerhard A. 3D Crack propagation in unreinforced concrete. A two-step algorithm for tracking 3D crack paths. *Computer Methods in Applied Mechanics and Engineering*, 195(37-40):5198–5219, 2006.
168. Oliver, J. and Huespe, a. E. and Samaniego, E. and Chaves, E. W. V. Continuum approach to the numerical simulation of material failure in concrete. *International Journal for Numerical and Analytical Methods in Geomechanics*, 28(78):609–632, 2004.
169. Oliver, J. and Huespe, A. E. Continuum approach to material failure in strong discontinuity settings. *Computer Methods in Applied Mechanics and Engineering*, 193(30-32):3195–3220, 2004.
170. Beese, Steffen and Loehnert, Stefan and Wriggers, Peter. Modeling of Fracture in Polycrystalline Materials. In *Advances in Discretization Methods*, pages 79–102. Springer, Cham, 2016.
171. Huespe, A. E. and Needleman, A. and Oliver, J. and Sánchez, P. J. A finite thickness band method for ductile fracture analysis. *International Journal of Plasticity*, 25(12):2349–2365, 2009.
172. Huespe, A. E. and Needleman, A. and Oliver, J. and Sánchez, P. J. A finite strain, finite band method for modeling ductile fracture. *International Journal of Plasticity*, 28(1):53–69, 2012.
173. Riccardi, Francesco and Kishta, Ejona and Richard, Benjamin. A step-by-step global crack-tracking approach in E-FEM simulations of quasi-brittle materials. *Engineering Fracture Mechanics*, 170:44–58, 2017.
174. Chaves, Eduardo W V. Tracking 3D Crack Path. In *International Conference on Mathematical and Statistical Modeling in Honor of Enrique Castillo.*, Ciudad Real, Spain, 2006.
175. Jäger, Philippe and Steinmann, Paul and Kuhl, Ellen. Towards the treatment of boundary conditions for global crack path tracking in three-dimensional brittle fracture. *Computational Mechanics*, 45(1):91–107, 2009.
176. Osher, Stanley and Sethian, James A. Fronts propagating with curvature-dependent speed: Algorithms based on Hamilton-Jacobi formulations. *Journal of Computational Physics*, 79(1):12–49, 1988.
177. Belytschko, T. and Moës, N. and Usui, S. and Parimi, C. Arbitrary discontinuities in finite elements. *International Journal for Numerical Methods in Engineering*, 50(4):993–1013, 2001.

178. Stolarska, M. and Chopp, David L and Moës, Nicolas and Belytschko, Ted. Modelling crack growth by level sets in the extended finite element method. *International Journal for Numerical Methods in Engineering*, 51(8):943–960, 2001.
179. Sethian, James Albert. and Sethian, James Albert. *Level set methods and fast marching methods : evolving interfaces in computational geometry, fluid mechanics, computer vision, and materials science*. Cambridge University Press, 1999. ISBN 9780521645577. 378 pp.
180. Gravouil, A. and Moës, N. and Belytschko, T. Non-planar 3D crack growth by the extended finite element and level sets-Part II: Level set update. *International Journal for Numerical Methods in Engineering*, 53(11): 2569–2586, 2002.
181. Stolarska, M. and Chopp, D. L. Modeling thermal fatigue cracking in integrated circuits by level sets and the extended finite element method. *International Journal of Engineering Science*, 41(20):2381–2410, 2003.
182. Colombo, Daniele and Massin, Patrick. Fast and robust level set update for 3D non-planar X-FEM crack propagation modelling. *Computer Methods in Applied Mechanics and Engineering*, 200(25-28):2160–2180, 2011.
183. Ventura, G. and Budyn, E. and Belytschko, T. Vector level sets for description of propagating cracks in finite elements. *International Journal for Numerical Methods in Engineering*, 58(10):1571–1592, 2003.
184. Fries, Thomas-Peter and Baydoun, Malak. Crack propagation with the extended finite element method and a hybrid explicit-implicit crack description. *International Journal for Numerical Methods in Engineering*, 89(12): 1527–1558, 2012.
185. Colombo, Daniele. An implicit geometrical approach to level sets update for 3D non planar X-FEM crack propagation. *Computer Methods in Applied Mechanics and Engineering*, 237-240:39–50, 2012.
186. Sukumar, N. and Prévost, J. H. Modeling quasi-static crack growth with the extended finite element method Part I: Computer implementation. *International Journal of Solids and Structures*, 40(26):7513–7537, 2003.
187. Sukumar, N. and Chopp, D. L. and Béchet, E. and Moës, N. Three-dimensional non-planar crack growth by a coupled extended finite element and fast marching method. *International Journal for Numerical Methods in Engineering*, 76(5):727–748, oct 2008.
188. Shi, Jianxu and Chopp, David and Lua, Jim and Sukumar, N. and Belytschko, Ted. Abaqus implementation of extended finite element method using a level set representation for three-dimensional fatigue crack growth and life predictions. *Engineering Fracture Mechanics*, 77(14):2840–2863, 2010.
189. Duflot, Marc. A study of the representation of cracks with level sets. *International Journal for Numerical Methods in Engineering*, 70(11):1261–1302, 2007.
190. Holl, Matthias and Rogge, Timo and Loehnert, Stefan and Wriggers, Peter and Rolfes, Raimund. 3D multiscale crack propagation using the XFEM applied to a gas turbine blade. *Computational Mechanics*, 53(1):173–188, 2014.
191. Sadeghirad, Alireza and Chopp, David L. and Ren, Xiang and Fang, Eugene and Lua, Jim. A novel hybrid approach for level set characterization and tracking of non-planar 3D cracks in the extended finite element method. *Engineering Fracture Mechanics*, 160:1–14, 2016.
192. Moës, N. and Gravouil, A. and Belytschko, T. Non-planar 3D crack growth by the extended finite element and level sets-Part I: Mechanical model. *International Journal for Numerical Methods in Engineering*, 53(11): 2549–2568, 2002.
193. Bordas, Stéphane and Moran, Brian. Enriched finite elements and level sets for damage tolerance assessment of complex structures. *Engineering Fracture Mechanics*, 73(9):1176–1201, 2006.
194. Paul, B. and Ndeffo, M. and Massin, P. and Moës, N. An integration technique for 3D curved cracks and branched discontinuities within the extended Finite Element Method. *Finite Elements in Analysis and Design*, 123(May 2016):19–50, 2017.
195. Agathos, Konstantinos and Ventura, Giulio and Chatzi, Eleni and Bordas, Stéphane P. A. Stable 3D XFEM/vector level sets for non-planar 3D crack propagation and comparison of enrichment schemes. *International Journal for Numerical Methods in Engineering*, 113(2):252–276, jan 2018.
196. Haghighat, E. and Pietruszczak, S. On modeling of discrete propagation of localized damage in cohesive-frictional materials. *International Journal for Numerical and Analytical Methods in Geomechanics*, 39(16): 1774–1790, 2015.
197. Feist, C. and Hofstetter, G. An embedded strong discontinuity model for cracking of plain concrete. *Computer Methods in Applied Mechanics and Engineering*, 195(52):7115–7138, 2006.
198. Feist, C. and Hofstetter, G. Three-dimensional fracture simulations based on the SDA. *International Journal for Numerical and Analytical Methods in Geomechanics*, 31(2):189–212, 2007.
199. Armero, F. and Kim, J. Three-dimensional finite elements with embedded strong discontinuities to model material failure in the infinitesimal range. *International Journal for Numerical Methods in Engineering*, 91(12): 1291–1330, 2012.
200. Dias, I. F. and Oliver, J. and Lemos, J. V. and Lloberas-Valls, O. Modeling tensile crack propagation in concrete gravity dams via crack-path-field and strain injection techniques. *Engineering Fracture Mechanics*, 154:288–310, 2016.
201. Dias, I. F. *Crack path field and strain injection techniques in numerical modeling of propagating material failure*. PhD thesis, Universitat Politècnica de Catalunya (UPC-BarcelonaTech), 2012.
202. Dias, I. F. and Oliver, J. and Huespe, A.E. Strain injection techniques in numerical modeling of propagating material failure. *Monography CIMNE*, 134, 2012.
203. Oliver, J. and Caicedo, M. and Roubin, E. and Huespe, A.E. and Hernández, J.A. Continuum approach to computational multiscale modeling of propagating fracture. *Computer Methods in Applied Mechanics and Engineering*, 294:384–427, 2015.
204. Tamayo-Mas, Elena and Rodríguez-Ferran, Antonio. A medial-axis-based model for propagating cracks in a regularised bulk. *International Journal for Numerical Methods in Engineering*, 101(7):489–520, 2015.
205. Tamayo-Mas, E. *Continuous-discontinuous modelling for quasi-brittle failure : propagating cracks in a regularised bulk*. PhD thesis, Universitat Politècnica de Catalunya (UPC-BarcelonaTech), 2013.
206. Tamayo-Mas, Elena and Rodríguez-Ferran, Antonio. A new continuous-discontinuous damage model: Cohesive cracks via an accurate energy-transfer process. *Theoretical and Applied Fracture Mechanics*, 69:90–101, 2014.

207. Bouchard, P.O. and Bay, F. and Chastel, Y. Numerical modelling of crack propagation: automatic remeshing and comparison of different criteria. *Computer Methods in Applied Mechanics and Engineering*, 192(35-36): 3887–3908, 2003.
208. Unger, Jörg F. and Eckardt, Stefan and Könke, Carsten. Modelling of cohesive crack growth in concrete structures with the extended finite element method. *Computer Methods in Applied Mechanics and Engineering*, 196:4087–4100, 2007.
209. Erdogan, F. and Sih, G.C. On the Crack Extension in Plates under Loading and Transverse Shear. *Journal of Fluids Engineering*, 85(4):519–527, 1963.
210. Schöllmann, Matthias and Richard, Hans A. and Kullmer, Gunter and Fulland, Markus. A new criterion for the prediction of crack development in multiaxially loaded structures. *International Journal of Fracture*, 117(2):129–141, 2002.
211. Sih, G.C. Some basic problems in fracture mechanics and new concepts. *Engineering Fracture Mechanics*, 5 (2):365–377, 1973.
212. Sih, G. C. GC. Strain-energy-density factor applied to mixed mode crack problems. *International Journal of fracture*, 10(3):305–321, 1974.
213. Sih, G. C. and Macdonald, B. Fracture mechanics applied to engineering problems-strain energy density fracture criterion. *Engineering Fracture Mechanics*, 6(2): 361–386, 1974.
214. Ingraffea, Anthony R and Gerstle, Walter and Gergely, Peter and Saoume, Victor. Fracture mechanics of bond in reinforced concrete. *Journal of Structural Engineering*, 110(4):871–890, 1984.
215. Byskov, Esben. The calculation of stress intensity factors using the finite element method with cracked elements. *International Journal of Fracture Mechanics*, 6 (2):159–167, 1970.
216. Tracey, Dm. Finite elements for determination of crack tip elastic stress intensity factors. *Engineering Fracture Mechanics*, 3(3):255–265, 1971.
217. Barsoum, Roshdy S. Triangular quarter-point elements as elastic and perfectly-plastic crack tip elements. *International Journal for Numerical Methods in Engineering*, 11(1):85–98, 1977.
218. Henshell, R. D. and Shaw, K. G. Crack tip finite elements are unnecessary. *International Journal for Numerical Methods in Engineering*, 9(3):495–507, 1975.
219. Barsoum, Roshdy S. On the use of isoparametric finite elements in linear fracture mechanics. *International Journal for Numerical Methods in Engineering*, 10(1): 25–37, jan 1976.
220. Lim, I. L. and Johnston, I. W. and Choi, S. K. A finite element code for fracture propagation analysis within elasto-plastic continuum. *Engineering fracture mechanics*, 53(2):193–211, 1996.
221. Moës, N. and Belytschko, T. Extended finite element method for cohesive crack growth. *Engineering Fracture Mechanics*, 69(7):813–833, 2002.
222. Zi, Goangseup and Belytschko, Ted. New crack-tip elements for XFEM and applications to cohesive cracks. *International Journal for Numerical Methods in Engineering*, 57(15):2221–2240, 2003.
223. Natarajan, S. and Mahapatra, R. and Bordas, Stéphane. Integrating strong and weak discontinuities without integration subcells and example applications in an XFEM/GFEM framework. *International journal for numerical methods in engineering*, 83:269–294, 2010.
224. Vu-Bac, N. and Nguyen-Xuan, H. and Chen, L. and Lee, C. K. and Zi, G. and Zhuang, X. and Liu, G. R. and Rabczuk, T. A phantom-node method with edge-based strain smoothing for linear elastic fracture mechanics. *Journal of Applied Mathematics*, 2013(1), 2013.
225. Griffith, A. A. The Phenomena of Rupture and Flow in Solids. *Philosophical Transactions of the Royal Society A: Mathematical, Physical and Engineering Sciences*, 221:163–198, 1921.
226. Griffith, A. The theory of rupture. In C.Biereno and J.Burgers, editors, *First International Congress of Applied Mechanic*, pages 54–63, Delft, 1924.
227. Nuismer, R. J. An energy release rate criterion for mixed mode fracture. *International Journal of Fracture*, 11(2): 245–250, 1975.
228. Wu, C.-H. Fracture Under Combined Loads by Maximum-Energy-Release-Rate Criterion. *Journal of Applied Mechanics, Transactions ASME*, 45(3):553–558, 1978.
229. Xie, Ming and Gerstle, Walter H and Rahulkumar, Pakal. Energy-Based Automatic Mixed-Mode Crack-Propagation Modeling. *Journal of Engineering Mechanics*, 121(8):914–923, 1995.
230. Meschke, Günther and Dumstorff, Peter. Energy-based modeling of cohesive and cohesionless cracks via X-FEM. *Computer Methods in Applied Mechanics and Engineering*, 196(21-24):2338–2357, 2007.
231. Wells, G. N. and Sluys, L. J. A new method for modelling cohesive cracks using finite elements. *International Journal for Numerical Methods in Engineering*, 50(12):2667–2682, 2001.
232. Mergheim, J. and Kuhl, E. and Steinmann, P. A finite element method for the computational modelling of cohesive cracks. *International Journal for Numerical Methods in Engineering*, 63(2):276–289, 2005.
233. Verhoosel, Clemens V. and Remmers, Joris J. C. and Gutiérrez, Miguel A. A partition of unityâĂŘbased multiscale approach for modelling fracture in piezoelectric ceramics. *International Journal for Numerical Methods in Engineering*, 82(8):966–994, 2010.
234. Gálvez, J. C. and Planas, J. and Sancho, J. M. and Reyes, E. and Cendón, D. a. and Casati, M. J. An embedded cohesive crack model for finite element analysis of quasi-brittle materials. *Engineering Fracture Mechanics*, 109:369–386, 2013.
235. Alfaiate, J and Pires, E B and Martins, J a C. A Finite Element Analysis of Non-Prescribed creck propation in concrete. *Computers and Structures*, 63(I):17–26, 1997.
236. Mariani, S. and Perego, U. Extended finite element method for quasi-brittle fracture. *International Journal for Numerical Methods in Engineering*, 58(1):103–126, 2003.
237. Hill, R. Acceleration waves in solids. *Journal of the Mechanics and Physics of Solids*, 10(1):1–16, 1962.
238. Rudnicki, J. W. and Rice, J. R. Conditions for the localization of deformation in pressure-sensitive dilatant materials. *Journal of the Mechanics and Physics of Solids*, 23(6):371–394, 1975.
239. Rice, J. R. and Rudnicki, J. W. A note on some features of the theory of localization of deformation. *International Journal of Solids and Structures*, 16(7):597–605, 1980.
240. Ottosen, Niels Saabye and Runesson, Kenneth. Discontinuous bifurcations in a nonassociated Mohr material. *Mechanics of Materials*, 12(3-4):255–265, 1991.

241. Oliver, Javier. Modelling strong discontinuities in solid mechanics via strain softening constitutive equations. Part 1: fundamentals. *International Journal for Numerical Methods in Engineering*, 39(21):3575–3600, 1996.
242. Peerlings, R. H J and de Borst, R. and Brekelmans, W. A M and Geers, M. G D. Localisation issues in local and nonlocal continuum approaches to fracture. *European Journal of Mechanics, A/Solids*, 21(2):175–189, 2002.
243. Runesson, Kenneth and Saabye Ottosen, Niels and Dunja, Perić. Discontinuous bifurcations of elastic-plastic solutions at plane stress and plane strain. *International Journal of Plasticity*, 7(1-2):99–121, 1991.
244. Benallal, Ahmed and Comi, Claudia. Localization analysis via a geometrical method. *International Journal of Solids and Structures*, 33(1):99–119, 1996.
245. Oliver, J. and Cervera, M. and Manzoli, O. Strong discontinuities and continuum plasticity models: the strong discontinuity approach. *International Journal of Plasticity*, 15(3):319–351, 1999.
246. Mosler, J. Numerical analyses of discontinuous material bifurcation: Strong and weak discontinuities. *Computer Methods in Applied Mechanics and Engineering*, 194(9-11):979–1000, 2005.
247. Oliver, J. and Huespe, A. E. and Cante, J. C. and Díaz, G. On the numerical resolution of the discontinuous material bifurcation problem. *International Journal for Numerical Methods in Engineering*, 83(6):786–804, 2010.
248. Wu, Jian-Ying and Cervera, Miguel. On the equivalence between traction- and stress-based approaches for the modeling of localized failure in solids. *Journal of the Mechanics and Physics of Solids*, 82:137–163, 2015.
249. Oliver, J. and Linero, D. L. and Huespe, A. E. and Manzoli, O. L. Two-dimensional modeling of material failure in reinforced concrete by means of a continuum strong discontinuity approach. *Computer Methods in Applied Mechanics and Engineering*, 197(5):332–348, 2008.
250. Cervera, M. and Chiumenti, M. and Di Capua, D. Benchmarking on bifurcation and localization in J2 plasticity for plane stress and plane strain conditions. *Computer Methods in Applied Mechanics and Engineering*, 241-244:206–224, 2012.
251. Rabczuk, T. and Belytschko, T. Cracking particles: A simplified meshfree method for arbitrary evolving cracks. *International Journal for Numerical Methods in Engineering*, 61(13):2316–2343, 2004.
252. Rabczuk, T. and Belytschko, T. A three-dimensional large deformation meshfree method for arbitrary evolving cracks. *Computer Methods in Applied Mechanics and Engineering*, 196(29-30):2777–2799, 2007.
253. Weed, D. A. and Foster, C. D. and Motamedi, M. H. A robust numerical framework for simulating localized failure and fracture propagation in frictional materials. *Acta Geotechnica*, 12(2):253–275, 2017.
254. Armero, Francisco and Linder, Christian. Numerical simulation of dynamic fracture using finite elements with embedded discontinuities. *International Journal of Fracture*, 160(2):119–141, 2009.
255. Daux, Christophe and Moes, N. and Dolbow, John. Arbitrary branched and intersecting cracks with the extended finite element method. *International Journal for Numerical Methods in Engineering*, 48(September 1999):1741–1760, 2000.
256. Duarte, C. A. and Reno, L. G. and Simone, A. and Van Der Giessen, E. Hp generalized finite elements for three-dimensional branched cracks and polycrystals. *AIP Conference Proceedings*, 973(February):39–44, 2008.
257. Saloustros, Savvas and Pelà, Luca and Cervera, Miguel and Roca, Pere. An Enhanced Finite Element Macro-Model for the Realistic Simulation of Localized Cracks in Masonry Structures: A Large-Scale Application. *International Journal of Architectural Heritage*, 12(3): 432–447, 2018.
258. COMET. Coupled Mechanical and Thermal analysis, http://www.cimne.com/comet/, 2016.
259. GiD. The personal pre and post-processor, http://www.gidhome.com/, 2014.
260. Saloustros, Savvas. *Tracking Localized Cracks in the Computational Analysis of Masonry Structures*. PhD thesis, Universitat Politècnica de Catalunya (UPC-BarcelonaTech), 2017.
261. Lourenço, Paulo B. *Computational strategies for masonry structures*. PhD thesis, Delft University of Technology, 1996.
262. Fouchal, Fazia and Lebon, Frédéric and Titeux, Isabelle. Contribution to the modelling of interfaces in masonry construction. *Construction and Building Materials*, 23 (6):2428–2441, 2009.
263. Zhang, Yiming. *Simulation methods for durability assessment of concrete structures: multifield framework and strong discontinuity embedded approach*. PhD thesis, Vienna University of Technology, 2013.
264. Reyes, E. and Gálvez, J. C. and Casati, M. J. and Cendón, D. A. and Sancho, J. M. and Planas, J. An embedded cohesive crack model for finite element analysis of brickwork masonry fracture. *Engineering Fracture Mechanics*, 76(12):1930–1944, 2009.
265. ASTM:C496/C496M. Standard Test Method for Splitting Tensile Strength of Cylindrical Concrete Specimens. *ASTM International*, (336):1–5, 2011.
266. ASTM:D3967-08. Standard Test Method for Splitting Tensile Strength of Intact Rock Core Specimens. *ASTM International*, 2008.
267. Malárics, Viktória. *Ermittlung der Betonzugfestigkeit aus dem Spaltzugversuch an zylindrischen Betonproben*. PhD thesis, Karlsruher Institut für Technologie, 2010.
268. Malárics, V and Müller, H S. Evaluation of the splitting tension test for concrete from a fracture mechanical point of view the. *Proceedings of the Fracture Mechanics of Concrete and Concrete Structures - Assessment, Durability, Monitoring and Retrofitting of Concrete Structures*, pages 709–716, 2010.
269. Nakamura, Hikaru and Takeshi, Higai. Compressive Fracture Energy and Fracture Zone Length of Concrete. In *US-Japan Seminar on Post-Peak Behavior of Reinforced Concrete Structures Subjected to Seismic Loads: Recent Advances and Challenges on Analysis and Design*, pages 471–487, Tokyo, Japan, 2000.
270. Hendriks, M.A.N. and de Boer, A. and Belletti, B. Guidelines for Nonlinear Finite Element Analysis of Concrete Structures. Technical report, Rijkswaterstaat Centre for Infrastructure, 2017.
271. Augenti, N. and Parisi, F. and Prota, A. and Manfredi, G. In-Plane Lateral Response of a Full-Scale Masonry Subassemblage with and without an Inorganic Matrix-Grid Strengthening System. *Journal of Composites for Construction*, 15(4):578–590, 2011.
272. Saloustros, S. and Pelà, L. and Cervera, M. and Roca, P. A macro-modelling finite element technique for the realistic simulation of cracking in masonry structures. *Structural Analysis of Historical Constructions - Anamnesis, diagnosis, therapy, controls*, (2010):284–

290, 2016.
273. Roca, Pere and Cervera, Miguel and Pelà, Luca and Clemente, Roberto and Chiumenti, Michele. Continuum FE models for the analysis of Mallorca Cathedral. *Engineering Structures*, 46:653–670, 2013.
274. Petromichelakis, Yiannis and Saloustros, Savvas and Pelà, Luca. Seismic assessment of historical masonry construction including uncertainty. In Á.Cunha, E.Caetano, P.Ribeiro, C.Papadimitriou, C.Moutinho, and F.Magalhães, editors, *9th International Conference on Structural Dynamics, EURODYN 2014*, pages 297–304, Porto, Portugal, 2014. ISBN 9789727521654.
275. Saloustros, S. and Pelà, L. and Cervera, M. and Roca, P. and D'Ayala, D. F. Effect of pier-spandrel geometry on the in-plane response of masonry structures. In C.Modena, F.da Porto, and M.Valluzzi, editors, *16th International Brick and Block Masonry Conference*, pages 339–346, Padova, Italy, 2016. CRC Press 2016. ISBN 9781138029996.
276. Anthoine, A. and Magenes, G. and Magonette, G. Shear compression testing and analysis of brick masonry walls. In *10th European Conference on Earthquake Engineering*, pages 1657–1662, Vienna, 1994.
277. Anthoine, Armelle. Research of unreinforced masonry at the joint research center of the European Commision. In D. P.Abrams and G. M.Calvi, editors, *U.S.-Italy Workshop on Guidelines for Seismic Evaluation and Rehabilitation of Unreinforced Masonry Buildings*, Pavia, 1994. National Center for Earthquake Engineering Research.
278. Binda, Luigia and Mirabella Roberti, Giulio and Tiraboschi, Claudia and Abbaneo, Silvia. Measuring Masonry Material Properties. *U.S.-Italy Workshop on Guidelines for Seismic Evaluation and Rehabilitation of Unreinforced Masonry Buildings*, pages 326–347, 1994.
279. Magenes, Guido and Calvi, Gian Michele. In-plane seismic response of brick masonry walls, 1997. ISSN 0098-8847.
280. Brencich, A and Gambarotta, L and Lagomarsino, S. Catania Project: Research on the seismic response of two masonry buildings. Chapter 6: Analysis of a masonry building in Via Martoglio. *CNR Gruppo Nazionale per la Difesa dei Terremoti*, pages 107–143, 2000.
281. Milani, Gabriele and Lourenço, P.B. and Tralli, A. Homogenised limit analysis of masonry walls, Part II: Structural examples. *Computers & Structures*, 84(3-4): 181–195, 2006.
282. Addessi, D and Liberatore, D and Masiani, R. Force-Based Beam Finite Element (FE) for the Pushover Analysis of Masonry Buildings. *International Journal of Architectural Heritage*, 9(3):231–243, 2015.
283. Italian Ministry of Infrastructure and Transport. *Circolare 2 febbraio 2009, n. 617, Istruzioni per l'applicazione delle "Nuove norme tecniche per le costruzion" di cui al decreto ministeriale 14 gennaio 2008.* Rome, Italy, 2009.
284. Lemaitre, J and Chaboche, J L. Aspect Phenomenologique de la Rupture par Endommagement. *Journal de Mécanique Appliquée*, 2(3), 1978.
285. Ju, J. W. On energy-based coupled elastoplastic damage theories: Constitutive modeling and computational aspects. *International Journal of Solids and Structures*, 25(7):803–833, 1989.
286. Faria, R. and Oliver, Javier. *A Rate Dependent Plastic-Damage Constitutive Model for Large Scale Computations in Concrete Structures, Monography N-17.* CIMNE, 1993. ISBN 9788578110796.
287. Petracca, Massimo and Pelà, Luca and Rossi, Riccardo and Oller, Sergio and Camata, Guido and Spacone, Enrico. Regularization of first order computational homogenization for multiscale analysis of masonry structures. *Computational Mechanics*, 57(2):257–276, 2016.
288. Petracca, Massimo. *Computational Multiscale Analysis of Masonry Structures.* PhD thesis, University G. d'Annunzio of Chieti- Pescara (UNICH) - Universitat Politècnica de Catalunya (UPC-BarcelonaTech), 2016.
289. Oliver, Javier and Cervera, Miguel and Oller, Sergio and Lubliner, J. Isotropic damage models and smeared crack analysis of concrete. In *SCI-C Computer Aided Analysis and Design of Concrete Structures*, pages 945–957, 1990.
290. Oliver, J. A consistent characteristic length for smeared cracking models. *International Journal for Numerical Methods in Engineering*, 28(2):461–474, 1989.
291. Slobbe, A.T. and Hendriks, M.A.N. and Rots, J.G. Systematic assessment of directional mesh bias with periodic boundary conditions: Applied to the crack band model. *Engineering Fracture Mechanics*, 109:186–208, 2013.